Theses and Dissertations   1. Thesis and Dissertation Collection, all items

2009-09

Analysis and experimentation of control strategies for underactuated spacecraft

Hall, Jason S.

Monterey, California: Naval Postgraduate School

http://hdl.handle.net/10945/10468

NAVAL
POSTGRADUATE
SCHOOL

MONTEREY, CALIFORNIA

DISSERTATION

ANALYSIS AND EXPERIMENTATION OF CONTROL STRATEGIES FOR UNDERACTUATED SPACECRAFT

by

Jason S. Hall

September 2009

Dissertation Supervisor: Marcello Romano

THIS PAGE INTENTIONALLY LEFT BLANK

REPORT DOCUMENTATION PAGE		*Form Approved OMB No. 0704-0188*

1. AGENCY USE ONLY *(Leave blank)*	2. REPORT DATE September 2009	3. REPORT TYPE AND DATES COVERED Dissertation	
4. TITLE AND SUBTITLE: Analysis and Experimentation of Control Strategies for Underactuated Spacecraft		**5. FUNDING NUMBERS**	
6. AUTHOR Jason S. Hall			

7. PERFORMING ORGANIZATION NAME(S) AND ADDRESS(ES)
  Naval Postgraduate School
  Monterey, CA 93943-5000
		8. PERFORMING ORGANIZATION REPORT NUMBER	

9. SPONSORING / MONITORING AGENCY NAME(S) AND ADDRESS(ES) N/A		**10. SPONSORING / MONITORING AGENCY REPORT NUMBER**	
11. SUPPLEMENTARY NOTES The views expressed in this dissertation are those of the author and do not reflect the official policy or position of the Department of Defense or the U.S. Government.			
12a. DISTRIBUTION / AVAILABILITY STATEMENT Approved for public release; distribution is unlimited		**12b. DISTRIBUTION CODE** A	

13. ABSTRACT (maximum 200 words)

A laboratory spacecraft simulator testbed is first introduced to examine the problem of multiple spacecraft interacting in close proximity. This testbed enables validation of guidance, navigation and control (GNC) algorithms by combining 6-Degrees of Freedom (DoF) computer simulation with 3-DoF Hardware-In-the-Loop (HIL) experimentation. The presented 3-DoF spacecraft simulator employs a novel control actuator configuration consisting of a Miniature Single Gimbaled Control Moment Gyroscope (MSGCMG) and dual on/off cold-gas in-plane vectorable thrusters. The dual vectorable thruster design enables simultaneous translation and attitude control allowing it to act both in conjunction with the MSGCMG as well as provide sole actuator control throughout a commanded closed-path maneuver. Small-time local controllability (STLC) of this uniquely actuated system via Lie Algebra methods is formally demonstrated and results of experiments conducted on the described testbed are included. From this study in 3-DoF, a 6-DoF minimally control actuated asymmetric spacecraft design is proposed. Six-DoF control of this underactuated mechanical system is achieved via two oppositely mounted hemispherically vectorable thrusters. In order to capitalize on the unique nature of this system with only two control torques, a quaternion feedback regulator is developed to yield three-axis stabilization of its attitude. This regulator capitalizes on recent advancements in generalized inversion and perturbed feedback linearizing control to stabilize the dynamics of an underactuated asymmetric spacecraft and extends this to include stabilization of the kinematics of the system. Two control design methodologies are derived. The first is Lyapunov based, yielding a globally stable system, while the second yields local stability within a domain of attraction through perturbed feedback linearization. Results of several numerical simulations are presented for an asymmetric spacecraft with two bounded body-fixed control torques. The proposed attitude control method is not intended to provide attitude maintenance for attitude tracking or in the presence of relatively large disturbance torques; however, it may prove widely applicable for detumbling and reorientation maneuvers of spacecraft with only two available control torques.

14. SUBJECT TERMS Underactuated Spacecraft; Hardware-in-the-Loop; Vectorable Thrusters; Control Moment Gyros; Small-Time Local Controllability; Generalized Inverse			15. NUMBER OF PAGES 181
			16. PRICE CODE
17. SECURITY CLASSIFICATION OF REPORT Unclassified	18. SECURITY CLASSIFICATION OF THIS PAGE Unclassified	19. SECURITY CLASSIFICATION OF ABSTRACT Unclassified	20. LIMITATION OF ABSTRACT UU

THIS PAGE INTENTIONALLY LEFT BLANK

**ANALYSIS AND EXPERIMENTATION OF CONTROL
STRATEGIES FOR UNDERACTUATED SPACECRAFT**

Jason S. Hall
Lieutenant Commander, United States Navy
B.S., U.S. Naval Academy, 1997
M.S., Naval Postgraduate School, 2006

Submitted in partial fulfillment of the
requirements for the degree of

DOCTOR OF PHILOSOPHY IN MECHANICAL ENGINEERING

from the

**NAVAL POSTGRADUATE SCHOOL
September 2009**

Author: _____
                         Jason S. Hall

Approved by: _____   _____

Marcello Romano	Brij Agrawal
Professor of Mechanical	Professor of Mechanical
and Astronautical Engineering	and Astronautical Engineering
Dissertation Supervisor	Dissertation Committee Chair

_____   _____

Roberto Cristi	Fotis Papoulias
Professor of Electrical and	Professor of Mechanical
Computer Engineering	and Astronautical Engineering

_____

Xiaoping Yun
Professor of Electrical and
Computer Engineering

Approved by: _____
                  Knox Millsaps, Chair, Department of Mechanical and Astronautical
Engineering

Approved by: _____
                  Douglas Moses, Vice Provost for Academic Affairs

THIS PAGE INTENTIONALLY LEFT BLANK

ABSTRACT

A laboratory spacecraft simulator testbed is first introduced to examine the problem of multiple spacecraft interacting in close proximity. This testbed enables validation of guidance, navigation and control (GNC) algorithms by combining 6-Degrees of Freedom (DoF) computer simulation with 3-DoF Hardware-In-the-Loop (HIL) experimentation. The presented 3-DoF spacecraft simulator employs a novel control actuator configuration consisting of a Miniature Single Gimbaled Control Moment Gyroscope (MSGCMG) and dual on/off cold-gas in-plane vectorable thrusters. The dual vectorable thruster design enables simultaneous translation and attitude control allowing it to act both in conjunction with the MSGCMG as well as provide sole actuator control throughout a commanded closed-path maneuver. Small-time local controllability (STLC) of this uniquely actuated system via Lie Algebra methods is formally demonstrated and results of experiments conducted on the described testbed are included. From this study in 3-DoF, a 6-DoF minimally control actuated asymmetric spacecraft design is proposed. Six-DoF control of this underactuated mechanical system is achieved via two oppositely mounted hemispherically vectorable thrusters. In order to capitalize on the unique nature of this system with only two control torques, a quaternion feedback regulator is developed to yield three-axis stabilization of its attitude. This regulator capitalizes on recent advancements in generalized inversion and perturbed feedback linearizing control to stabilize the dynamics of an underactuated asymmetric spacecraft and extends this to include stabilization of the kinematics of the system. Two control design methodologies are derived. The first is Lyapunov based, yielding a globally stable system, while the second yields local stability within a domain of attraction through perturbed feedback linearization. Results of several numerical simulations are presented for an asymmetric spacecraft with two bounded body-fixed control torques. The proposed attitude control method is not intended to provide attitude maintenance for attitude tracking or in the presence of relatively large disturbance torques; however, it may prove widely applicable for detumbling and reorientation maneuvers of spacecraft with only two available control torques.

THIS PAGE INTENTIONALLY LEFT BLANK

TABLE OF CONTENTS

THIS PAGE INTENTIONALLY LEFT BLANK

LIST OF FIGURES

THIS PAGE INTENTIONALLY LEFT BLANK

LIST OF TABLES

THIS PAGE INTENTIONALLY LEFT BLANK

ACKNOWLEDGMENTS

Additionally, the author would like to thank the following for their invaluable assistance in completion of this Dissertation:

My beautiful wife, Meredith, and now three wonderful children, Carter, Morgen and Isaiah, who have kept me smiling despite the long hours away from home and often pre-occupied thoughts at inopportune times.

Drs. Brij Agrawal, Marcello Romano, Roberto Cristi, Xiaoping Yun and Fotis Papoulias for their time, energy and direct support as PhD Committee members to make this a reality.

I would like to specifically thank Dr. Marcello Romano for his invaluable assistance as my advisor throughout this process, always being there to provide timely expertise, guidance and validation of the research being conducted.

I would also like to specifically thank Dr. Roberto Cristi for the timeless hours spent assisting the development of the included stability proofs.

Mr. Bob Reehm who has continued to remind me of the purpose of it all and kept me spiritually grounded.

Dr. Riccardo Bevilacqua for his friendship and partnership throughout these years.

Dr. Abdulrahman Bajodah for his work in generalized inversion control methods and the many fruitful discussions.

LCol Fred Kennedy, PhD, for many helpful discussions and encouragement along the way.

THIS PAGE INTENTIONALLY LEFT BLANK

I.   INTRODUCTION

The traditional spacecraft system is a monolithic structure with a single mission focused design and lengthy production and qualification schedules coupled with enormous cost.   Additionally, there rarely, if ever, are any designed preventive maintenance plans or re-fueling capability. There has been much research in recent years into alternative options. One option involves autonomous on-orbit servicing of current or future monolithic spacecraft systems. The U.S. Department of Defense (DoD) embarked on a highly successful venture to prove such a concept with the Defense Advanced Research Projects Agency's (DARPA) Orbital Express program.   Orbital Express demonstrated all of the enabling technologies required for autonomous on-orbit servicing to include refueling, component transfer, autonomous satellite grappling and berthing, rendezvous, inspection, proximity operations, docking and undocking, and autonomous fault recognition and anomaly handling (Kennedy 2008).   Another potential option involves a paradigm shift from the monolithic spacecraft system to one involving multiple interacting spacecraft that can autonomously assemble and reconfigure. Numerous benefits are associated with autonomous spacecraft assemblies, ranging from a removal of significant intra-modular reliance that provides for parallel design, fabrication, assembly and validation processes to the inherent smaller nature of fractionated systems that allows for each module to be placed into orbit separately on more affordable launch platforms (Mathieu and Weigel 2005).

A.   GROUND-BASED   HARDWARE-IN-THE-LOOP   EXPERIMENTAL VALIDATION

With respect specifically to the validation process, the significantly reduced dimensions and mass of aggregated spacecraft when compared to the traditional monolithic spacecraft allow for not only component but even full-scale on-the-ground Hardware-In-the-Loop (HIL) experimentation.   Likewise,   much   of   the   HIL experimentation required for on-orbit servicing of traditional spacecraft systems can also be accomplished in ground-based laboratories (Creamer 2007).   This type of HIL experimentation   complements   analytical   methods   and   numerical   simulations   by

providing a low-risk, relatively low-cost and potentially high-return method for validating the technology, navigation techniques and control approaches associated with spacecraft systems. Several approaches exist for the actual HIL testing in a laboratory environment with respect to spacecraft guidance, navigation and control. One such method involves reproduction of the kinematics and vehicle dynamics for 3-DoF (two horizontal translational degrees and one rotational degree about the vertical axis) through the use of robotic spacecraft simulators that float via planar air bearings on a flat horizontal floor. This particular method is currently being employed by several research institutions and is the validation method of choice for our research into GNC algorithms for proximity operations at the Naval Postgraduate School (Machida, Toda, and Iwata 1992; Ullman 1993; Corrazzini and How 1998; Marchesi, Angrilli and Venezia 2000; Ledebuhr et al. 2001; Nolet, Kong, and Miller 2005; LeMaster, Schaechter, and Carrington 2006; Romano, Friedman, and Shay 2007).

For spacecraft involved in proximity operations, the in-plane and cross-track dynamics are decoupled, as modeled by the Hill-Clohessy-Wiltshire (HCW) equations, thus the reduction to 3-Degree of Freedom (DoF) does not appear to be a critical limiter. One consideration involves the reduction of the vehicle dynamics to one of a double integrator. However, the orbital dynamics can be considered to be a disturbance that needs to be compensated for by the spacecraft navigation and control system during the proximity navigation and assembly phase of multiple systems. Thus, the flat floor testbed can be used to capture many of the critical aspects of an actual autonomous proximity maneuver that can then be used for validation of numerical simulations. Portions of the here-in described testbed, combined with the first generation robotic spacecraft simulator of the Spacecraft Robotics Laboratory (SRL) at the Naval Postgraduate School (NPS), have been employed to propose and experimentally validate control algorithms. The interested reader is referred to Romano et al. (2007) for a full description of this robotic spacecraft simulator and the associated HIL experiments involving its demonstration of successful autonomous spacecraft approach and docking maneuvers to a collaborative target with a prototype docking interface of the Orbital Express program.

A unique control problem exists, given a requirement for spacecraft aggregates to rendezvous and dock during the final phases of assembly and a desire to maximize the useable surface area of the spacecraft for power generation, sensor packages, docking mechanisms and payloads while minimizing thruster impingement. In fact, control of such systems using the standard control actuator configuration of fixed thrusters on each face coupled with momentum exchange devices can be challenging, if not impossible. For such systems, a new and unique configuration is proposed consisting of vectorable thrusters that may capitalize, for instance, on the recently developed carpal robotic joint invented by Canfield and Reinholtz (1998) with its hemispherical vector space. It is here demonstrated through Lie algebra analytical methods and experimental results that two vectorable in-plane thrusters in an opposing configuration can yield a minimum set of actuators for a controllable reduced order (3-DoF) system. It will be shown that by coupling the proposed set of vectorable in-plane thrusters with a single degree of freedom torquer such as a Control Moment Gyroscope, an additional degree of redundancy can be gained for the reduced order system. Experimental results are included using SRL's second-generation, reduced-order spacecraft simulator with a state feedback linearized controller to demonstrate its ability to navigate a closed circular path with the proposed actuator configuration. A general overview of this spacecraft simulator is presented with additional details on the simulators being found in: Hall (2006), Eikenberry (2006), Price (2006), Romano and Hall (2006), Hall and Romano (2007a), and Hall and Romano (2007b).

B.   ROTO-TRANSLATION OF AN UNDERACTUATED SPACECRAFT

With respect to the full order (6-DoF) system of roto-translation, it will be demonstrated that a set of two vectorable hemispherical thrusters in an opposing configuration can yield a minimum set of actuators for a controllable relative motion spacecraft system. The proposed actuator configuration can readily be seen to yield an underactuated mechanical system, that is to say the number of controls N_u is fewer than the degrees of freedom. It will be shown that by adding a single-degree of freedom torque, the system can become fully actuated and a state-feedback linearizing controller

3

can be designed to drive the system to the desired position and orientation. Without the single-degree of freedom torque, this control actuator configuration equates to only two of the three body-fixed axes being directly torque controlled while the third can be indirectly controlled by capitalizing on the coupling of the terms of the moments of inertia for the system that appear in the Euler equations. Furthermore, given the cascaded nature of the angular motion equations whereby the angular rates drive the orientation, there has been much research to date to develop control algorithms to provide three-axis stabilization for an underactuated spacecraft with only two control torques. However, to date, there has not been a smooth time-invariant control algorithm to provide attitude stabilization of such a spacecraft with arbitrary inertia. By considering the attitude stabilization for the underactuated spacecraft system of angular motion equations in the general case, it may prove to be widely applicable to not only proximity operations but also de-tumbling and reorientation maneuvers of underactuated spacecraft that may either be designed with only two directly actuated control axes or be experiencing control actuator failure about one of its control axes during their mission life.

C.   STATE-OF-THE-ART   IN   UNDERACTUATED   RIGID   BODY STABILIZATION

The problem of stabilization of a rigid spacecraft's attitude dynamics and kinematics has been studied over the years in many papers and articles. However, the vast majority of the proposed control laws assume that the spacecraft is fully actuated. Wie and Barba (1985), Wie, Weiss and Arapostathis (1989), Vadali (1989), and Bajodah (2009a) address several nonlinear control techniques that provide time-invariant global asymptotic stability of the fully actuated spacecraft system of equations. Although these control laws provide for the necessary control of a nominally designed three-axis stabilized spacecraft in which three control torques exist, the question of control of underactuated spacecraft naturally enters when discussing actuator failures or when proposing minimally designed spacecraft systems. It is well understood that full order (3-DoF) control of the kinematics of such underactuated systems presents a challenging control problem; however, it should also be recognized that it has the distinct potential to provide several key benefits. Specifically, under the present thrust of Operationally

Responsive Space, where one focus is on transitioning from the typical large monolithic spacecraft design to one that embraces the new spacecraft paradigm of smaller, faster to manufacture and cheaper to produce and employ, underactuated control could provide a key enabling technology. Furthermore, in light of many current traditional spacecraft systems remaining in operation well past their intended design life despite actuator failures that degrade their capabilities, underactuated control could enable these aging systems to satisfy their original missions.

The investigation of stabilization of underactuated spacecraft kinematics and attitude dynamics began with the theoretical establishment of the necessary and sufficient conditions for the controllability of a rigid body's attitude with either gas thrusters or momentum exchange devices by Crouch (1984). He concluded that, for a spacecraft with momentum exchange devices, controllability is impossible with fewer than three, while for a spacecraft with independent paired jets, controllability is possible with two. It was later demonstrated by Kerai (1995), by using geometric control theory, that small-time local controllability of the rigid body equations assuming paired gas jets can indeed be achieved with only two control torques. Byrnes and Isidori (1991) proved that the full angular motion equations for a rigid spacecraft with only two controls cannot be asymptotically stabilized by smooth pure state feedback because they violate Brockett's (1983) theorem on non-holonomic underactuated systems. With this in mind, they proposed a smooth feedback controller to affect partial stabilization of the rigid body model resulting in a revolute constant-rate motion about the uncontrolled axis of rotation. Later, Krishnan, McClamroch and Reyhanoglu (1995) proposed a hybrid control design combining continuous time features with discrete event features to affect a discontinuous feedback control strategy to stabilize any equilibrium attitude of an underactuated spacecraft with two momentum wheel actuators in finite time under the restriction that the total angular momentum vector of the system is zero. This control methodology translates directly to a study of an underactuated axi-symmetric spacecraft. Tsiotras, Corless, and Longuski (1995) and Tsiotras and Luo (2000) also dealt with control of underactuated axi-symmetric spacecraft by proposing a time-invariant feedback control law to asymptotically stabilize the orientation of two of the three body-fixed axes. In

addition to only providing for partial attitude stabilization of axi-symmetric spacecraft, their discussion was limited to cases where the angular velocity about the unactuated axis is zero at the start of the maneuver. Tsiotras and Schleicher (2000), and Tsiotras and Doumtchenko (2000) relaxed the restriction on the symmetry of the spacecraft slightly to consider a nearly axi-symmetric spacecraft by a small parameter and a set of time-invariant control laws are proposed to stabilize the angular velocity and attitude of a spacecraft about a certain axis by virtual control inputs of the two actuated angular rates.

The global asymptotic rate stabilization problem without concern for kinematics of a fully asymmetric underactuated rigid spacecraft was addressed by Coverstone-Carroll (1996) through the use of a Variable Structure Controller (VSC). Bajodah (2009b) also addressed the rate-only stabilization problem for detumbling maneuvers through the use of singularly perturbed feedback linearization and generalized inverse control methodologies. Although both of these controllers prove to be robust to large initial angular velocities around all three axes in the presence of actuator torque limitations, they both require an additional controller to provide desired kinematic alignment after the detumbling maneuver. One such controller, as proposed by Coverstone-Carroll (1996), is a simple linear controller that is used to perform a series of eigenaxis rotations which precludes smooth attitude tracking.

The problem of stabilization of both the kinematics and dynamics of an underactuated asymmetric spacecraft was most recently addressed by Casagrande, Astolfi, and Parisini (2008) who proposed a time-variant switching control law to effect global asymptotic stabilization of the closed-loop system. Although novel, the proposed law lacks detailed simulation results by considering only the case where the initial angular rates about two of the axes to include the unactuated axis are initially zero. Furthermore, real-world spacecraft with flexible parts, antennas, fuel slosh, etc., may preclude the use of time-variant control laws because they have the distinct potential of producing unacceptable transient response and might therefore lead to instability (Tsiotras and Doumtchenko, 2000). Behal et al. (2002) address the nonlinear tracking control of an axi-symmetric spacecraft by developing a kinematic controller to determine the desired actuated angular rates which are in turn used as control inputs to the dynamic

system through the use of standard back-stepping techniques. This method yields only asymptotic dynamic and kinematic stabilization results for an axi-symmetric rigid body given the restriction that the angular rate about the unactuated axis is close to zero but it does yield bounded results otherwise.

The goal of this work is to extend the research into control algorithms for underactuated rigid spacecraft attitude control by proposing a novel, time-invariant smooth quaternion feedback regulator based on generalized inverse methods to affect three-axis attitude stabilization of the error quaternion kinematics for an underactuated rigid spacecraft with arbitrary inertia matrices and two realistically bounded body-fixed torques for required reorientation maneuvers. The problem of three-axis stabilization of the attitude of an underactuated spacecraft with direct control about only two of the body-fixed control axes will be addressed in the general case where the spacecraft's attitude is referenced to an inertially fixed frame. From this, the proposed quaternion feedback regulator can be shown to be seamlessly modified to account for attitude control with respect to a relative motion frame of reference as is the case for a chaser-target rendezvous maneuver. After affecting attitude error stabilization, a spacecraft can be propelled towards another spacecraft via various navigation schemes such as conventional waypoint navigation.

D.   SCOPE OF THE DISSERTATION

This dissertation advances the body of knowledge with respect to control of underactuated spacecraft in three key areas:

1. Laboratory experimentation of a reduced-order underactuated spacecraft simulator with vectorable thrusters and a miniature control moment gyroscope. Using feedback linearizing control methodology coupled with Schmitt Trigger and Pulse Width Modulation logic, experimental results are presented which validate the capability of this novel control actuator design to propel the spacecraft simulator around a tightly constrained path.

2. Analytical determination of the small-time local controllability of a generic full-order spacecraft under variations on the control inputs. This study is able

to provide the interested spacecraft systems engineer with the ability to determine the minimum number of control actuators necessary to maintain controllability. Furthermore, this analysis can be used to aid in dealing with both control actuator failures on existing spacecraft systems or planning for minimally designed spacecraft.

3. A smooth time-invariant state feedback control logic based on quaternion feedback regulation is derived to yield stabilization of the error kinematics of a spacecraft with only two control torques and arbitrary inertia. Two separate control designs are presented, the first being Lyapunov function based and the other being perturbed feedback linearizing in nature. Results of the numerical results considering both of these designs are presented for various maneuvers.

II.   LABORATORY EXPERIMENTATION OF GUIDANCE AND CONTROL OF SPACECRAFT DURING PROXIMITY MANEUVERS

While presenting an overview of a robotic testbed for HIL experimentation of guidance and control algorithms for on-orbit proximity maneuvers, this chapter specifically focuses on exploring the feasibility, design and evaluation in a 3-DoF environment of a vectorable thruster configuration combined with optional miniature single gimbaled control moment gyro (MSGCMG) for an agile small spacecraft. Specifically, the main aims are to present and practically confirm the theoretical basis of small-time local controllability for this unique actuator configuration through both analytical and numerical simulations performed in previous works (Romano and Hall 2006; Hall and Romano 2007a; Hall and Romano 2007b) and to validate the viability of using this minimal control actuator configuration on a small spacecraft in a practical way. Furthermore, the experimental work is used to confirm the controllability of this configuration along a fully constrained trajectory through the employment of a smooth feedback controller based on state feedback linearization and linear quadratic regulator techniques and proper state estimation methods. The chapter is structured as follows: First the design of the experimental testbed including the floating surface and the second generation 3-DoF spacecraft simulator is introduced. Then the dynamics model for the spacecraft simulator with vectorable thrusters and momentum exchange device are formulated. The controllability associated with this uniquely configured system is then addressed with a presentation of the minimum number of control inputs to ensure small time local controllability. Next, a formal development is presented for the state feedback linearized controller, state estimation methods, Schmitt trigger and Pulse Width Modulation scheme. Finally, experimental results are presented that demonstrate a closed-path circular trajectory about an arbitrary reference that is representative of a possible inspection of a target spacecraft by a given chaser.

A. THE NPS ROBOTIC SPACECRAFT SIMULATOR TESTBED

Three generations of robotic spacecraft simulators have been developed at the NPS Spacecraft Robotics Laboratory, in order to provide for relatively low-cost HIL experimentation of GNC algorithms for spacecraft proximity maneuvers (see Figure 1). In particular, the second generation robotic spacecraft simulator testbed is used for the here-in presented research. The whole spacecraft simulator testbed consists of three components. The two components specifically dedicated to HIL experimentation in 3-DoF are a floating surface with an indoor pseudo-GPS (iGPS) measurement system and one 3-DoF autonomous spacecraft simulator. The third component of the spacecraft simulator testbed is a 6-DoF simulator stand-alone computer based spacecraft simulator and is separated from the HIL components. Additionally, an off-board desktop computer is used to support the 3-DoF spacecraft simulator by providing the capability to upload software, initiate experimental testing, receive logged data during testing and process the iGPS position coordinates. Figure 2 depicts the robotic spacecraft simulator in the Proximity Operations Simulator Facility (POSF) at NPS with key components identified. The main testbed systems are briefly described in the next sections with further details given in Hall (2006), Price (2006), Eikenberry (2006), Romano and Hall (2006), Hall and Romano (2007a), and Hall and Romano (2007b).

Figure 1.   Three Generations of Spacecraft Simulators at the NPS Spacecraft
Robotics Laboratory (first, second and third generations, from left to right)

1.   Floating Surface

A 4.9 m by 4.3 m epoxy floor surface provides the base for the floatation of the
spacecraft simulator. The use of planar air bearings on the simulator reduces the friction
to a negligible level and with an average residual slope angle of approximately 2.6×10^{-3}
deg for the floating surface, the average residual acceleration due to gravity is
approximately 1.8×10^{-3} ms^{-2}. This value of acceleration is two orders of magnitude lower
than the nominal amplitude of the measured acceleration differences found during
reduced gravity phases of parabolic flights (Romano et al. 2007).
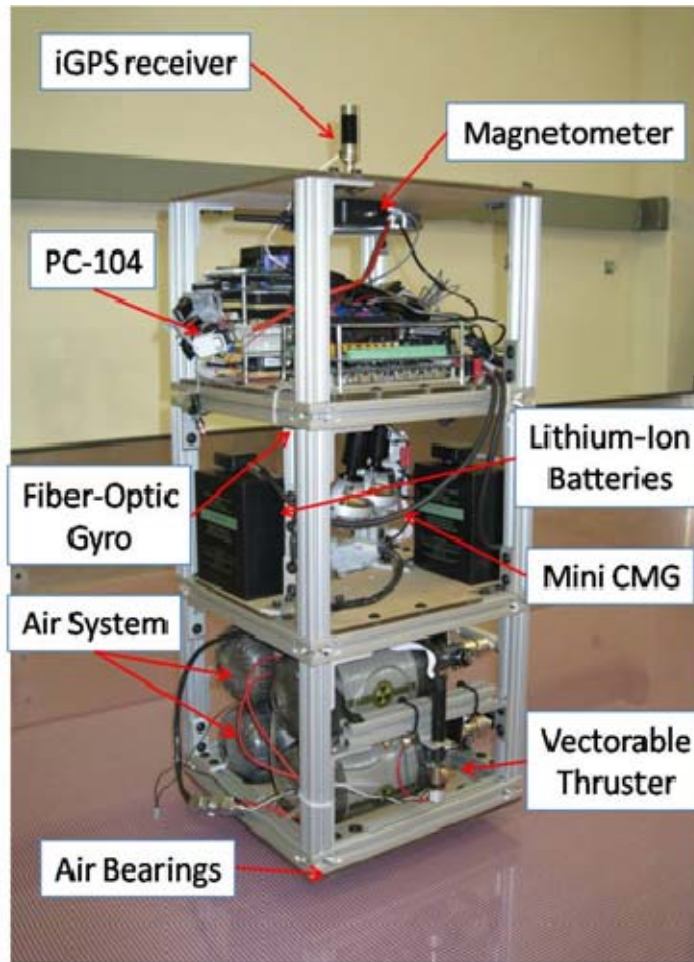
Figure 2.   SRL's 2nd Generation 3-DoF Spacecraft Simulator

2.   Three-DoF Robotic Spacecraft Simulator

SRL's second generation robotic spacecraft simulator is modularly constructed with three easily assembled sections dedicated to each primary subsystem. Prefabricated 6105-T5 Aluminum fractional t-slotted extrusions form the cage of the vehicle while one square foot, 0.25 inch thick static dissipative rigid plastic sheets provide the upper and lower decks of each module.   The use of these materials for the basic structural requirements provides a high strength to weight ratio and enable rapid assembly and reconfiguration. Table 1 reports the key parameters of the 3-DoF spacecraft simulator.

Subsystem	Characteristic	Parameter
Structure	Length and width	0.30 m
	Height	0.69 m
	Mass	26 kg
	J_z	0.40 kg-m^2
Propulsion	Propellant	Compressed Air
	Equiv. storage capacity	0.05 m^3 @ 31.03 MPa
	Operating pressure	0.41 MPa
	Thrust (x2)	0.159 N
	ISP	34.3 s
	Total ΔV	31.1 m/s
Flotation	Propellant	Air
	Equiv. storage capacity	0.05 m^3 @ 31.03 MPa
	Operating pressure	.51 MPa
	Linear air bearing (x4)	32 mm diameter
	Continuous operation	~40 min
CMG Attitude Control	Max torque	0.668 Nm
	Momentum storage	0.098 Nms
Electrical & Electronic	Battery type	Lithium-Ion
	Storage capacity	12 Ah @ 28V
	Continuous Operation	~6 h
	Computer	1 PC104 Pentium III
Sensors	Fiber optic gyro	KVH Model DSP-3000
	Position sensor	Metris iGPS
	Magnetometer	MicroStrain 3DM-GX1

Table 1.   Key Parameters of the 2nd Generation 3-DoF Robotic Spacecraft Simulator

a.   *Propulsion and Flotation Subsystems*

The lowest module houses the flotation and propulsion subsystems. The flotation subsystem is composed of four planar air bearings, an air filter assembly, dual 4500 PSI (31.03 MPa) carbon-fiber spun air cylinders and a dual manifold pressure reducer to provide 75 PSI (0.51 MPa). This pressure with a volume flow rate for each air bearing of 3.33 slfm (3.33 x 10^{-3} m^3/min) is sufficient to keep the simulator in a friction-free state for nearly 40 minutes of continuous experimentation time. The propulsion subsystem is composed of dual vectorable supersonic on-off cold-gas thrusters and a separate dual carbon-fiber spun air cylinder and pressure reducer package regulated at 60 PSI (0.41 MPa) and has the capability of providing the system 31.1 m/s ΔV.

b. Electronic and Power Distribution Subsystems

The power distribution subsystem is composed of dual lithium-ion batteries wired in parallel to provide 28 volts for up to 12 Amp-Hours and is housed in the second deck of the simulator. A four port DC-DC converter distributes the requisite power for the system at 5, 12 or 24 volts DC. An attached cold plate provides heat transfer from the array to the power system mounting deck in the upper module. The current power requirements include a single PC-104 CPU stack, a wireless router, three motor controllers, three separate normally-closed solenoid valves for thruster and air bearing actuation, a fiber optic gyro, a magnetometer and a wireless server for transmission of the vehicle's position via the pseudo-GPS system.

c. Translation and Attitude Control System Actuators

The 3-DoF robotic spacecraft simulator includes actuators to provide both translational control and attitude control. A full development of the controllability for this unique configuration of dual rotating thrusters and one-axis Miniature-Single Gimbaled Control Moment Gyro (MSGCMG) will be demonstrated in subsequent sections of this paper. The translational control is provided by two cold-gas on-off supersonic nozzle thrusters in a dual vectorable configuration. Each thruster is limited in a region $\pm \pi/2$ with respect to the face normal and, through experimental testing at the supplied pressure, has been demonstrated to have an ISP of 34.3 s and able to provide 0.159 N of thrust with less than 10 msec actuation time (Lugini and Romano 2009). The MSGCMG is capable of providing 0.668 Nm of torque with a maximum angular momentum of 0.098 Nms.

3. Six-DoF Computer-based Numerical Spacecraft Simulator

A separate component of SRL's spacecraft simulator testbed at NPS is a 6-DoF computer-based spacecraft simulator. This simulator enables full 6-DoF numerical simulations to be conducted with realistic orbital perturbations including aerodynamic, solar pressure and third-body effects, and earth oblateness up to J4. Similar to the 3-DoF robotic simulator, the numerical simulator is also modularly designed within a

MATLAB®/Simulink® architecture to allow near seamless integration and testing of developed guidance and control algorithms. Additionally, by using the MATLAB®/Simulink® architecture with the added Real Time Workshop™ toolbox, the developed control algorithms can be readily transitioned into C-code for direct deployment onto the 3-DoF robotic simulator's onboard processor. A full discussion of the process by which this is accomplished and simplified for rapid real-time experimentation on the 3-DoF testbed for either the proprietary MATLAB® based XPCTarget™ operating system is given in (Hall 2006; Price 2006) or for an open-source Linux based operating system with the Real Time Application Interface (RTAI) is given in (Bevilacqua, Hall, Horning, and Romano 2009).

B. DYNAMICS OF A 3-DOF SPACECRAFT SIMULATOR WITH VECTORABLE THRUSTERS AND MOMENTUM EXCHANGE DEVICE

Two sets of coordinate frames are established for reference: an inertial frame $\mathcal{I}$ with orthogonal axes defined by the unit vectors $\left\{ \hat{i}_1, \hat{i}_2, \hat{i}_3 \right\}$ and body-fixed frame $\mathcal{B}$ with orthogonal axes defined by the unit vectors $\left\{ \hat{b}_1, \hat{b}_2, \hat{b}_3 \right\}$. These reference frames are depicted in Figure 4 along with the necessary external forces and parameters required to properly define the simulators motion. The origin of the body-fixed coordinate system is taken to be the center of mass C of the spacecraft simulator and is assumed to be collocated with the simulator's geometric center. By the effects of the flat floor, $\hat{b}_3$ is maintained aligned with $\hat{i}_3$ while $\hat{b}_1$ is defined to be in line with the thrusters points of action. The position and velocity vectors of $\mathcal{B}$ with respect to $\mathcal{I}$ expressed in $\mathcal{B}$ are given by $\mathbf{r}$ and $\mathbf{v}$ so that $\mathbf{r}_{BI}$ marks the position of the simulator with respect to the origin of $\mathcal{I}$ as measured by the inertial measurement sensors and provides the vehicle's two degrees of translational freedom. The vehicle's rotational freedom is described by an angle of rotation θ_3 between $\hat{b}_1$ and $\hat{i}_1$ about $\hat{b}_3$. The angular velocity of $\mathcal{B}$ with respect to $\mathcal{I}$ expressed in $\mathcal{B}$ is thus limited to one degree of freedom and is denoted by ω_3. The

spacecraft simulator is assumed to be rigid and therefore a constant moment of inertia (J_3) exists about the $\hat{b}_3$. Furthermore, any changes to the mass of the simulator (m) due to thruster firing are neglected.

The forces imparted at a distance L from the center of mass by the vectorable on-off thrusters are denoted by F_a and F_b respectively. The thrust angle α_a defines the orientation of thruster a in $\mathcal{B}$ and is the angle measured from $\hat{b}_1$ in a clockwise direction (right-hand rotation) to $\mathbf{F}_a$. Likewise, thrust angle α_b defines the orientation of thruster b in $\mathcal{B}$ and is the angle measured from $-\hat{b}_1$ in a clockwise direction (right-hand rotation) to $\mathbf{F}_b$. The torque imparted on the vehicle by a momentum exchange device such as the MSGCMG is denoted by T_{CMG} and can be constrained to exist only about the $\hat{b}_3$ axis.
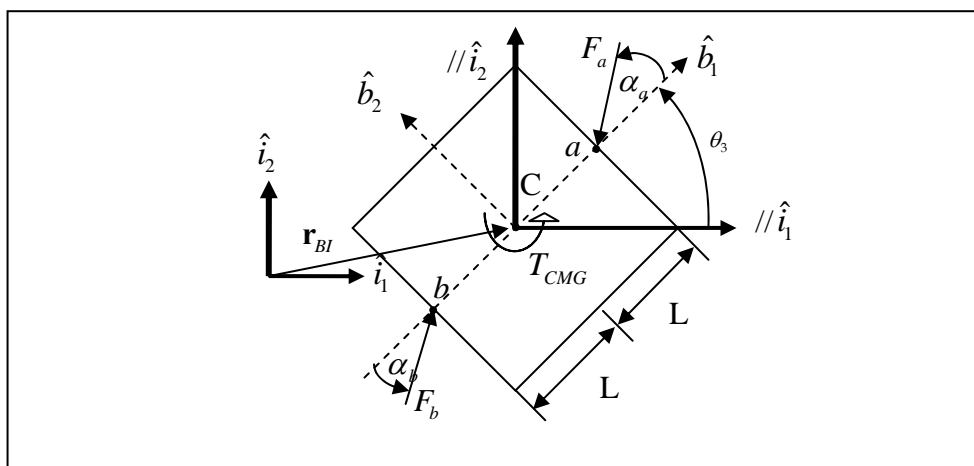
Figure 3.   Schematic of SRL's 2nd Generation Spacecraft Simulator

1.   **Controllability Analysis of a Single-Gimbaled Control Moment Gyroscope for a Reduced Order System**

The feasibility and utility of using a single-gimbaled control moment gyroscope for the actuation of a 3-DoF spacecraft simulator can easily be demonstrated through development of the reduced order angular motion equations for the vehicle and the

MSGCMG. Beginning with the full order angular motion equations equipped with a momentum exchange device such as a MSGCMG given by Wie (1998, p. 437)

$$^S\dot{\mathbf{H}} + \boldsymbol{\omega} \times {}^S\mathbf{H} = \mathbf{T} \tag{1}$$

where $^S\mathbf{H}(t) \in \mathbb{R}^3$, $\forall\, ^S\mathbf{H} = \begin{bmatrix} ^SH_1, {}^SH_2, {}^SH_3 \end{bmatrix}^T$ the total system's angular momentum vector is expressed in the body-fixed control frame with respect to an inertial frame, $\mathbf{T}_{EXT}(t) \in \mathbb{R}^3$, $\forall \mathbf{T}_{EXT} = \begin{bmatrix} T_{EXT,1}, T_{EXT,2}, T_{EXT,3} \end{bmatrix}^T$ is the external torque vector acting on the body-fixed frame and $\boldsymbol{\omega}(t) \in \mathbb{R}^3$, $\forall \boldsymbol{\omega} = \begin{bmatrix} \omega_1, \omega_2, \omega_3 \end{bmatrix}^T$ is the angular velocity vector of the body-fixed frame with respect to an inertial frame.

The total system's angular momentum vector includes both the rigid body's angular momentum and the MSGCMG's angular momentum. Therefore

$$^S\mathbf{H} = J_T\boldsymbol{\omega} + \mathbf{h} \tag{2}$$

where $J_T \in \mathbb{R}^{3x3}$ is the total moment of inertia of the spacecraft with the SGCMG such that

$$J_T = J_B + J_{CMG} \tag{3}$$

where $J_B \in \mathbb{R}^{3x3}$

$$J_B = J_P + \begin{bmatrix} 1 & 0 & 0 \\ 0 & 1 & 0 \\ 0 & 0 & m_{CMG}r_{CMG}^2 \end{bmatrix} \tag{4}$$

represents the sum of the second moment of inertia dyadic of the SGCMG platform $J_P \in \mathbb{R}^{3x3}$ and the second moment of inertia of a point mass concentrated in the center of mass m_{CMG} of the SGCMG with respect to the center of mass of the spacecraft r_{CMG} assuming the SCCMG is aligned with the spacecraft's third control axis. $J_{CMG} \in \mathbb{R}^{3x3}$ is the second moment of inertia dyadic of the MSGCMG cluster represented in the body-

17

fixed frame. This represents the summation of the second moment of inertia dyadic of the MSGCMG body and includes both the contribution of its spinning inertia disc and associated hardware (Bevilacqua, Izzo, and Valente 2003). Finally, $\mathbf{h}(t) \in \mathbb{R}^3, \forall \mathbf{h} = [h_1, h_2, h_3]^T$ represents the total momentum vector of the SGCMG expressed in the body-fixed frame. Differentiation of (2) yields

$$
\begin{aligned}
{}^S\dot{\mathbf{H}} &= J_T \dot{\boldsymbol{\omega}} + \dot{J}_T \boldsymbol{\omega} + \dot{\mathbf{h}} \\
&= J_T \dot{\boldsymbol{\omega}} + \omega^\times J_T \boldsymbol{\omega} + \dot{\mathbf{h}}
\end{aligned}
\tag{5}
$$

where $\omega^\times \in \mathbb{R}^{3x3}$ represents the skew symmetric matrix with respect to $\boldsymbol{\omega}$

$$
\omega^x = \begin{bmatrix} 0 & -\omega_3 & \omega_2 \\ \omega_3 & 0 & -\omega_1 \\ -\omega_2 & \omega_1 & 0 \end{bmatrix}
\tag{6}
$$

By combining (1), (2), and (5), we get

$$
J_T \dot{\boldsymbol{\omega}} + \omega^\times J_T \boldsymbol{\omega} + \dot{\mathbf{h}} + \boldsymbol{\omega} \times (J_T \boldsymbol{\omega} + \mathbf{h}) = \mathbf{T}_{EXT}
\tag{7}
$$

Furthermore, by introducing the control torque vector generated on the body-fixed frame by the MSGCMG denoted as $\mathbf{T}_{CMG}(t) \in \mathbb{R}^{3x1}, \forall \mathbf{T}_{CMG} = [T_{CMG,1}, T_{CMG,2}, T_{CMG,3}]^T$ and a control vector $\mathbf{T}(t) \in \mathbb{U}^{3x1}, \forall \mathbf{T} = [T_1, T_2, T_3]^T$ to represent the torque required by a given control law, (7) becomes

$$
J_T \dot{\boldsymbol{\omega}} + \omega^x J_T \boldsymbol{\omega} = \mathbf{T}_{CMG} + \mathbf{T}_{EXT}
\tag{8}
$$

where

$$
\mathbf{T}_{CMG} = -(\omega^\times J_T \boldsymbol{\omega} + \dot{\mathbf{h}} + \boldsymbol{\omega} \times \mathbf{h}) = \mathbf{T}
\tag{9}
$$

(9) can be solved for the time derivative of the angular momentum vector as

$$
\dot{\mathbf{h}} = -\mathbf{T} - \omega^\times J_T \boldsymbol{\omega} - \boldsymbol{\omega} \times \mathbf{h}
\tag{10}
$$

18
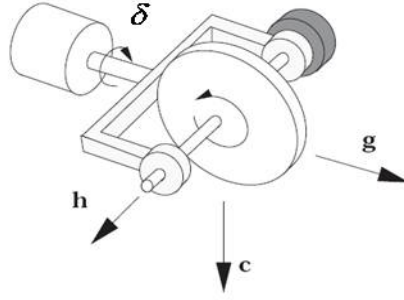
Figure 4.   Orthonormal Vectors of MSGCMG Unit (After Kurokawa 1998)

Figure 4 depicts the internal vectors of the MSGCMG unit. Three mutually orthogonal unit vectors exist where $\mathbf{g}$ is the gimbal vector, $\mathbf{h}$ is the angular momentum vector, and $\mathbf{c}$ is the torque vector where

$$\mathbf{c} = \frac{\partial \mathbf{h}}{\partial \delta} = \mathbf{g} \times \mathbf{h} \tag{11}$$

The gimbal vectors are constant while the others are dependent upon the MSGCMG's gimbal angle δ. The total angular momentum becomes a general function of the CMG gimbal angles δ and the constant angular momentum of the unit's rotor wheel denoted by h_w such that

$$\mathbf{h} = h_w \left[0, \cos \delta, \sin \delta \right]^T \tag{12}$$

The total output torque of the MSGCMG in the absence of coupling terms due to spacecraft motion then can be found by taking the time derivative of (12) as

$$\mathbf{T}_{CMG} = -\dot{\mathbf{h}} = \left[0, h_w \sin \delta \dot{\delta}, -h_w \cos \delta \dot{\delta} \right]^T \tag{13}$$

By taking the third body-fixed axis to be the yaw axis as depicted in Figure 4, and considering only the components about this axis due to compensation of the other two axes by the reactions of the floor, (8) and (9) simplify to

$$J_3 \dot{\omega}_3 = T_3 = -h_w \cos \delta \dot{\delta} \tag{14}$$

19

To determine the steering logic for the instantaneous angular rate to command the MSGCMG's gimbal motor, it is thus necessary to solve (14) for the gimbal rate $\dot{\delta}$ given the desired torque as generated by a given attitude control law. Once the gimbal angular position reaches $\pm\pi/2$, the MSGCMG cannot generate any torque about the third body-fixed axis and it is therefore in a saturated singular configuration.

2. Reduced Order Dynamics with Dual Rotating Thrusters and MSGCMG

The translation and attitude motion of the simulator are governed by the equations

$$
\begin{aligned}
\dot{\mathbf{r}}_{BI} &= \mathbf{v}_{BI} \\
\dot{\mathbf{v}}_{BI} &= m^{-1}\,{}^{I}R_B\,{}^{B}\mathbf{F} \\
\dot{\theta}_3 &= \omega_3 \\
\dot{\omega}_3 &= J_3^{-1}T_3
\end{aligned}
\tag{15}
$$

where ${}^{B}\mathbf{F}(t) \in \mathbb{R}^2, \forall\, {}^{B}\mathbf{F} = \begin{bmatrix} {}^{B}F_1, {}^{B}F_2 \end{bmatrix}^{T}$ represents the thrusters' inputs limited to the region $\pm\pi/2$ with respect to each face normal and $T_3(t) \in \mathbb{R}$ is the attitude input. ${}^{I}R_B$, ${}^{B}\mathbf{F}$ and T_3 are given by

$$
{}^{I}R_B = \begin{bmatrix} c\,\theta_3 & -s\,\theta_3 \\ s\,\theta_3 & c\,\theta_3 \end{bmatrix}
\tag{16}
$$

$$
{}^{B}\mathbf{F}^{T} = {}^{B}\mathbf{F}_a^{T} + {}^{B}\mathbf{F}_b^{T} = \begin{bmatrix} -F_a\,c\,\alpha_a + F_b\,c\,\alpha_b, & -F_a\,s\,\alpha_a + F_b\,s\,\alpha_b \end{bmatrix}^{T}
\tag{17}
$$

$$
T_3 = \begin{bmatrix} T_{CMG} + L\left(-F_a\,s\,\alpha_a - F_b\,s\,\alpha_b\right) \end{bmatrix}
\tag{18}
$$

where $s\bullet = \sin(\bullet), c\bullet = \cos(\bullet)$.

The internal dynamics of the vectorable thrusters are assumed to be linear according to the following equations

$$
\dot{\alpha}_a = \beta_a,\ \dot{\beta}_a = J_a^{-1}T_a,\ \dot{\alpha}_b = \beta_b,\ \dot{\beta}_b = J_b^{-1}T_b
\tag{19}
$$

where J_a and J_b represent the moments of inertia about each thruster rotational axis respectively and $T_a \in \mathbb{R}$, $T_b \in \mathbb{R}$ represent the corresponding thruster rotation control input.

The system's state equation given by (15) can be rewritten in control-affine system form as (LaValle 2006)

$$\dot{\mathbf{x}} = \mathbf{f}(\mathbf{x}) + \sum_{i=1}^{N_u} u_i \mathbf{g}_i(\mathbf{x}) = \mathbf{f}(\mathbf{x}) + G(\mathbf{x})\mathbf{u}, \; x \in \mathbb{R}^{N_x} \tag{20}$$

where N_u is the number of controls. With $\mathbb{R}^{N_x}$ representing a smooth N_x-dimensional manifold defined be the size of the state-vector and the control vector to be in $\mathbb{U}^{N_u}$.

Defining the state vector $\mathbf{x} \in \mathbb{R}^{10}$ as $\mathbf{x}^T = [x_1, x_2, ..., x_{10}] = [r_{BI,1}, r_{BI,2}, \theta_3, \alpha_a, \alpha_b, v_{BI,1}, v_{BI,2}, \omega_3, \beta_a, \beta_b]$ and the control vector $\mathbf{u} \in \mathbb{U}^5$ as $\mathbf{u}^T = [u_1, u_2, ..., u_5] = [{}^B F_a, {}^B F_b, T_{CMG}, T_a, T_b]$, the system's state equation becomes

$$\dot{\mathbf{x}} = \mathbf{f}(\mathbf{x}) + G(\mathbf{x})\mathbf{u} = [x_6, x_7, x_8, x_9, x_{10}, \mathbf{0}_{1x5}]^T + \begin{bmatrix} \mathbf{0}_{5x5} \\ G_1(\mathbf{x}) \end{bmatrix} \mathbf{u} \tag{21}$$

where the matrix $G_1(\mathbf{x}) \in \mathbb{R}^{5x5}$ is obtained from (15) as

$$G_1(\mathbf{x}) = \begin{bmatrix} -m^{-1}[c\,x_3\,c\,x_4 - s\,x_3\,s\,x_4] & m^{-1}[c\,x_3\,c\,x_5 - s\,x_3\,s\,x_5] & 0 & 0 & 0 \\ -m^{-1}[c\,x_3\,s\,x_4 + s\,x_3\,c\,x_4] & m^{-1}[c\,x_3\,s\,x_5 + s\,x_3\,c\,x_5] & 0 & 0 & 0 \\ -J_3^{-1}s\,x_4 L & -J_3^{-1}s\,x_5 L & J_3^{-1} & 0 & 0 \\ 0 & 0 & 0 & J_a^{-1} & 0 \\ 0 & 0 & 0 & 0 & J_b^{-1} \end{bmatrix} \tag{22}$$

With the system in the form of (20) given the vector fields in (21) and (22), and given that $\mathbf{f}(\mathbf{x}) \in \mathbb{R}^{10}$ (the drift term) and $G(\mathbf{x}) \in \mathbb{R}^{10x5}$ (the control matrix of control vector fields) are smooth functions, it is important to note that it is not necessarily possible to obtain zero velocity due to the influence of the drift term. This fact places the system in the unique subset of control-affine systems with drift and, as seen later, will

21

call for an additional requirement for determining the controllability of the system. Furthermore, when studying controllability of systems, the literature to date restricts the consideration to cases where the control is proper. Having a proper control implies that the affine hull of the control space is equal to $\mathbb{U}^{N_u}$ or that the smallest subspace of $\mathbb{U}$ is equal to the number of control vectors and that it is closed (Sussman 1987; Sussman 1990; Bullo and Lewis 2005; LaValle 2006). With a system such as a spacecraft in general or the simplified model of the 3-DoF simulator in particular, the use of on-off cold-gas thrusters restrict the control space to only positive space with respect to both thrust vectors leading to an unclosed set and thus improper control space. In order to overcome this issue, a method which leverages the symmetry of the system is used by which the controllability of the system is studied by considering only one virtual rotating thruster that is positioned a distance *L* from the center of mass with the vectored thrust resolved into a y and x-component. In considering this system perspective, the thruster combination now spans $\mathbb{R}^2$ and therefore is proper and is analogous to the planar body with variable-direction force vector considered in (Lewis and Murray 1997; Bullo and Lewis 2005). Furthermore, under the assumption that the control bandwidth of the thrusters' rotation is much larger than the control bandwidth of the system dynamics, the internal dynamics of the vectorable thrusters can be decoupled from the state and control vectors for the system yielding a thrust vector dependent on simply a commanded angle. Thus the system's state vector, assuming that both thrusters and a momentum exchange device are available, becomes $\mathbf{x}^T = \left[x_1, x_2, ..., x_6 \right] = [r_{BI,1}, r_{BI,2}, \theta_3, v_{BI,1}, v_{BI,2}, \omega_3] \in \mathbb{R}^6$ and the control vector is $\mathbf{u}^T = \left[u_1, u_2, u_3 \right] = [^B F_1, {}^B F_2, T_3] = \mathbb{U}^3$ so that the system's state equation becomes

$$\dot{\mathbf{x}} = \mathbf{f}(\mathbf{x}) + G(\mathbf{x})\mathbf{u} = \left[x_4, x_5, x_6, 0, 0, 0 \right]^T + \begin{bmatrix} \mathbf{0}_{3x3} \\ G_1(\mathbf{x}) \end{bmatrix} \mathbf{u} \qquad (23)$$

where $\mathbf{f}(\mathbf{x}) \in \mathbb{R}^6$ and $G(\mathbf{x}) \in \mathbb{R}^{6x3}$ are again smooth functions. The matrix $G_1(\mathbf{x})$ can be obtained by considering the relation of the desired control vector to the body centered

reference system, in the two cases of positive force needed in $\hat{b}_1$ ($^B U_1 > 0$) and negative force needed in $\hat{b}_1$ ($^B U_1 < 0$). In this manner, the variables in (22) and (23) can be defined as

$$
\begin{aligned}
&^B U_1 < 0 \rightarrow \begin{cases} \mathbf{u}^T = [^B F_1, {}^B F_2, T_3] = \left[-F_a \, c \, x_4, -F_a \, s \, x_4, T_{CMG} \right] \\ d = -L, F_b = 0 \end{cases} \\
&^B U_1 > 0 \rightarrow \begin{cases} \mathbf{u}^T = [^B F_1, {}^B F_2, T_3] = \left[F_b \, c \, x_5, F_b \, s \, x_5, T_{CMG} \right] \\ d = L, F_a = 0 \end{cases}
\end{aligned}
\tag{24}
$$

yielding the matrix in $G_1(\mathbf{x}) \in \mathbb{R}^{3x3}$ through substitution into (22) as

$$
G_1(\mathbf{x}) = \begin{bmatrix} m^{-1} c \, x_3 & -m^{-1} s \, x_3 & 0 \\ m^{-1} s \, x_3 & m^{-1} c \, x_3 & 0 \\ 0 & -dJ_3^{-1} & J_3^{-1} \end{bmatrix}
\tag{25}
$$

When the desired control input to the system along $\hat{b}_1$ is zero, both thrusters can be used to provide a control force along $\hat{b}_2$, while a momentum exchange device provides any required torque. In this case, the control vector $\mathbf{u}$ becomes $\mathbf{u}^T = [u_1, u_2] = [^B F_2, T_3] = \mathbb{U}^2$ and control matrix of control fields becomes $G(\mathbf{x}) \in \mathbb{R}^{6x2}$ in (23) such that the variables in (22) and (23) can be defined as

$$
^B U_2 = 0 \rightarrow \begin{cases} \mathbf{u}^T = [^B F_2, T_3] = \left[Fs\alpha, T_{CMG} \right] \\ F = F_a = F_b, \alpha = x_4 = -x_5 = -\dfrac{\pi}{2} sign\left({}^B U_2 \right) \end{cases}
\tag{26}
$$

yielding the matrix $G_1(\mathbf{x}) \in \mathbb{R}^{3x2}$ through substitution into (22) as

$$
G_1(\mathbf{x}) = \begin{bmatrix} -2m^{-1} s \, x_3 & 0 \\ 2m^{-1} c \, x_3 & 0 \\ 0 & J_3^{-1} \end{bmatrix}
\tag{27}
$$

23

As will be demonstrated later, the momentum exchange device is not necessary to ensure small time controllability for this system. In considering this situation, which also occurs when a control moment gyroscope is present but is near the singular conditions and therefore requires desaturation, the thruster not being used for translation control can be slewed to $\pm\pi/2$ depending on the required torque compensation and fired to affect the desired angular rate change. The desired control input to the system with respect to $\hat{b}_1\left({}^B U_1\right)$ can again be used to define the desired variables such that

$$
\begin{aligned}
{}^B U_1 \leq 0 \rightarrow & \begin{cases} \mathbf{u}^T = [{}^B F_1, {}^B F_2, T_3] = [{}^B F_1, {}^B F_2, {}^B F_{2/rot3}] = \left[-F_a\, \mathrm{c}\, x_4, -F_a\, \mathrm{s}\, x_4, F_b d\, \mathrm{s}\, x_5\right] \\ d = -L,\ x_5 = \pm\pi/2 \end{cases} \\
{}^B U_1 > 0 \rightarrow & \begin{cases} \mathbf{u}^T = [{}^B F_1, {}^B F_2, T_3] = [{}^B F_1, {}^B F_2, {}^B F_{2/rot3}] = \left[F_b\, \mathrm{c}\, x_5, F_b\, \mathrm{s}\, x_5, -F_a d\, \mathrm{s}\, x_4\right] \\ d = L,\ x_4 = \pm\pi/2 \end{cases}
\end{aligned}
\tag{28}
$$

yielding the matrix $G_1\left(\mathbf{x}\right) \in \mathbb{R}^{3x3}$ through substitution into (22) as

$$
G_1(\mathbf{x}) = \begin{bmatrix} m^{-1}\, \mathrm{c}\, x_3 & -m^{-1}\, \mathrm{s}\, x_3 & -(md)^{-1}\, \mathrm{s}\, x_3 \\ m^{-1}\, \mathrm{s}\, x_3 & m^{-1}\, \mathrm{c}\, x_3 & (md)^{-1}\, \mathrm{c}\, x_3 \\ 0 & -dJ_3^{-1} & J_3^{-1} \end{bmatrix}
\tag{29}
$$

In case of zero force requested along x with only thrusters acting, the system cannot in general provide the requested torque value.

A key design consideration with this type of control actuator configuration is that with only the use of an on/off rotating thruster to provide the necessary torque compensation, fine pointing can be difficult and more fuel is required to affect a desired maneuver involving both translation and rotation.

C.   SMALL-TIME LOCAL CONTROLLABILITY

Before studying the controllability for a nonlinear control-affine system of the form in (20), it is important to review several definitions. First, the set of states reachable in time at most T is given by $R_\Sigma\left(\mathbf{x}_0, \leq T\right)$ by solutions of the nonlinear control-affine system.

Definition 1 (Accessibility)

A system is *accessible* from $\mathbf{x}_0$ (the initial state) if there exists $\tau > 0$ such that the interior of $R_\Sigma\left(\mathbf{x}_0, \leq t\right)$ is not an empty set for $t \in \left]0, \tau\right]$ (Bullo and Lewis 2005).

Definition 2 (Proper Small-time Local Controllability)

A system is *small-time locally controllable* (STLC) from $\mathbf{x}_0$ if there exists $\tau > 0$ such that $\mathbf{x}_0$ lies in the interior of $R_\Sigma\left(\mathbf{x}_0, \leq t\right)$ for each $t \in \left]0, \tau\right]$ for every proper control set U (Bullo & Lewis, 2005). Assuming that at $\mathbf{x}(0) = \mathbf{0}$ this can also be seen under time reversal as the equilibrium for the system x_0 can be reached from a neighborhood in small time (Sussman 1987; Sussman 1990).

Definition 3 (Proper Control Set)

A control set $\mathbf{u}^T = \left[u_1, ..., u_k\right]$ is termed to be *proper* if the set satisfies a constraint $\mathbf{u} \in K$ where K affinely spans $\mathbb{U}^k$ (Sussman 1990; Bullo and Lewis 2005; LaValle 2006).

Definition 4 (Lie derivative)

The *Lie derivative* of a smooth scalar function $g\left(\mathbf{x}\right) \in \mathbb{R}$ with respect to a smooth vector field $\mathbf{f}\left(\mathbf{x}\right) \in \mathbb{R}^{N_x}$ is a scalar function defined as (Slotine 1991, p. 229)

$$L_{\mathbf{f}} g = \nabla g \ \mathbf{f} = \left[\frac{\partial g}{\partial x_1} ... \frac{\partial g}{\partial x_{N_x}}\right] \begin{bmatrix} f_1(\mathbf{x}) \\ \vdots \\ f_{N_x}(\mathbf{x}) \end{bmatrix}. \tag{30}$$

<u>Definition 5</u> (Lie Bracket)

The Lie bracket of two vector fields $\mathbf{f}(\mathbf{x}) \in \mathbb{R}^{N_x}$ and $\mathbf{g}(\mathbf{x}) \in \mathbb{R}^{N_x}$ is a third vector field $[\mathbf{f},\mathbf{g}] \in \mathbb{R}^{N_x}$ defined by $[\mathbf{f},\mathbf{g}] = \nabla \mathbf{g}\, \mathbf{f} - \nabla \mathbf{f}\, \mathbf{g}$, where the i-th component can be expressed as (Slotine 1991, p. 230)

$$[\mathbf{f},\mathbf{g}]_i = \sum_{j=1}^{N_x} \left(f_j \frac{\partial g_i}{\partial x_j} - g_j \frac{\partial f_i}{\partial x_j} \right). \tag{31}$$

Using Lie bracketing methods that produce motions in directions that do not seem to be allowed by the system distribution, sufficient conditions can be met to determine a system's STLC even in the presence of a drift vector as in the equations of motion developed above. These sufficient conditions involve the Lie Algebra Rank Condition (LARC).

<u>Definition 6</u> (Associated Distribution $\Delta(\mathbf{x})$)

Given a system as in (6), the associated distribution $\Delta(\mathbf{x})$ is defined as the vector space (subspace of $\mathbb{R}^{N_x}$) spanned by the system vector fields $\mathbf{f}, \mathbf{g}_1, \dots \mathbf{g}_{N_u}$.

<u>Definition 7</u>

The Lie algebra of the associated distribution $\mathcal{L}(\Delta)$ is defined to be the distribution of all independent vector fields that can be obtained by applying subsequent Lie bracket operations to the system vector fields. Of note, no more than N_x vector fields can be produced (LaValle 2006). With $\dim\left[\mathcal{L}(\Delta)\right] \leq N_x$, the computation of the elements of $\mathcal{L}(\Delta)$ ends either when N_x independent vector fields are obtained or when all subsequent Lie brackets are vector fields of zeros.

<u>Definition 8</u> (Lie Algebra Rank Condition [LARC])

The *Lie Algebra Rank Condition* is satisfied at a state $\mathbf{x}$ if the rank of the matrix obtained by concatenating the vector fields of the Lie algebra distribution at $\mathbf{x}$ is equal to N_x (the number of state).

For a driftless control-affine system, following the Chow-Rashevskii Theorem, the system is STLC if the LARC is satisfied (Lewis and Murray 1997; Bullo and Lewis 2005; LaValle 2006). However, given a system with drift, in order to determine the STLC, the satisfaction of the LARC it is not sufficient: In addition to the LARC, it is necessary to examine the combinations of the vectors used to compose the Lie brackets of the Lie algebra. From Sussman's General Theorem on Controllability, if the LARC is satisfied and if there are no ill formed brackets in $\mathcal{L}(\Delta)$, then the system is STLC from its equilibrium point (Sussman 1987). The Sussman's theorem, formally stated is reported here below.

Theorem 1 (Sussman's General Theorem on Controllability)

Consider a system given by (20) and an equilibrium point $\mathbf{p} \in \mathbb{R}^{N_x \times 1}$ such that $\mathbf{f}(\mathbf{p}) = \mathbf{0}$. Assume $\mathcal{L}(\Delta)$ satisfies the LARC at $\mathbf{p}$. Furthermore, assume that whenever a potential Lie bracket consists of the drift vector $\mathbf{f}(\mathbf{x})$ appearing an odd number of times while $\mathbf{g}_1(\mathbf{x}), ..., \mathbf{g}_{N_u}(\mathbf{x})$ all appear an even number of times to include zero times (indicating an ill formed Lie bracket), there are sufficient successive Lie brackets to overcome this ill formed Lie bracket to maintain LARC. Then the system is STLC from $\mathbf{p}$ (Sussman 1987; Sussman 1990).

As it is common in literature, an ill formed bracket is dubbed a "bad" bracket (Sussman 1987; Sussman 1990; Lewis and Murray, 1997, Bullo and Lewis, 2005; LaValle 2006). Conversely, if a bracket is not "bad," it is termed "good". As an example, for a system with a drift vector and two control vectors, the bracket $\left[\mathbf{f}, \left[\mathbf{g}_1, \mathbf{g}_1\right]\right]$ is bad, as the drift vector occurs only once while the first control vector appears twice and the second control vector appears zero times. Similarly, the bracket $\left[\mathbf{f}, \left[\mathbf{f}, \left[\mathbf{f}, \mathbf{g}_1\right]\right]\right]$ is good as the first control vector appears only once. Therefore, it can be summarized that if the rank of the Lie algebra of a control-affine system with drift is

equal to the number of states and there exist sufficient "good" brackets to overcome the "bad" brackets to reach the required LARC rank, then the system is small time locally controllable.

D. SMALL-TIME LOCAL CONTROLLABILITY CONSIDERATIONS FOR THE 3-DOF SPACECRAFT SIMULATOR

The concept of small time local controllability is better suitable than the one of accessibility for the problem of spacecraft rendezvous and docking, as a spacecraft is required to move in any directions in a small interval of time dependent on the control actuator capabilities (e.g., to avoid obstacles). The finite time τ can be arbitrary if the control input is taken to be unbounded and proper (Sussman 1990; Bullo and Lewis 2005; LaValle 2006).

While no theory yet exists for the study of the general controllability for a non-linear system, the STLC from an equilibrium condition can be studied by employing Sussman's theorem. For the case of spacecraft motion, in order to apply Sussman's theorem, we hypothesize that the spacecraft is moving from an initial condition with velocity close to zero (relative to the origin of an orbiting reference frame).

In applying Sussman's General Theorem on Controllability to the reduced system equations of motion presented in (23) with $G_1(\mathbf{x})$ given in (25), the Lie algebra evaluates to

$$\mathcal{L}(\Delta) = span\{\mathbf{g}_1, \mathbf{g}_2, \mathbf{g}_3[\mathbf{f},\mathbf{g}_1],[\mathbf{f},\mathbf{g}_2],[\mathbf{f},\mathbf{g}_3]\} \tag{32}$$

so that $\dim[\mathcal{L}(\Delta)] = N_x = 6$. In order to verify that this is the minimum number of actuators required to ensure STLC, the Lie algebra is reinvestigated for each possible combination of controls. Appendix A includes a developed MATLAB® function for determining the Lie algebra for an arbitrary nonlinear system. The resulting analysis, as summarized in Table 2, demonstrates that the system is STLC from the systems equilibrium point at $\mathbf{f}(\mathbf{p}) = \mathbf{0}$ given either two rotating thrusters in complementary semi-circle planes or fixed thrusters on opposing faces providing a normal force vector to the

face in opposing directions and a momentum exchange device about the center of mass. For instance, in considering the case of control inputs $\mathbf{u}^T = [u_1, u_2] = [{}^B F_y, T_z] \in U^2$, (23) given (27) becomes

$$\dot{\mathbf{x}} = \mathbf{f}(\mathbf{x}) + \mathbf{g}_1(\mathbf{x})u_1 + \mathbf{g}_2(\mathbf{x})u_2$$
$$= [x_4, x_5, x_6, 0, 0, 0]^T + [0, 0, 0, 2m^{-1}sx_3, 2m^{-1}cx_3, 0]^T u_1 + [0, 0, 0, 0, 0, J_3^{-1}]^T u_2 \qquad (33)$$

with the equilibrium point $\mathbf{p}$ such that $\mathbf{f}(\mathbf{p}) = \mathbf{0}$ is $\mathbf{p} = [x_1, x_2, x_3, 0, 0, 0]^T$. The $\mathcal{L}(\Delta)$ is formed by considering the associated distribution $\Delta(\mathbf{x})$ and successive Lie brackets as

$$\begin{array}{llll}
\mathbf{f}, & \mathbf{g}_1, & \mathbf{g}_2 & \\
[\mathbf{f}, \mathbf{g}_1], & [\mathbf{g}_1, \mathbf{g}_2], & [\mathbf{f}, \mathbf{g}_2] & \\
[\mathbf{f}, [\mathbf{f}, \mathbf{g}_1]], & [\mathbf{f}, [\mathbf{g}_1, \mathbf{g}_2]], & [\mathbf{f}, [\mathbf{f}, \mathbf{g}_2]], & \\
[\mathbf{g}_1, [\mathbf{f}, \mathbf{g}_1]], & [\mathbf{g}_1, [\mathbf{g}_1, \mathbf{g}_2]], & [\mathbf{g}_1, [\mathbf{f}, \mathbf{g}_2]], & \\
[\mathbf{g}_2, [\mathbf{f}, \mathbf{g}_1]], & [\mathbf{g}_2, [\mathbf{g}_1, \mathbf{g}_2]], & [\mathbf{g}_2, [\mathbf{f}, \mathbf{g}_2]], & [\mathbf{f}, [\mathbf{f}, [\mathbf{f}, \mathbf{g}_1]]], \\
[\mathbf{f}, [\mathbf{f}, [\mathbf{f}, \mathbf{g}_2]]], & [\mathbf{f}, [\mathbf{f}, [\mathbf{g}_1, \mathbf{g}_2]]], & [\mathbf{f}, [\mathbf{f}, [\mathbf{f}, \mathbf{g}_2]]], & [\mathbf{f}, [\mathbf{g}_1, [\mathbf{f}, \mathbf{g}_2]]]
\end{array}$$

The sequence can first be reduced by considering any "bad" brackets in which the drift vector appears an odd number of times and the control vector fields each appear an even number of times to include zero. In this manner the Lie brackets $[\mathbf{g}_1, [\mathbf{f}, \mathbf{g}_1]]$ and $[\mathbf{g}_2, [\mathbf{f}, \mathbf{g}_2]]$ can be disregarded.

By evaluating each remaining Lie bracket at the equilibrium point $\mathbf{p}$, the linearly independent vector fields can be found as

29

$$\mathbf{g}_1 = \left[\mathbf{0}_{3x1}, -m^{-1}sx_3, m^{-1}cx_3, -J_3^{-1}L \right]^T$$

$$\mathbf{g}_2 = \left[\mathbf{0}_{5x1}, J_3^{-1} \right]^T$$

$$[\mathbf{f}, \mathbf{g}_1] = \nabla \mathbf{g}_1 \cdot \mathbf{f} - \nabla \mathbf{f} \cdot \mathbf{g}_1 = \left[m^{-1}sx_3, -m^{-1}cx_3, \mathbf{0}_{4x1} \right]^T$$

$$[\mathbf{f}, \mathbf{g}_2] = \nabla \mathbf{g}_2 \cdot \mathbf{f} - \nabla \mathbf{f} \cdot \mathbf{g}_2 = \left[\mathbf{0}_{2x1}, -J_3^{-1}, \mathbf{0}_{3x1} \right]^T$$

$$\left[\mathbf{g}_1, [\mathbf{f}, \mathbf{g}_2] \right] = \nabla [\mathbf{f}, \mathbf{g}_2] \cdot \mathbf{g}_1 - \nabla \mathbf{g}_1 \cdot [\mathbf{f}, \mathbf{g}_2] = \left[\mathbf{0}_{3x1}, -(mJ_3)^{-1}cx_3, -(mJ_3)^{-1}sx_3, 0 \right]^T$$

$$\left[\mathbf{f}, \left[\mathbf{g}_1, [\mathbf{f}, \mathbf{g}_2] \right] \right] = \nabla \left[\mathbf{g}_1, [\mathbf{f}, \mathbf{g}_2] \right] \cdot \mathbf{f} - \nabla \mathbf{f} \cdot \left[\mathbf{g}_1, [\mathbf{f}, \mathbf{g}_2] \right] = \left[2L(mJ_3)^{-1}cx_3, 2L(mJ_3)^{-1}sx_3, \mathbf{0}_{4x1} \right]^T$$

$$(34)$$

Therefore, the Lie algebra comprised of these vector fields is

$$\mathcal{L}(\Delta) = span\left\{ \mathbf{g}_1, \mathbf{g}_2, [\mathbf{f}, \mathbf{g}_1], [\mathbf{f}, \mathbf{g}_2], \left[\mathbf{g}_1, [\mathbf{f}, \mathbf{g}_2] \right], \left[\mathbf{f}, \left[\mathbf{g}_1, [\mathbf{f}, \mathbf{g}_2] \right] \right] \right\} \qquad (35)$$

yielding $\dim\left[\mathcal{L}(\Delta) \right] = N_x = 6$, and therefore the system is small time locally controllable.

Control Inputs	Thruster Positions	$\dim(\mathcal{L}(\Delta))$	Controllability
$^B F_1$	$\alpha_a = \alpha_b = 0$	2	Inaccessible
$^B F_2$	$\alpha_a = -\alpha_b = \mp\pi/2$	5	Inaccessible
T_{CMG}	NA	2	Inaccessible
$^B F_1, T_{CMG}$	$\alpha_a = \alpha_b = 0$	6	STLC
$\left(^B F_2, T_{CMG} \right)$ or $\left(^B F_2, ^B F_{2/rot3} \right)$	$\alpha_a = -\alpha_b = \mp\pi/2$	6	STLC
$^B F_1, ^B F_2$	$|\alpha_a| \leq \pi/2, |\alpha_b| \leq \pi/2$	6	STLC

Table 2.   STLC Analysis for the 3-DoF Spacecraft Simulator

E.   NAVIGATION AND CONTROL OF THE 3-DOF SPACECRAFT SIMULATOR

In the current research, the assumption is made that the spacecraft simulator is maneuvering in the proximity of an attitude stabilized target spacecraft and that this spacecraft follows a Keplarian orbit. Furthermore, the proximity navigation maneuvers are considered to be fast with respect to the orbital period. A pseudo-GPS inertial measurement system by Metris, Inc. (iGPS) is used to fix the ICS in the laboratory setting

for the development of the state estimation algorithm and control commands. The *X*-axis is taken to be the vector between the two iGPS transmitters with the *Y* and *Z* axes forming a right triad through the origin of a reference system located at the closest corner of the epoxy floor to the first iGPS transmitter. Navigation is provided by fusing of the magnetometer data and fiber optic gyro through a discrete Kalman filter to provide attitude estimation and through the use of a linear quadratic estimator to estimate the translation velocities given inertial position measurements. Control is accomplished through the combination of a state feedback linearized controller, a linear quadratic regulator, Schmitt trigger logic and Pulse Width Modulation using the minimal control actuator configuration of the 3-DoF spacecraft simulator. Figure 5 reports a block diagram representation of the control system.
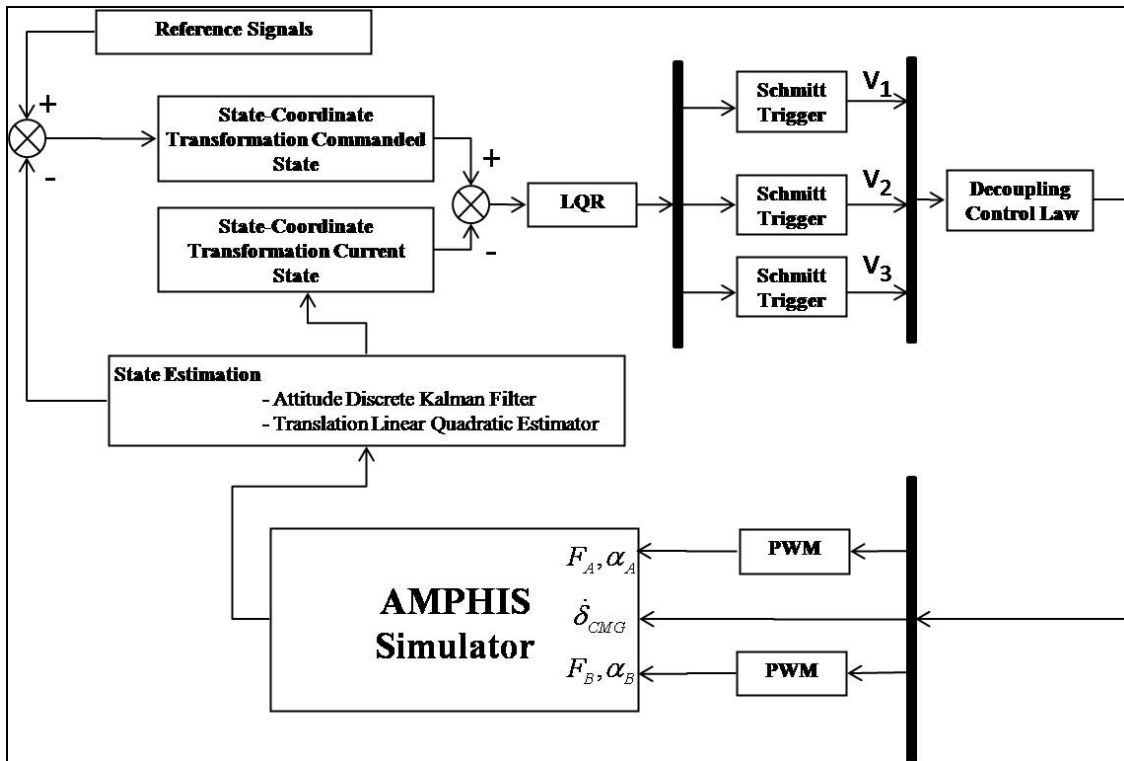
Figure 5. Block diagram of the control system of the 3-DoF spacecraft simulator, (v_1, v_2, v_3 control inputs to the system)

1. Navigation Using Inertial Measurements with Kalman Filter and Linear Quadratic Estimator

In the presence of the high accuracy, low noise, high bandwidth iGPS sensor with position accuracy to within 5.4 mm with a standard deviation of 3.6 mm and asynchronous measurement availability with a nominal frequency of 40 Hz, a full-order linear quadratic estimator with respect to the translation states is implemented to demonstrate the capability to estimate the inertial velocities in the absence of accelerometers. Additionally, due to the effect of noise and drift rate in the fiber-optic gyro, a discrete-time linear Kalman filter is employed to fuse the data from the magnetometer and the gyro. Both the gyro and magnetometer are capable of providing new measurements asynchronously at 100 Hz. Experimental results are presented in subsequent sections to demonstrate the filter's effectiveness.

a. Attitude Discrete-time Kalman Filter

With the attitude rate being directly measured, the measurement process can be modeled in state-space equation form as:

$$\begin{bmatrix} \omega_z \\ \dot{\beta}_g \end{bmatrix} = \underbrace{\begin{bmatrix} 0 & -1 \\ 0 & 0 \end{bmatrix}}_{A} \begin{bmatrix} \dot{\psi} \\ \beta_g \end{bmatrix} + \underbrace{\begin{bmatrix} 1 \\ 0 \end{bmatrix}}_{B} \omega_g + \underbrace{\begin{bmatrix} -1 & 0 \\ 0 & 1 \end{bmatrix}}_{G} \begin{bmatrix} \eta_{\omega g} \\ \eta_{\beta g} \end{bmatrix} \tag{36}$$

$$z = \psi_m = \underbrace{\begin{bmatrix} 1 & 0 \end{bmatrix}}_{H} \begin{bmatrix} \psi \\ \beta_g \end{bmatrix} + \eta_{\psi m} \tag{37}$$

where ω_g is the measured gyro rate, β_g is the gyro drift rate, $\eta_{\omega g}$ and $\eta_{\beta g}$ are the associated gyro output measurement noise and the drift rate noise respectively. ψ_m is the measured angle from the magnetometer, and $\eta_{\psi m}$ is the associated magnetometer output measurement noise. It is assumed that $\eta_{\omega g}$, $\eta_{\beta g}$ and $\eta_{\psi m}$ are zero-mean Gaussian white-noise processes with variances given by $\sigma_{\omega g}^2$, $\sigma_{\beta g}^2$ and $\sigma_{\psi m}^2$ respectively. Introducing

the state variables $\mathbf{x}^T = [\psi, \beta_g]$, control variables $u = \omega_g$, and error variables $\mathbf{w}^T = [\eta_{\omega g}, \eta_{\beta g}]$ and $v = \eta_{\psi m}$, (36) and (37) can be expressed compactly in matrix form as

$$\dot{\mathbf{x}}(t) = A(t)\mathbf{x}(t) + B(t)\mathbf{u}(t) + G(t)\mathbf{w}(t) \tag{38}$$

$$\mathbf{z}(t) = H\mathbf{x}(t) + \mathbf{v}(t) \tag{39}$$

In assuming a constant sampling interval Δt in the gyro output, the system equation (38) and observation equations (39) can be discretized and rewritten as

$$\mathbf{x}_{k+1} = \Phi_k \mathbf{x}_k + \Gamma_k \mathbf{u}_k + \Upsilon_k \mathbf{w}_k \tag{40}$$

$$\mathbf{z}_k = H_k \mathbf{x}_k + \mathbf{v}_k \tag{41}$$

where

$$\Phi_k = e^{A\Delta t} = \begin{bmatrix} 1 & -\Delta t \\ 0 & 1 \end{bmatrix} \tag{42}$$

and

$$\Gamma_k = \int_0^{\Delta t} e^{A\tau} B d\tau = \begin{bmatrix} \Delta t \\ 0 \end{bmatrix} \tag{43}$$

The process noise covariance matrix used in the propagation of the estimation error covariance given by (Gelb 1974; Crassidis and Junkins 2004)

$$(\Upsilon_k Q_k \Upsilon_k)^T = \int_{t_k}^{t_{k+1}} \int_{t_k}^{t_{k+1}} \Phi(t_{k+1}, \tau) G(\tau) E\{\mathbf{w}(\tau)\mathbf{w}^T(\alpha)\} G^T(\alpha)\Phi(t_{k+1}, \alpha) d\tau d\alpha \tag{44}$$

can be properly numerically estimated given a sufficiently small sampling interval by following the numerical solution by van Loan (Crassidis and Junkins 2004). First, the following $2n$ x $2n$ matrix is formed:

$$a = \begin{bmatrix} -A & GQG^T \\ 0 & A^T \end{bmatrix} \Delta t \tag{45}$$

33

where Δt is the constant sampling interval, A and G are the constant continuous-time state matrix and error distribution matrix given in (38), and Q is the constant continuous-time process noise covariance matrix

$$Q = E\left\{\mathbf{w}(t)\mathbf{w}^T(t)\right\} = \begin{bmatrix} \sigma_g^2 & 0 \\ 0 & \sigma_{\beta g}^2 \end{bmatrix} \tag{46}$$

The matrix exponential of (45) is then computed by

$$\mathcal{B} = e^a \equiv \begin{bmatrix} \mathcal{B}_{11} & \mathcal{B}_{12} \\ 0 & \mathcal{B}_{22} \end{bmatrix} = \begin{bmatrix} \mathcal{B}_{11} & \Phi_k^{-1}\mathcal{Q}_k \\ 0 & \Phi_k^T \end{bmatrix} \tag{47}$$

where Φ_k is the state transition matrix from (42) and $\mathcal{Q}_k = \left(\Upsilon_k Q_k \Upsilon_k\right)^T$. Therefore, the discrete-time process noise covariance is

$$\mathcal{Q}_k = \left(\Upsilon_k Q_k \Upsilon_k\right)^T = \Phi_k \mathcal{B}_{12} = \begin{bmatrix} 1/3\sigma_{\beta g}^2 \Delta t^3 + \sigma_g^2 \Delta t & -1/2\sigma_{\beta g}^2 \Delta t^2 \\ -1/2\sigma_{\beta g}^2 \Delta t^2 & \sigma_{\beta g}^2 \Delta t \end{bmatrix} \tag{48}$$

The discrete-time measurement noise covariance is

$$r_k = E\left\{\mathbf{v}_k \mathbf{v}_k^T\right\} = \sigma_{\theta m}^2 \tag{49}$$

Given the filter model as expressed in (36) and (37), the estimated states and error covariance are initialized where this initial error covariance is given by $P_0 = E\left\{\tilde{\mathbf{x}}(t_0)\tilde{\mathbf{x}}^T(t_0)\right\}$. If a measurement is given at the initial time, then the state and covariance are updated using the Kalman gain formula

$$K_k = P_k^- H_k^T \left[H_k P_k^- H_k^T + r_k \right]^{-1} \tag{50}$$

where P_k^- is the *a priori* error covariance matrix and is equal to P_0. The updated or *a posteriori* estimates are determined by

34

$$\hat{\mathbf{x}}_k^+ = \hat{\mathbf{x}}_k^- + K_k \left[z_k - H_k \hat{\mathbf{x}}_k^- \right]$$
$$P_k^+ = \left[I_{2x2} - K_k H_k \right] P_k^-$$

<div align="right">(51)</div>

where again with a measurement given at the initial time, the *a priori* state $\hat{\mathbf{x}}_k^-$ is equal to $\hat{\mathbf{x}}_0$. The state estimate and covariance are propagated to the next time step using

$$\hat{\mathbf{x}}_{k+1}^- = \Phi_k \hat{\mathbf{x}}_k^+ + \Gamma_k u_k$$
$$P_{k+1}^- = \Phi_k P_k^+ \Phi_k^T + Q_k$$

<div align="right">(52)</div>

If a measurement is not given at the initial time step, or any time step during the process, the estimate and covariance are propagated to the next available measurement point using (52).

b. *Translation Linear Quadratic Estimator*

With the measured translation state from the iGPS sensor being given by

$$\mathbf{z} = \underbrace{\begin{bmatrix} 1 & 0 & 0 & 0 \\ 0 & 1 & 0 & 0 \end{bmatrix}}_{C} \underbrace{\left[\mathbf{r}_{BI}, \mathbf{v}_{BI} \right]^T}_{\tilde{\mathbf{x}}}$$

<div align="right">(53)</div>

the dynamics of a full-order state estimator is described by the equation

$$\begin{aligned}
\dot{\tilde{\mathbf{x}}} = \dot{\mathbf{x}} - \dot{\hat{\mathbf{x}}} &= \left[A\mathbf{x} + B\mathbf{u} \right] - \left[A\hat{\mathbf{x}} + B\mathbf{u} + L_{QE} \left(\mathbf{z} - C\hat{\mathbf{x}} \right) \right] \\
&= A \left(\mathbf{x} - \hat{\mathbf{x}} \right) - L_{QE} \left(C\mathbf{x} - C\hat{\mathbf{x}} \right) \\
&= \left(A - L_{QE} C \right) \tilde{\mathbf{x}}
\end{aligned}$$

<div align="right">(54)</div>

where

$$A\mathbf{x} + B\mathbf{u} \quad : \quad \text{linearized plant dynamics}$$
$$A\hat{\mathbf{x}} + B\mathbf{u} \quad : \quad \text{system model}$$
$$L_{QE} \quad : \quad \text{linear quadratic estimator gain matrix}$$
$$C\hat{\mathbf{x}} \quad : \quad \text{predicted measurement}$$

The observer gain matrix L_{LQE} can be solved using standard linear quadratic estimator methods as (Bryson 1993)

$$L_{LQE} = PC^T R_T^{-1} \qquad (55)$$

where P is the solution to the algebraic Riccati equation

$$AP + PA^T - PC^T R_T^{-1} CP + Q_T = 0 \qquad (56)$$

and Q_T and R_T are the associated weighting matrices with respect to the translational degree of freedom defined as

$$\begin{aligned}
Q_T &= diag\left(1/\|\Delta\mathbf{r}_{max}\|^2, 1/\|\Delta\mathbf{r}_{max}\|^2, 1/\|\Delta\mathbf{v}_{max}\|^2, 1/\|\Delta\mathbf{v}_{max}\|^2\right) \\
R_T &= diag\left(1/(F_{max})^2, 1/(F_{max})^2\right)
\end{aligned} \qquad (57)$$

where $\|\Delta\mathbf{r}_{max}\|, \|\Delta\mathbf{v}_{max}\|$ are taken to be the maximum allowed errors between the current and estimated translational states and F_{max} is the maximum possible imparted force from the thrusters.

Table 3 lists the values of the attitude Kalman filter and translation state observer used for the experimental tests.

Δt	10^{-2} s
$\sigma_{\beta g}$	3.76 x 10^{-3} rad-s$^{-3/2}$
$\sigma_{\omega g}$	1.43 x 10^{-4} rad-s$^{-3/2}$
$\sigma_{\psi m}$	5.59 x 10^{-3} rad
P_0	$diag\left[10^{-15}, 10^{-8}\right]$
$\hat{\mathbf{x}}_0$	$[0,0]^T$
$\left\|\Delta\mathbf{r}_{max}\right\|$	10^{-2} m
$\left\|\Delta\mathbf{v}_{max}\right\|$	3 x 10^{-3} m-s^{-1}
F_{max}	0.159 N
L_{LQE}	$\begin{bmatrix} 18.9423 & 0 \\ 0 & 18.9423 \\ 53 & 0 \\ 0 & 53 \end{bmatrix}$

Table 3.   Kalman Filter Estimation Parameters

2. Smooth Feedback Control via State Feedback Linearization and Linear Quadratic Regulation

Considering a Multi-Input Multi-Output (MIMO) nonlinear system in control-affine form, the state feedback linearization problem of nonlinear systems can be stated as follows: obtain a proper state transformation

$$\mathbf{z} = \Phi(\mathbf{x}) \text{ where } \mathbf{z} \in \mathbb{R}^{N_x} \tag{58}$$

and a static feedback control law

$$\mathbf{u} = \alpha(\mathbf{x}) + \beta(\mathbf{x})\mathbf{v} \text{ where } \mathbf{v} \in \mathbb{R}^{N_u} \tag{59}$$

such that the closed-loop system in the new coordinates and controls become

$$\dot{\mathbf{z}} = \left\{\frac{\partial\Phi}{\partial\mathbf{x}}\left[\mathbf{f}(\mathbf{x}) + G(\mathbf{x})\alpha(\mathbf{x})\right]\right\}\bigg|_{\mathbf{x}=\Phi^{-1}(\mathbf{z})} + \left\{\frac{\partial\Phi}{\partial\mathbf{x}}\left[G(\mathbf{x})\boldsymbol{\beta}(\mathbf{x})\right]\right\}\bigg|_{\mathbf{x}=\Phi^{-1}(\mathbf{z})}\mathbf{v} \tag{60}$$

is both linear and controllable. The necessary conditions for a MIMO system to be considered for input-output linearization are that the system must be square or $N_u = N_y$

where N_u is defined as above to be the number of control inputs and N_y is the number of outputs for a system of the expanded form (Isidori 1989; Slotine 1990)

$$\dot{\mathbf{x}} = \mathbf{f}(\mathbf{x}) + G(\mathbf{x})\mathbf{u}$$

$$\mathbf{y} = \sum_{i=1}^{N_y} h_i(\mathbf{x}) = \mathbf{h}(\mathbf{x}) \tag{61}$$

The input-output linearization is determined by differentiating the outputs y_i in (61) until the inputs appear. Following the method outlined in Slotine (1990, chap. 6) by which the assumption is made that the partial relative degree r_i is the smallest integer such that at least one of the inputs appears in $y_i^{(r_i)}$, then

$$y_i^{(r_i)} = L_{\mathbf{f}}^{r_i} h_i + \sum_{j=1}^{N_y} L_{\mathbf{g}_j} L_{\mathbf{f}}^{r_i-1} h_i(\mathbf{x}) u_j \tag{62}$$

with the restriction that $L_{\mathbf{g}_j} L_{\mathbf{f}}^{r_i-1} h_i(\mathbf{x}) \neq 0$ for at least one j in a neighborhood of the equilibrium point $\mathbf{x}_0$. Letting

$$E(\mathbf{x}) = \begin{bmatrix} L_{\mathbf{g}_1} L_{\mathbf{f}}^{r_1-1} h_1(\mathbf{x}) & \cdots & L_{\mathbf{g}_{N_u}} L_{\mathbf{f}}^{r_1-1} h_1(\mathbf{x}) \\ L_{\mathbf{g}_1} L_{\mathbf{f}}^{r_2-1} h_2(\mathbf{x}) & \cdots & L_{\mathbf{g}_{N_u}} L_{\mathbf{f}}^{r_2-1} h_2(\mathbf{x}) \\ \cdots & \cdots & \cdots \\ L_{\mathbf{g}_1} L_{\mathbf{f}}^{r_{N_y}-1} h_{N_y}(\mathbf{x}) & \cdots & L_{\mathbf{g}_{N_u}} L_{\mathbf{f}}^{r_{N_y}-1} h_{N_y}(\mathbf{x}) \end{bmatrix} \tag{63}$$

so that (63) is in the form

$$\begin{bmatrix} y_1^{(r_1)} \\ y_2^{(r_2)} \\ \cdots \\ y_{N_y}^{(r_{N_y})} \end{bmatrix} = \begin{bmatrix} L_{\mathbf{f}}^{r_1} h_1(\mathbf{x}) \\ L_{\mathbf{f}}^{r_2} h_2(\mathbf{x}) \\ \cdots \\ L_{\mathbf{f}}^{r_{N_y}} h_{N_y}(\mathbf{x}) \end{bmatrix} + E(\mathbf{x})\mathbf{u} \tag{64}$$

the decoupling control law can be found where the $N_y \times N_y$ matrix $E(\mathbf{x})$ is invertible over the finite neighborhood of the equilibrium point for the system as

38

$$\mathbf{u} = E(\mathbf{x})^{-1} \begin{bmatrix} v_1 - L_{\mathbf{f}}^{r_1} h_1(\mathbf{x}) \\ v_2 - L_{\mathbf{f}}^{r_2} h_2(\mathbf{x}) \\ \dots \\ v_{N_y} - L_{\mathbf{f}}^{r_{N_y}} h_{N_y}(\mathbf{x}) \end{bmatrix} \tag{65}$$

With the above stated equations for the simulator dynamics in (23) given $G_1(\mathbf{x})$ as defined in (25), if we choose

$$\mathbf{h}(\mathbf{x}) = [\mathbf{r}_{BI}, \theta_3]^T \tag{66}$$

the state transformation can be chosen as

$$\mathbf{z}^T = [h_1(\mathbf{x}), h_2(\mathbf{x}), h_3(\mathbf{x}), L_{\mathbf{f}} h_1(\mathbf{x}), L_{\mathbf{f}} h_2(\mathbf{x}), L_{\mathbf{f}} h_3(\mathbf{x})] = [\mathbf{r}_{BI}, \theta_3, \mathbf{v}_{BI}, \omega_3] \tag{67}$$

where $\mathbf{z}(t) \in \mathbb{R}^6, \forall \mathbf{z} = [z_1, z_2, ..., z_6]^T$ are new state variables, and the system in (23) is transformed into

$$\dot{\mathbf{z}} = \left[z_4, z_5, z_6, m^{-1} \left(c z_3 \, {}^B F_1 - s z_3 \, {}^B F_2 \right), m^{-1} \left(s z_3 \, {}^B F_1 + c z_3 \, {}^B F_2 \right), J_3^{-1} T_3 \right]^T \tag{68}$$

The dynamics given by (23) considering the switching logic described in (24), (26) and (28) can now be transformed using (68) and the state feedback control law

$$\left[{}^B \mathbf{F}, T_z \right] = E(\mathbf{x})^{-1} (\mathbf{v} - \mathbf{b}) \tag{69}$$

into a linear system

$$\dot{\mathbf{z}} = \begin{bmatrix} \mathbf{0}_{3x3} & \mathbf{I}_{3x3} \\ \mathbf{0}_{3x3} & \mathbf{0}_{3x3} \end{bmatrix} \mathbf{z} + \begin{bmatrix} \mathbf{0}_{3x3} \\ \mathbf{I}_{3x3} \end{bmatrix} \mathbf{v} \tag{70}$$

where

$$\mathbf{b} = \left[L_{\mathbf{f}}^{r_1} h_1(\mathbf{x}), L_{\mathbf{f}}^{r_2} h_2(\mathbf{x}), L_{\mathbf{f}}^{r_3} h_3(\mathbf{x}) \right]^T \tag{71}$$

and $E(\mathbf{x})$ given by (63) with equivalent inputs $\mathbf{v}(t) \in \mathbb{R}^3, \forall \mathbf{v} = [v_1, v_2, v_3]^T$ and relative degree of the system at the equilibrium point $\mathbf{x}_0$ is $(r_1, r_2, r_3) = (2, 2, 2)$. Therefore the total relative degree of the system at the equilibrium point, which is defined as the sum of the relative degree of the system, is six. Given that the total relative degree of the system is equal to the number of states, the nonlinear system can be exactly linearized by state feedback and with the equivalent inputs v_i, both stabilization and tracking can be achieved for the system without concern for the stability of the internal dynamics (Slotine 1990).

One of the noted limitations of a feedback linearized based control system is the reliance on a fully measured state vector (Slotine 1990). This limitation can be overcome through the employment of proper state estimation. HIL experimentation on SRL's second generation robotic spacecraft simulator using these navigation algorithms combined with the state feedback linearized controller as described above coupled with a linear quadratic regulator to ensure the poles of (70) lie in the open left half plane demonstrate satisfactory results as reported in the following section.

a.   *Feedback Linearized Control Law with CMG Rotational Control and Thruster Translational Control*

By applying (69) to the dynamics in (23) given $G_1(\mathbf{x})$ as defined in (25) where the system is taken to be observable in the state vector $\mathbf{y} = [\mathbf{r}_{BI}, \theta_3]^T = [x_1, x_2, x_3]^T$ and by using thruster b for translational control (i.e., for the case ${}^B U_1 > 0$ where ${}^B U_1 = v_1 \, \mathrm{c}\, \theta_3 + v_2 \, \mathrm{s}\, \theta_3$ and ${}^B U_2 = -v_1 \, \mathrm{s}\, \theta_3 + v_2 \, \mathrm{c}\, \theta_3$), the feedback linearized control law is

$$\mathbf{u}^T = \left[{}^B F_1, {}^B F_2, T_3 \right] = \left[m\,{}^B U_1, m\,{}^B U_2, mL\,{}^B U_2 + J_3 v_3 \right] \tag{72}$$

which is valid for all $\mathbf{x}$ in a neighborhood of the equilibrium point $\mathbf{x}_0$. Similarly, the feedback linearized control law when ${}^B U_1 < 0$ (thruster a is providing translation control)

$$\mathbf{u}^T = \left[{}^B F_1, {}^B F_2, T_3 \right] = \left[m\,{}^B U_1, m\,{}^B U_2, -mL\,{}^B U_2 + J_3 v_3 \right] \tag{73}$$

Finally, when $^BU_3 = 0$ (both thrusters used for translational control) given $G_1(\mathbf{x})$ as defined in (27) is

$$\mathbf{u}^T = \begin{bmatrix} ^BF_2, T_3 \end{bmatrix} = \begin{bmatrix} m\,^BU_2/2, J_3v_3 \end{bmatrix} \tag{74}$$

b. Feedback Linearized Control Law for Thruster Roto-Translational Control

As mentioned previously, by considering a momentum exchange device for rotational control, momentum storage must be managed. For a control moment gyroscope based moment exchange device, desaturation is necessary near gimbal angles of $\pi/2$. In this region, due to the mathematical singularity that exists, very little torque can be exchanged with the vehicle and thus it is essentially ineffective as an actuator. To accommodate these regions of desaturation, logic can be easily employed to define controller modes as follows: If the MSGCMG is being used as a control input and if the gimbal angle of the MSGCMG is greater than 75 degrees, the controller mode is switched from normal operation mode to desaturation mode and the gimbal angle rate is directly commanded to bring the gimbal angle to a zero degree nominal position while the thruster not being directly used for translational control is slewed as appropriate to provide torque compensation. In these situations, the feedback linearizing control law for the system dynamics in (23) given $G_1(\mathbf{x})$ as defined in (29) where thruster b is providing translational control ($^BU_x > 0$), and thruster a is providing the requisite torque is

$$\mathbf{u}^T = \begin{bmatrix} ^BF_1, ^BF_2, T_3 \end{bmatrix} = \begin{bmatrix} m\,^BU_1, (mL\,^BU_2 - J_3v_3)/2L, (mL\,^BU_2 + J_3v_3)/2 \end{bmatrix} \tag{75}$$

Similarly, the feedback linearizing control law for the system assuming thruster a is providing translational control $\left(^BU_1 \le 0 \right)$ while thruster b provides the requisite torque is

$$\mathbf{u}^T = \begin{bmatrix} ^BF_1, ^BF_2, T_3 \end{bmatrix} = \begin{bmatrix} m\,^BU_1, (mL\,^BU_2 + J_3v_3)/2L, (mL\,^BU_2 - J_3v_3)/2 \end{bmatrix} \tag{76}$$

3. Determination of the Thruster Angles, Forces and CMG Gimbal Rates

In either mode of operation, the pertinent decoupling control laws are used to determine the commanded angle for the thrusters and whether or not to open or close the solenoid for the thruster. For example, if ${}^{B}U_{1} > 0$, (72) or (75) can be used to determine the angle to command thruster b as

$$\alpha_{b} = \tan^{-1}\left({}^{B}F_{2}/{}^{B}F_{1}\right) \tag{77}$$

and the requisite thrust as

$$F_{b} = \sqrt{{}^{B}F_{1}^{2} + {}^{B}F_{2}^{2}} \tag{78}$$

If the MSGCMG is being used, the requisite torque commanded to the CMG is taken directly from (72). In the normal operation mode, with the commanded angle for thruster one not pertinent, it can be commanded to zero without affecting control of the system. Similarly, if ${}^{B}U_{1} < 0$, (73) or (76) can be used to determine the angle to command thruster b and the requisite thrust analogous to (77) and (78). The requisite torque commanded to the CMG is similarly taken directly from (73). The required CMG torques can be used to determine the gimbal rate $\dot{\delta}_{CMG}$ to command the MSGCMG by solving (14) given a desired body-fixed torque T_{3} such that

$$\dot{\delta}_{CMG} = -T_{3}/\left(h_{w}\cos\delta_{CMG}\right) \tag{79}$$

where h_{w} is the constant angular momentum of the rotor wheel and δ_{CMG} is the current angular displacement of the wheel's rotational axis with respect to the horizontal.

If the momentum exchange device is no longer available and ${}^{B}U_{1} > 0$, the thruster angle commands and required thrust value for the opposing thruster can be determined by using (75) as

$$\alpha_{a} = -\pi/2\, sign\left(mL\,{}^{B}U_{2} + J_{3}v_{3}\right) \tag{80}$$

and

$$F_a = -sign(\alpha_a)\left(mL\,^BU_2 + J_3 v_3\right)/L \tag{81}$$

given $T_3 = -F_a\,s\,\alpha_a L$. Likewise, the thruster angle commands and required thrust value for the opposing thruster given $^BU_3 < 0$ can be determined by using (76) as

$$\alpha_b = \pi/2\,sign\left(mL\,^BU_2 - J_3 v_3\right) \tag{82}$$

and

$$F_b = sign(\alpha_b)\left(mL\,^BU_2 - J_3 v_3\right)/L \tag{83}$$

given $T_3 = -F_b \sin\alpha_b L$.

4.   Linear Quadratic Regulator Design

In order to determine the linear feedback gains used to compute the requisite equivalent inputs v_i to regulate the three degrees of freedom, so that

$$
\begin{aligned}
&\lim_{t\to\infty} z_1(t) = r_{BI,1}(t) = r_{ref}, &&\lim_{t\to\infty} z_2(t) = r_{BI,2}(t) = r_{ref}, &&\lim_{t\to\infty} z_3(t) = \theta_3(t) = \theta_{ref}\\
&\lim_{t\to\infty} z_4(t) = v_{BI,1}(t) = v_{ref}, &&\lim_{t\to\infty} z_5(t) = v_{BI,2}(t) = v_{ref}, &&\lim_{t\to\infty} z_6(t) = \omega_3(t) = \omega_{ref}
\end{aligned}
\tag{84}
$$

a standard linear quadratic regulator is employed where the state-feedback law $\mathbf{v} = -K\mathbf{z}$ minimizes the quadratic cost function

$$J(\mathbf{v}) = \int_0^\infty \left(\mathbf{z}^T Q\mathbf{z} + \mathbf{v}^T R\mathbf{v}\right)dt \tag{85}$$

subject to the feedback linearized state-dynamics of the system given in (70) . Given the relation between the linearized state and true state of the system, the corresponding gain matrices R and Q in (85) are chosen to minimize the appropriate control and state errors as

43

$$Q = diag \begin{pmatrix} 1/\|\Delta \mathbf{r}_{\max}\|^2, 1/\|\Delta \mathbf{r}_{\max}\|^2, 1/(\Delta \theta_{\max})^2, \\ 1/\|\Delta \mathbf{v}_{\max}\|^2, 1/\|\Delta \mathbf{v}_{\max}\|^2, 1/(\Delta \omega_{\max})^2 \end{pmatrix}$$
$$R = diag \left(1/(F_{\max})^2, 1/(F_{\max})^2, 1/(T_{CMG,\max})^2 \right) \tag{86}$$

where $T_{CMG,\max}$ is taken to be the maximum possible imparted force and torques from the thrusters and MSGCMG.

Given the use of discrete cold-gas thrusters in the system for translational control throughout a commanded maneuver and rotational control when the continuously acting momentum exchange device is unavailable, Schmitt trigger switching logic is imposed. Schmitt triggers have the unique advantage of reducing undesirable chattering and subsequent propellant waste nearby the reference state through an output-versus-input logic that imposes a dead zone and hysteresis to the phase space as shown in Figure 8.
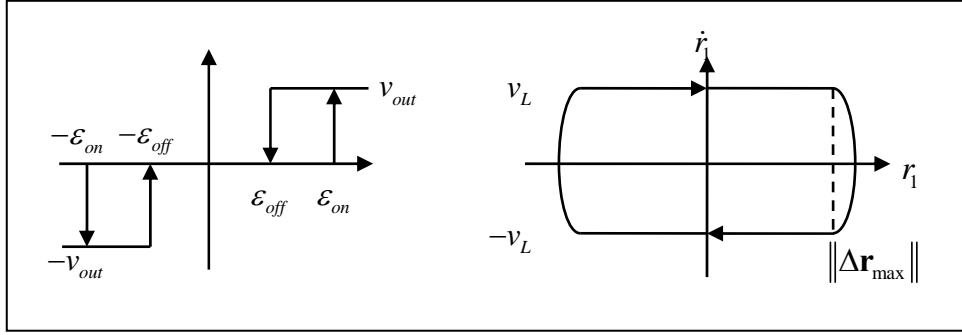
Figure 6.   Schmitt Trigger Characteristics with Design Parameters Considering $r_{BI,1}$ Coordinate Control Logic

Three separate Schmitt triggers are used with the design parameters of the Schmitt trigger shown in Figure 8 (as demonstrated for the $r_{BI,1}$ coordinate control logic). In the case of the two translational DoF Schmitt triggers, the parameters are chosen such that

$$\varepsilon_{on}(r) = K_r r_{db} + K_v v_L$$
$$\varepsilon_{off}(r) = K_r r_{db} - K_v v_L \tag{87}$$

where $v_L = F_{max}\Delta t/2m$. r_{db} is a free parameter that is constrained by mission requirements. v_{out} is chosen such that the maximum control command from the decoupling control law yields a value less than or equal to F_{max} for the translational thruster.

In the case of the rotational DoF Schmitt trigger when the momentum exchange device is unavailable, the parameters are chosen such that

$$\begin{aligned}\varepsilon_{on} &= K_\theta\theta_{db} + K_\omega\omega_L \\ \varepsilon_{off} &= K_\theta\theta_{db} - K_\omega\omega_L\end{aligned} \tag{88}$$

where $\omega_L = F_{max}L\Delta t/2J_3$. θ_{db} is a free parameter that is again constrained by mission requirements. For both modes of operation (i.e. with or without a momentum exchange device), (72) through (74) can be used to determine that

$$v_{1,max} = v_{2,max} = F_{max}/\sqrt{2}m \tag{89}$$

and when the thrusters are used for rotational control

$$v_{3,max} = F_{max}L/J_3 \tag{90}$$

When the momentum exchange device is available, the desired torque, as determined by the LQR control law described above, is passed directly through the Schmitt trigger to the decoupling control law to determine the required gimbal rate command to the MSGCMG.

The three Schmitt trigger blocks output the requested control inputs along the $\mathcal{I}$ frame. The appropriate feedback linearizing control law is then used to transform these control inputs into requested thrust, thruster angle and MSGCMG gimbal rate along the $\mathcal{B}$ frame. From these, a vector of specific actuator commands are formed such that

$$\mathbf{u}_c^T = \left[F_a, \alpha_a, F_b, \alpha_b, \dot{\delta}_{CMG} \right] \tag{91}$$

Each thruster command is normalized with respect to F_{max} and then fed with its corresponding commanded angle into separate Pulse Width Modulation (PWM) blocks. Each PWM block is then used to obtain an approximately linear duty cycle from on-off actuators by modulating the opening time of the solenoid valves (Wie 1998, p. 455). Additionally, due to the linkage between the thruster command and the thruster angle, the thruster firing sequence is held until the actual thruster angle is within a tolerance of the commanded thruster angle. Furthermore, in order to reduce over-controlling the system, the LQR, Schmitt trigger logic and decoupling control algorithm are run at the PWM bandwidth of 8.33 Hz. From each PWM, digital outputs (either zero or one) command the two thrusters while the corresponding angle is sent via RS-232 to the appropriate thruster gimbal motor.

$\Delta\theta_{max}$	1.8×10^{-2} rad
$\Delta\omega_{max}$	1.8×10^{-2} rad-s^{-1}
$T_{CMG,max}$	0.668 Nm
$K_r = K_{LQR}(1,1) = K_{LQR}(2,2)$	15.9
$K_v = K_{LQR}(1,4) = K_{LQR}(2,5)$	84.54 s
$K_\theta = K_{LQR}(3,3)$	1.39
$K_\omega = K_{LQR}(3,6)$	1.75 s
r_{db}	10^{-2} m
v_L	3.05×10^{-5} m-s^{-1}
θ_{db}	1.8×10^{-2} rad
ω_L	1.8×10^{-2} rad-s^{-1}
$\varepsilon_{on}(r)$	1.61×10^{-1} m
$\varepsilon_{off}(r)$	1.56×10^{-1} m
$\varepsilon_{on}(\theta)$	2.47×10^{-2} rad
$\varepsilon_{off}(\theta)$	2.37×10^{-2} rad
PWM min pulse width	10^{-2} s
PWM sample time	1.2×10^{-1} s

Table 4.   Values of the Control Parameters

Table 3 and Table 4 list the values of the control parameters used for the experimental tests reported in the following section. In particular, $\|\Delta \mathbf{v}_{max}\|$ is chosen based typical maximum relative velocities during rendezvous scenarios while $\Delta\theta_{max}$ is taken to be 1 degree and $\Delta\omega_{max}$ is chosen to be 1 degrees/sec which correspond to typical slew rate requirements for small satellites (Roser and Schedoni 1997; Lappas, Steyn, and Underwood 2002). The minimum opening time of the PWM was based on experimental results for the installed solenoid valves reported in (Lugini and Romano 2009).

F.   EXPERIMENTAL RESULTS

The navigation and control algorithms introduced above were coded in MATLAB®-Simulink® and run in real time using MATLAB XPC Target™ embedded on the SRL's second generation spacecraft simulator's on-board PC-104.   Two experimental tests are presented to demonstrate the effectiveness of the designed control system.   The scenario presented represents a potential real-world autonomous proximity operation mission where a small spacecraft is tasked with performing a full 360-degree circle around another spacecraft for the purpose of inspection or pre-docking.   These experimental tests validate the navigation and control approach and furthermore demonstrate the capability of the robotic spacecraft simulator testbed.

1.   Autonomous Proximity Maneuver Using Vectorable Thrusters and MSGCMG Along a Closed Circular Path

Figure 7, Figure 8, and Figure 9 report the results of an autonomous proximity maneuver along a closed circular trajectory of NPS SRL's second generation robotic spacecraft simulator using its vectorable thrusters and MSGCMG. The reference path for the center of mass of the simulator consists of 200 waypoints, taken at angular intervals of 1.8 deg along a circle of diameter 1m with a center at the point [2.0 m, 2.0 m] in the ICS, which can be assumed, for instance, to be the center of mass of the target. The reference attitude is taken to be zero throughout the maneuver. The entire maneuver lasts 147 s. During the first 10 s, the simulator is maintained fixed in order to allow the attitude Kalman filter time to converge to a solution. At 10 s into the experiment, the

solenoid valve regulating the air flow to the linear air bearings is opened and the simulator begins to float over the epoxy floor. At this point, the simulator begins to follow the closed path through autonomous control of the two thrusters and the MSGCMG.

As evidenced in Figure 7a through Figure 7d, the components of the center of mass of the simulator as estimated by the translation linear quadratic estimator are kept close to the reference signals by the action of the vectorable thrusters. Specifically, the mean of the absolute value of the tracking error is 1.3 cm for $\Delta r_{BI,1}$, with a standard deviation of 9.1 mm, 1.4 cm mean for $\Delta r_{BI,2}$ with a standard deviation of 8.6 mm, 2.4 mm/s mean for $\Delta v_{BI,1}$ with a standard deviation of 1.8 mm/s and 3.0 mm/s mean for $\Delta v_{BI,2}$ with a standard deviation of 2.7 mm/s. Furthermore, the mean of the absolute value of the estimated error in $r_{BI,1}$ is 2 mm with a standard deviation of 2 mm and 4 mm in $r_{BI,2}$ with a standard deviation of 3 mm. Likewise, Figure 7e and Figure 7f demonstrate the accuracy of the attitude tracking control through a comparison of the commanded and actual attitude and attitude rate. Specifically, the mean of the absolute value of tracking error for $\Delta \theta_3$ is 0.14 deg with a standard deviation of 0.11 deg and 0.14 deg/s for $\Delta \omega_3$ with a standard deviation of 0.15 deg/s. These control accuracies are in good agreement with the set parameters of the Schmitt triggers and the LQR design.

Figure 8a through Figure 8d report the command signals to the simulator's thrusters along with their angular positions. The commands to the thrusters demonstrate that the Schmitt trigger logic successfully avoids chattering behavior and the feedback linearized controller is able to determine the requisite thruster angles. Figure 8e and Figure 8f show the gimbal position of the miniature single-gimbaled control moment gyro and the delivered torque. Of note, the control system is able to autonomously maneuver the simulator without saturating the MSGCMG.
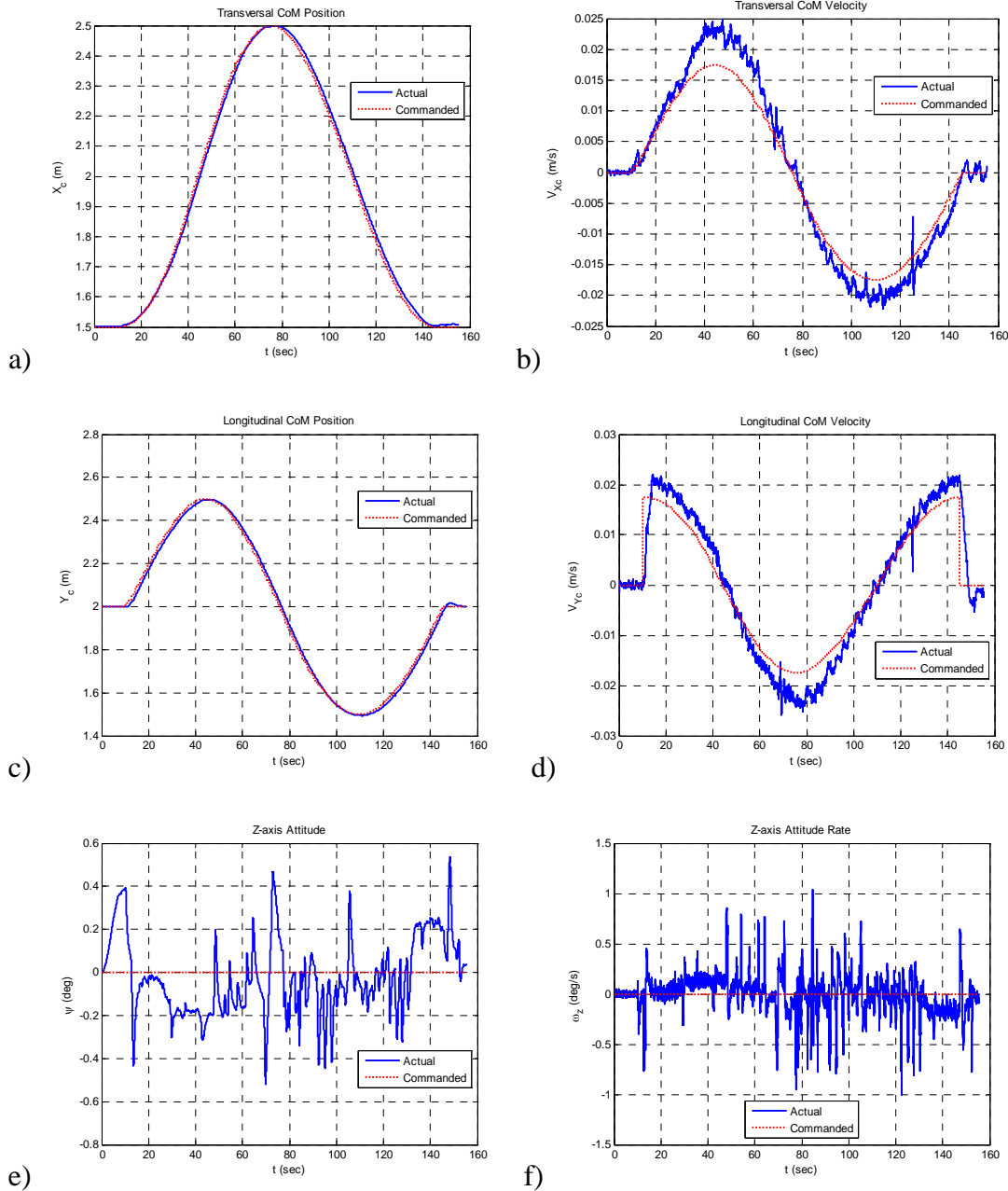
Figure 7.　　Logged data versus time of an autonomous proximity maneuver of NPS SRL's 3-DoF spacecraft simulator along a closed path using vectorable thrusters and MSGCMG. The simulator begins floating over the epoxy floor at t = 10 s.
a) Transversal position of the center of mass of the simulator in $\mathcal{I}$　b) Transversal velocity of the center of mass of the simulator in ICS c) Longitudinal position of the center of mass of the simulator d) Longitudinal velocity of the center of mass of the simulator e) Attitude f) Attitude rate
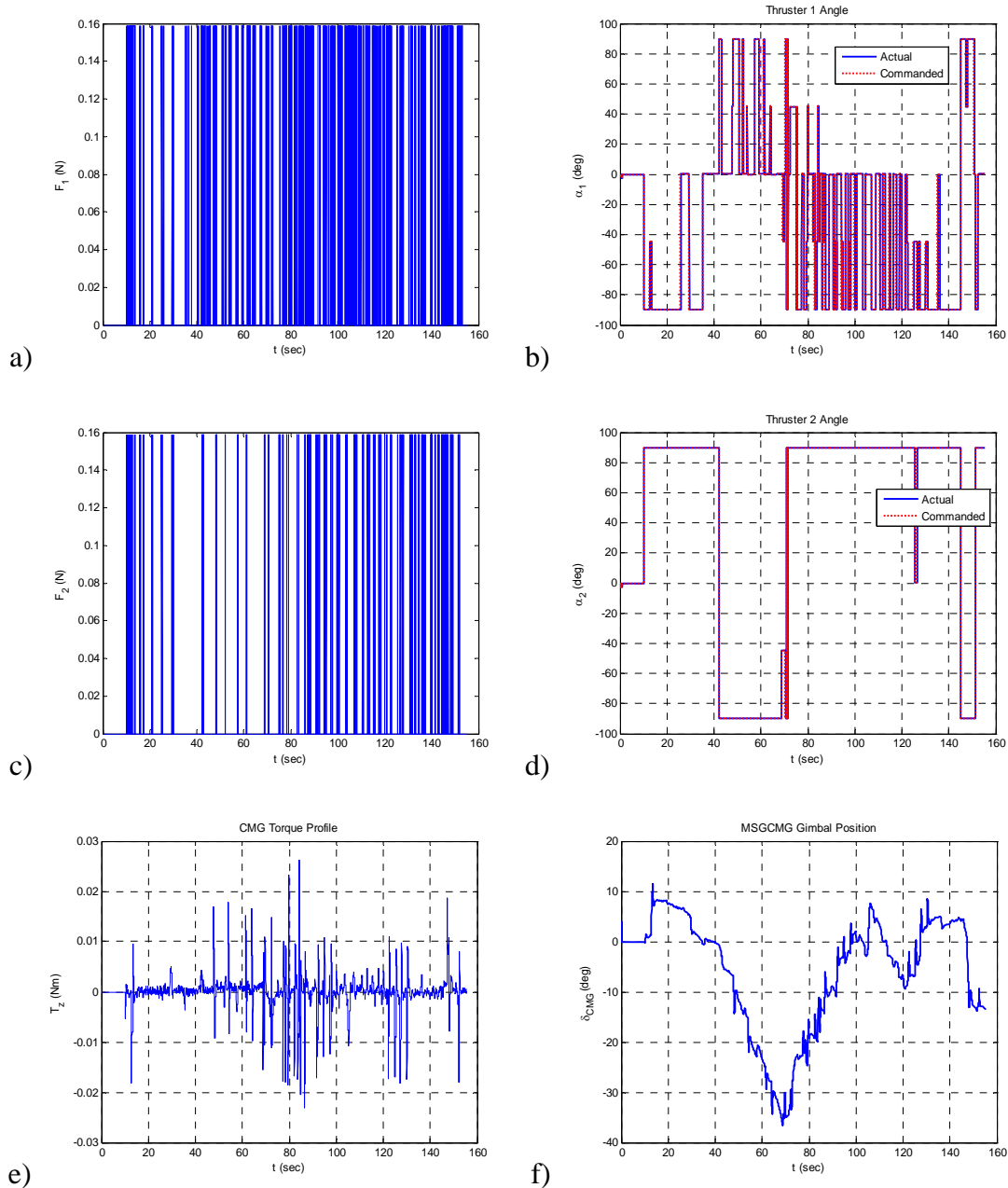
Figure 8. Control actuator actions during autonomous proximity maneuver of NPS SRL's 3-DoF spacecraft simulator along a closed path using vectorable thrusters and MSGCMG. a) Thruster 1 firing profile b) Thruster 1 position c) Thruster 2 firing profile d) Thruster 2 position f) MSGCMG torque profile e) MSGCMG gimbal position

Figure 9 depicts a bird's-eye view of the spacecraft simulator motion. Of particular note, the good control accuracy can be evaluated by the closeness of the actual ground-track line to the commanded circular trajectory and of the initial configuration of

the simulator to the final one. The total ΔV required during this experimental test was 0.294 m/s which correspond to a total impulse of 7.65 Ns.
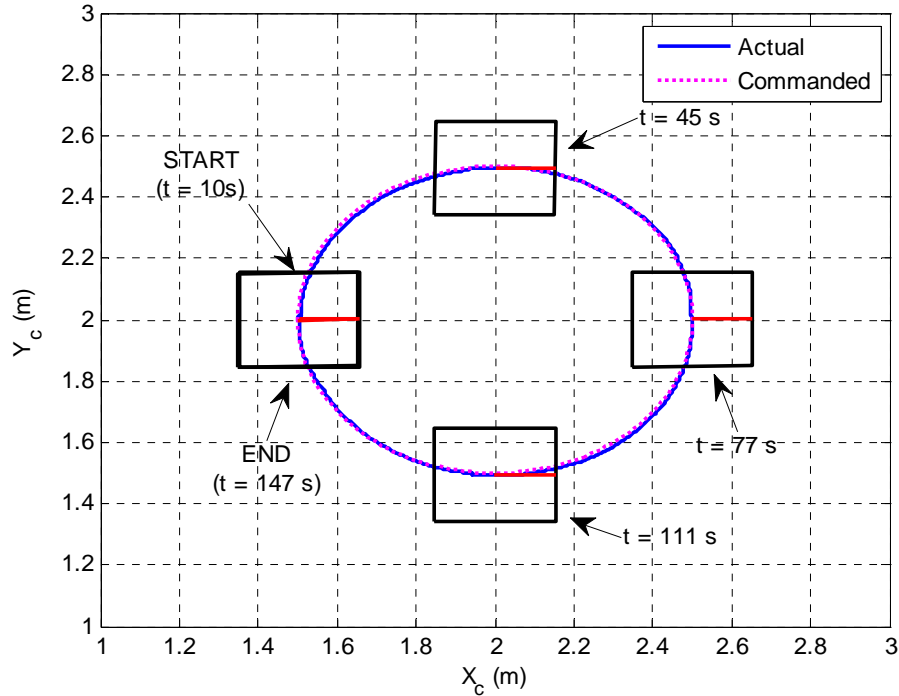
Figure 9.   Bird's-eye view of autonomous proximity maneuver of NPS SRL's 3-DoF spacecraft simulator along a closed path using vectorable thrusters and MSGCMG

2.   Autonomous Proximity Maneuver Using Vectorable Thrusters Along a Closed Circular Path

Figure 10, Figure 11, and Figure 12 report the results of maneuvering the spacecraft simulator along the same reference maneuver as in Section 6.1 but by using only the vectorable thrusters. This maneuver is presented to demonstrate the experimental validation of the STLC analytical results. As before, during the first 10 s, the simulator is not floating and kept stationary while the attitude Kalman filter converges.

The tracking and estimation errors for this maneuver are as follows with the logged positions, attitudes and velocities shown in Figure 10. The mean of the absolute value of the tracking error is 1.4 cm for $\Delta r_{BI,1}$, with a standard deviation of 8.5 mm, 1.4

cm mean for $\Delta r_{BI,2}$ with a standard deviation of 8.6 mm, 2.5 mm/s mean for $\Delta v_{BI,1}$ with a standard deviation of 1.9 mm/s and 3.1 mm/s mean for $\Delta r_{BI,2}$ with a standard deviation of 2.8 mm/s. The mean of the absolute value of the estimated error in $r_{BI,1}$ is 3 mm with a standard deviation of 3 mm and 4 mm in $r_{BI,2}$ with a standard deviation of 5 mm. The mean of the absolute value of tracking error for $\Delta\theta_3$ is 0.52 deg with a standard deviation of 0.31 deg and 0.24 deg/s for $\Delta\omega_3$ with a standard deviation of 0.20 deg/s. These control accuracies are in good agreement with the set parameters of the Schmitt triggers and LQR design.

Figure 11 reports the command signals to the simulator's thrusters with the commands to the thrusters again demonstrating that the feedback linearized controller is able to determine the requisite thruster angles to take advantage of this fully minimized actuation system. Figure 12 depicts a bird's-eye view of the motion of the simulator during this maneuver. The total ΔV required during this experimental test was 0.327 m/s which correspond to a total impulse of 8.55 Ns.
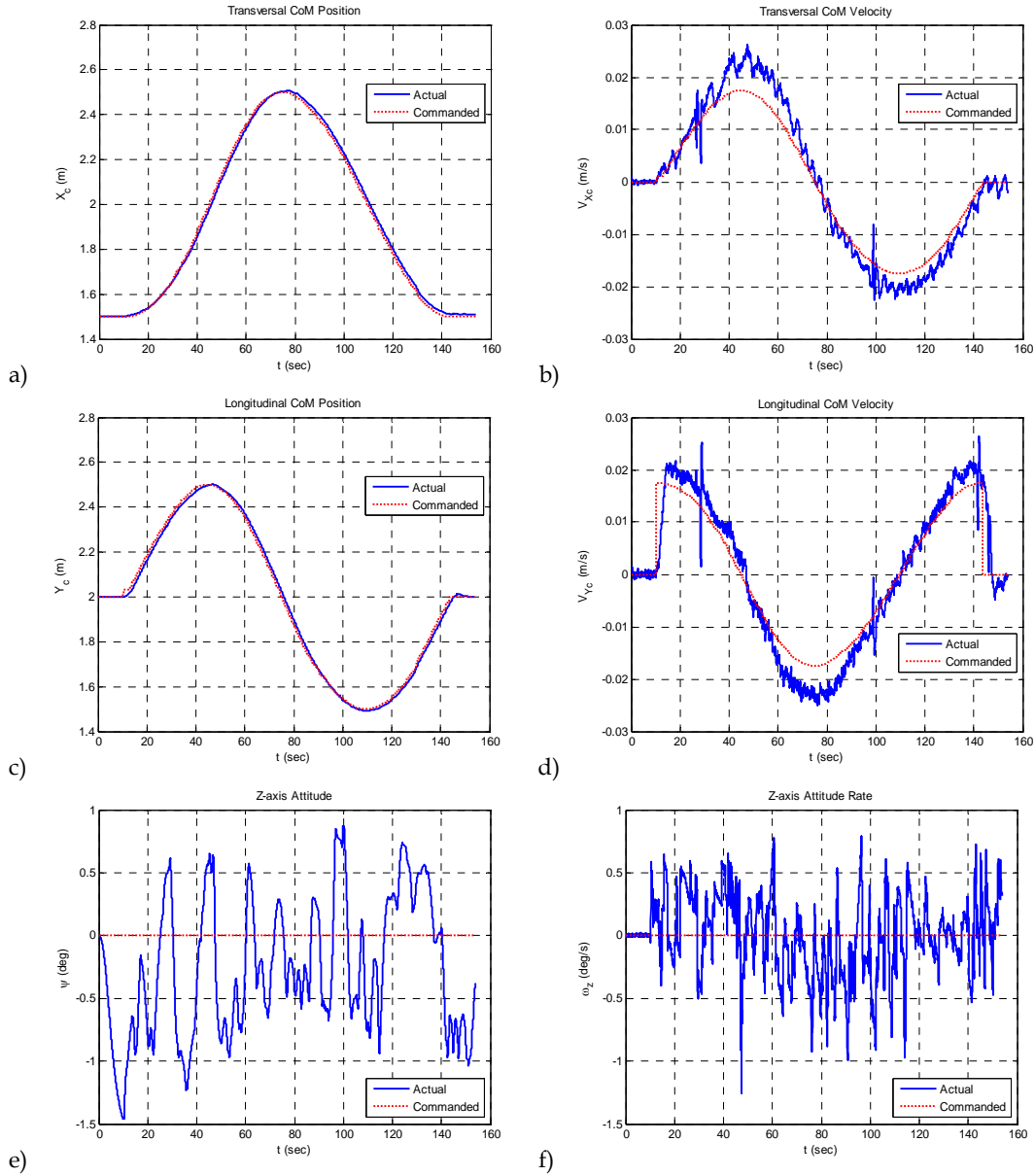
Figure 10. Logged data versus time of an autonomous proximity maneuver of NPS SRL's 3-DoF spacecraft simulator along a closed path using only vectorable thrusters. The simulator begins floating over the epoxy floor at t = 10 s. a) Transversal position of the center of mass of the simulator in the $\mathcal{I}$ b) Transversal velocity of the center of mass of the simulator in ICS c) Longitudinal position of the center of mass of the simulator d) Longitudinal velocity of the center of mass of the simulator e) Attitude f) Attitude rate
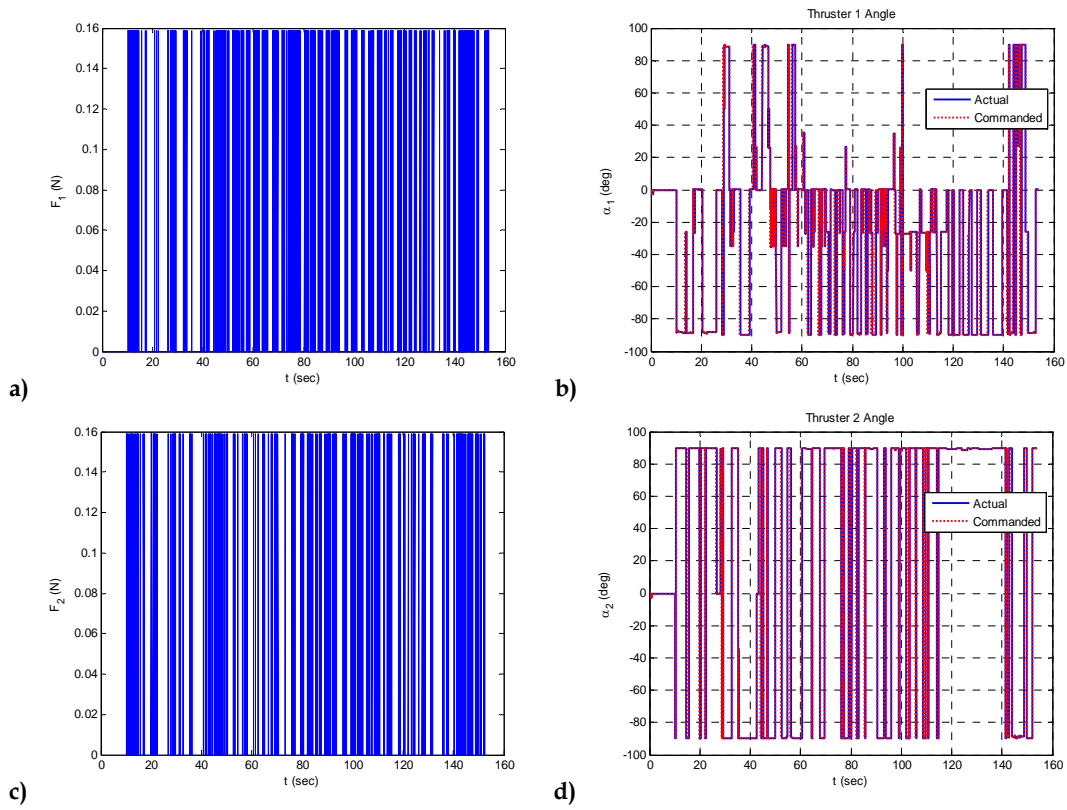
Figure 11.   Control actuator actions during autonomous proximity maneuver of NPS
SRL's 3-DoF spacecraft simulator along a closed path using only vectorable thrusters. a)
Thruster 1 firing profile b) Thruster 1 position c) Thruster 2 firing profile d) Thruster 2
position
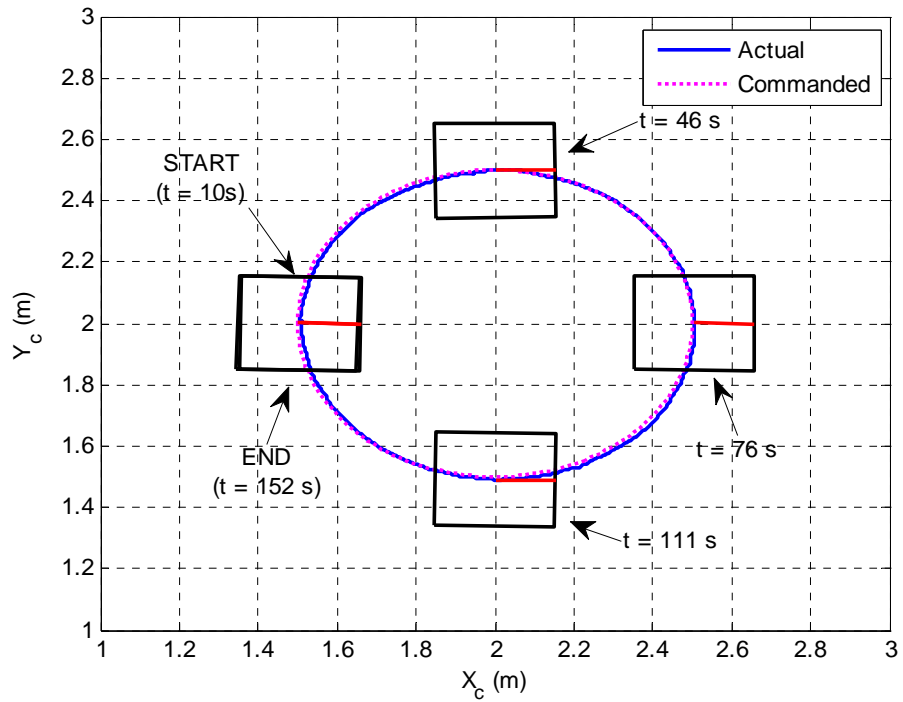
Figure 12.   Autonomous proximity maneuver of NPS SRL's 3-DoF spacecraft
simulator along a closed path using only thrusters

THIS PAGE INTENTIONALLY LEFT BLANK

III. VECTORABLE THRUSTER CONFIGURATION FOR ROTO-TRANSLATIONAL CONTROL OF SPACECRAFT

A novel configuration of two oppositely-mounted vectorable thrusters is presented to provide six DoF roto-translational control of a spacecraft. Figure 13 depicts a potential vectorable thruster solution based on the research presented by Canfield and Reinholz (1998). By allowing each thruster to be vectored within a hemispherical space, small-time local controllability of underactuated spacecraft is achieved.   This configuration of control actuators is proposed as a possible alternative to conventional fixed thruster-based architectures on rapidly deployable, low-cost, and low-mass spacecraft systems. It may also be used for more traditional spacecraft such as NASA's Crew Exploration Vehicle (CEV) and ESA's Automated Transfer Vehicle (ATV). The CEV's fixed thruster-based Reaction Control System (RCS) consists of a configuration of four pods of six thrusters to provide six DoF roto-translation control (Jackson and Gonzalez 2007). In comparison, the ATV achieves six DoF control via 32 fixed thrusters with 28 dedicated to the Attitude Control System (ACS) and 4 dedicated to the Orbital Control System (OCS) (Cavrois, Reynaud, Personne, Chavy and Strandmoe 2008). The potential advantages of reducing the number of thrusters required for 6-DoF roto-translational control include simplification of the overall spacecraft design, reduction of the required fuel for a desired maneuver, and a reduction in the overall size of the propulsion system.
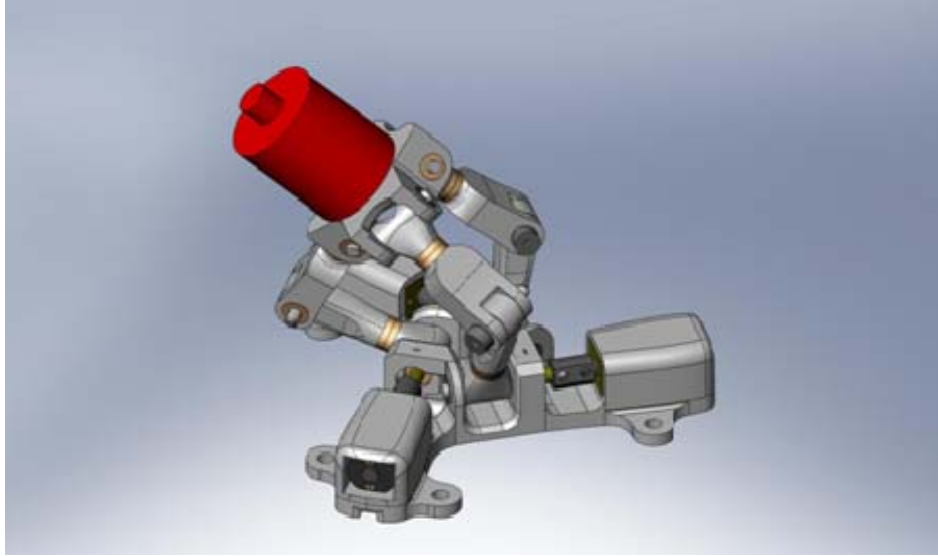
Figure 13.   Depiction of potential hemispherical vectorable thruster (Courtesy Dr. Steven Canfield, Tennesse Tech University)

This chapter presents the dynamics model of this novel unconventional spacecraft architecture within a proximity operations environment and, following the mathematical methods presented in the previous chapter, the small-time local controllability of this underactuated system is demonstrated. By adding two additional pairs of fixed thrusters, the system becomes fully actuated and thus input-output linearizable. Given this input-output linearizability, a feedback linearized control law is derived to that can control the 6-DoF roto-translation problem via traditional linear control methods. The reference spacecraft is assumed to be rigid with principal moments of inertia aligned with the body-fixed control axes.

A.   SPACECRAFT RELATIVE MOTION DYNAMICS

Consider two close-orbiting spacecraft moving in the gravitational field of Earth or one chaser spacecraft moving with respect to a reference point. It is assumed that the chaser-target pair are homogeneous rigid bodies and that the chaser-target pair are moving in a nearly circular orbit with the final desired state of the control problem being a soft dock of the two vehicles.

Three reference frames are established: an inertial frame $\mathcal{I}$ with orthogonal axes defined by the set of unit vectors $\{\hat{i}_1, \hat{i}_2, \hat{i}_3\}$, a rotating satellite reference frame $\mathcal{H}$ with orthogonal axes defined by the set of unit vectors $\{\hat{h}_1, \hat{h}_2, \hat{h}_3\}$ and a body-fixed frame $\mathcal{B}$ with orthogonal axes defined by the set of unit vectors $\{\hat{b}_1, \hat{b}_2, \hat{b}_3\}$. The rotating satellite reference frame $\mathcal{H}$ is used to define the reference coordinate system for the chaser-target rendezvous problem where the $\hat{h}_1$ is collinear with the position vector of the target spacecraft with respect to the Earth's center, $\hat{h}_2$ is in the direction of the velocity vector of the target spacecraft aligned with the local horizontal and $\hat{h}_3$ is normal to the orbit plane. In this manner, the angular velocity of $\mathcal{H}$ with respect to $\mathcal{I}$ is

$$\boldsymbol{\omega}_{HI} = -\omega_0 \hat{h}_3 \tag{92}$$

where ω_0 is the target spacecraft's mean motion. The angular velocity of $\mathcal{B}$ with respect to $\mathcal{I}$ is then given by

$$\boldsymbol{\omega}_{BI} = \boldsymbol{\omega}_{BH} + \boldsymbol{\omega}_{HI} = \boldsymbol{\omega}_{BH} - \omega_0 \hat{h}_3 \tag{93}$$

1. Translational Motion of the Chaser-Target Pair

The 3-DoF translational motion of the rigid chaser spacecraft with respect to $\mathcal{H}$ are given by Vallado (2001):

$$\begin{aligned}
\dot{\mathbf{r}}_{BH} &= \mathbf{v}_{BH} \\
\dot{\mathbf{v}}_{BH} &= \mathbf{f}\left(\mathbf{r}_{BH}, \mathbf{v}_{BH}\right) + m^{-1} {}^H\mathbf{F}
\end{aligned} \tag{94}$$

where $\mathbf{v}(t) \in \mathbb{R}^3, \forall \mathbf{v} = \left[v_{BH,1}, v_{BH,2}, v_{BH,3}\right]^T$ is the translational velocity vector of the chaser's body-fixed frame $\mathcal{F}$ with respect to the moving satellite reference frame $\mathcal{H}$ expressed in $\mathcal{H}$, $\mathbf{r}(t) \in \mathbb{R}^3, \forall \mathbf{r} = \left[r_{BH,1}, r_{BH,2}, r_{BH,3}\right]^T$ is the position vector of the chaser's body-fixed frame $\mathcal{B}$ with respect to the moving satellite reference frame $\mathcal{B}$ expressed

in $\mathcal{B}$, $^{H}\mathbf{F}(t) \in \mathbb{R}^{3}, \forall \, ^{H}\mathbf{F} = \left[^{H}F_{1}, \, ^{H}F_{2}, \, ^{H}F_{3} \right]$ is the control vector acting on $\mathcal{H}$, m is the mass of the chaser spacecraft and $\mathbf{f}\left(\mathbf{r}_{BH}, \mathbf{v}_{BH}\right) \in \mathbb{R}^{3}$ represents the drift vector

$$\mathbf{f}\left(\mathbf{r}_{BH}, \mathbf{v}_{BH}\right) = \begin{bmatrix} 3\omega_{0}^{2}r_{BH,1} + 2\omega_{0}v_{BH,2} \\ -2\omega_{0}v_{BH,1} \\ -\omega_{0}^{2}r_{BH,3} \end{bmatrix} \tag{95}$$

2. Rotational Motion of the Chaser Spacecraft with Respect to the Inertial Frame

The rotational motion of the chaser spacecraft about body-fixed axes with their origin located at the body's center of mass can be described using Euler's equations. For the general case, in which the control axes do not coincide with the principal axes of inertia and torquing devices such as independent gas thrusters are used to impart torques about these control axes, these become from Wie (1998, p. 341):

$$\dot{\boldsymbol{\omega}}_{BI} = -J^{-1}\omega_{BI}^{x}J\boldsymbol{\omega}_{BI} + J^{-1}\mathbf{T} \tag{96}$$

where $\boldsymbol{\omega}_{BI}(t) \in \mathbb{R}^{3}, \forall \boldsymbol{\omega}_{BI} = \left[\omega_{BI,1}, \omega_{BI,2}, \omega_{BI,3}\right]^{T}$ is the angular velocity vector of the body-fixed frame $\mathcal{B}$ with respect to an inertial frame $\mathcal{I}$ expressed in $\mathcal{B}$, $\mathbf{T}(t) \in \mathbb{R}^{3}, \forall \mathbf{T} = \left[^{B}T_{1}, \, ^{B}T_{2}, \, ^{B}T_{3}\right]^{T}$ is the control torque vector acting on $\mathcal{B}$. The notation $\omega_{BI}^{x} \in \mathbb{R}^{3x3}$ denotes the skew-symmetric matrix

$$\omega_{BI}^{x} = \begin{bmatrix} 0 & -\omega_{BI,3} & \omega_{BI,2} \\ \omega_{BI,3} & 0 & -\omega_{BI,1} \\ -\omega_{BI,2} & \omega_{BI,1} & 0 \end{bmatrix} \tag{97}$$

and $J \in \mathbb{R}^{3x3}$ is the inertia matrix with respect to the $\mathcal{F}$ given by

$$J = \begin{bmatrix} J_{11} & J_{12} & J_{13} \\ J_{21} & J_{22} & J_{23} \\ J_{31} & J_{32} & J_{33} \end{bmatrix} \tag{98}$$

3. Quaternion Kinematic Representation of the Chaser Spacecraft's Orientation

The orientation of a rigid spacecraft can be defined through various parameterizations of the special orthogonal group $SO(3)$. In this work, the quaternion is considered to parameterize this orientation due to their suitability for onboard real-time computation and subsequent common use for spacecraft attitude determination (Wie et al. 1989). The unit quaternion, first envisioned by Hamilton in 1843, can be separated into two parts, the first being a three-dimensional vector indicating the direction of the axis of rotation and the second being a scalar quantity which relates the angle of rotation about this axis of rotation such that

$$\hat{\mathbf{q}} = \mathbf{q} + q_4 = q_1\mathbf{i} + q_2\mathbf{j} + q_3\mathbf{k} + q_4 \tag{99}$$

where $\hat{\mathbf{q}}(t) \triangleq \{\mathbf{q}(t), q_4(t)\} \in \mathbb{R}^3 x \mathbb{R}$ and

$$q_i = b_i \sin(\delta/2), i = 1, 2, 3$$
$$q_4 = \cos(\delta/2) \tag{100}$$

where δ represents the magnitude of the rotation around the chosen axis and (b_1, b_2, b_3) are the direction cosines locating the axis of rotation to the inertial frame by Euler's Theorem (Wie and Barba 1985; Wie et al. 1989; Cristi and Burl 1993). The properties of the unit vectors $(\mathbf{i}, \mathbf{j}, \mathbf{k})$ with respect to the chosen reference frame when multiplied are such that 0

$$\mathbf{ij} = -\mathbf{ji} = \mathbf{k}, \mathbf{jk} = -\mathbf{kj} = \mathbf{i}, \mathbf{ki} = -\mathbf{ik} = \mathbf{j}, \mathbf{ii} = \mathbf{jj} = \mathbf{kk} = -1 \tag{101}$$

By considering the direction cosines expressed in (100) to be equivalent to the unit vectors $(\mathbf{i}, \mathbf{j}, \mathbf{k})$, the quaternion can be used to define a sequence of rotations about a series of Euler angles defined by $\phi, \theta,$ and ψ . By considering a 3-2-1 body-fixed rotation sequence from $\mathcal{B}$ to $\mathcal{I}$, as is typical for visualizing spacecraft orientations, a set of elementary quaternions can be defined from the three Euler angles similar to the three

sets of elementary rotation matrices (Wie 1998). In this manner, $\delta_1 = \phi, \delta_2 = \theta, \delta_3 = \psi$ and from (100) and (101), the quaternion associated with this sequence of rotations becomes

$$\hat{\mathbf{q}}_{BI} = \begin{bmatrix} q_{BI,1} \\ q_{BI,2} \\ q_{BI,3} \\ q_{BI,4} \end{bmatrix} = \begin{bmatrix} s_1 c_2 c_3 - c_1 s_2 s_3 \\ c_1 s_2 c_3 + s_1 c_2 s_3 \\ c_1 c_2 s_3 - s_1 s_2 c_3 \\ c_1 c_2 c_3 + s_1 s_2 s_3 \end{bmatrix} \tag{102}$$

where $s_i = \sin(\delta_i/2), c_i = \cos(\delta_i/2), i = 1, 2, 3$. Note that the order of elementary quaternion multiplications is reversed from the order of elementary rotation matrices due to the properties of quaternion multiplication expressed in (101).

The kinematic differential equation of the quaternion representing the orientation of the chaser spacecraft's body-fixed frame $\mathcal{B}$ to $\mathcal{I}$ is given as

$$\dot{\mathbf{q}}_{BI} = \frac{1}{2}\left(q_{BI,4}I_{3x3} + q_{BI}^x\right)\mathbf{\omega}_{BI}$$
$$\dot{q}_{BI,4} = -\frac{1}{2}\mathbf{q}_{BI}^T\mathbf{\omega}_{BI} \tag{103}$$

where $q_{BI}^x \in \mathbb{R}^{3x3}$ represents the skew-symmetric matrix

$$q_{BI}^x = \begin{bmatrix} 0 & -q_{BI,3} & q_{BI,2} \\ q_{BI,3} & 0 & -q_{BI,1} \\ -q_{BI,2} & q_{BI,1} & 0 \end{bmatrix} \tag{104}$$

and I_{3x3} represents a 3x3 identity matrix. One can quickly show using (100) that the quaternion is subject to the constraint

$$q_{BI,4}^2 = 1 - \mathbf{q}_{BI}^T\mathbf{q}_{BI} = 1 - \left\|\mathbf{q}_{BI}\right\|^2 \tag{105}$$

4. Angular Motion of the Chaser Spacecraft with Respect to the Satellite Reference Frame

Considering the rotating satellite reference frame $\mathcal{H}$, the quaternion describing the orientation of $\mathcal{B}$ with respect to $\mathcal{H}$ is defined as above so that $\hat{\mathbf{q}}_{BH}(t) \triangleq \{\mathbf{q}_{BH}(t), q_{BH,4}(t)\} \in \mathbb{R}^3 x \mathbb{R}$. From (103), the kinematic differential equation of $\hat{\mathbf{q}}_{BH}$ is given by

$$\dot{\mathbf{q}}_{BH} = \frac{1}{2}\left(q_{BH,4}I_{3x3} + q_{BH}^x\right)\boldsymbol{\omega}_{BH}$$

$$\dot{q}_{BH,4} = -\frac{1}{2}\mathbf{q}_{BH}^T\boldsymbol{\omega}_{BH} \tag{106}$$

Likewise, the constraint on the components of $\hat{\mathbf{q}}_{BH}$ hold so that (105) becomes

$$q_{BH,4}^2 = 1 - \|\mathbf{q}_{BH}\|^2 \tag{107}$$

The 3x3 rotation matrix that brings $\mathcal{H}$ onto $\mathcal{B}$ is given by

$$^B R_H = \left(q_{BH,4}^2 - \|\mathbf{q}_{BH}\|^2\right)I_{3x3} + 2\mathbf{q}_{BH}\mathbf{q}_{BH}^T - 2q_{BH,4}q_{BH}^x \tag{108}$$

so that

$$\begin{bmatrix} \hat{h}_1 \\ \hat{h}_1 \\ \hat{h}_1 \end{bmatrix} = {}^H R_B \begin{bmatrix} \hat{b}_1 \\ \hat{b}_2 \\ \hat{b}_3 \end{bmatrix} = \begin{bmatrix} R_{11} & R_{21} & R_{31} \\ R_{12} & R_{22} & R_{32} \\ R_{13} & R_{23} & R_{33} \end{bmatrix} \begin{bmatrix} \hat{b}_1 \\ \hat{b}_2 \\ \hat{b}_3 \end{bmatrix} \tag{109}$$

From (93) and (108), the angular velocity of the body-fixed frame $\mathcal{B}$ with respect to $\mathcal{H}$ expressed in $\mathcal{B}$ is therefore

$$\boldsymbol{\omega}_{BH} = \boldsymbol{\omega}_{BI} - \boldsymbol{\omega}_{HI} = \boldsymbol{\omega}_{BI} + {}^B R_H \left[0,0,\omega_0\right]^T \tag{110}$$

where $\boldsymbol{\omega}_{BH}(t) \in \mathbb{R}^3, \forall \boldsymbol{\omega}_{BH} = \left[\omega_{BH,1}, \omega_{BH,2}, \omega_{BH,3}\right]^T$.

Taking the time derivative of (110) yields

$$\dot{\mathbf{\omega}}_{BH} = \dot{\mathbf{\omega}}_{BI} + {}^{B}\dot{R}_{H}\left[0,0,\omega_{0}\right]^{T} \tag{111}$$

which, given

$$ {}^{B}\dot{R}_{H}\left[0,0,\omega_{0}\right]^{T} = \omega_{BH}^{x} R_{H}\left[0,0,\omega_{0}\right]^{T} \tag{112}$$

where $\omega_{BH}^{x} \in \mathbb{R}^{3x3}$ represents the skew-symmetric matrix

$$\omega_{BH}^{x} = \begin{bmatrix} 0 & -\omega_{BH,3} & \omega_{BH,2} \\ \omega_{BH,3} & 0 & -\omega_{BH,1} \\ -\omega_{BH,2} & \omega_{BH,1} & 0 \end{bmatrix} \tag{113}$$

yields

$$\dot{\mathbf{\omega}}_{BH} = \dot{\mathbf{\omega}}_{BI} + \omega_{BH}^{x} R_{H}\left[0,0,\omega_{0}\right]^{T} \tag{114}$$

Therefore, by substituting (96) into (114), the angular motion equations of the chaser spacecraft's body-fixed frame $\mathcal{B}$ with respect to the rotating satellite reference frame $\mathcal{H}$ expressed in $\mathcal{B}$ become

$$
\begin{aligned}
\dot{\mathbf{q}}_{BH} &= \frac{1}{2}\left(q_{BH,4}I_{3x3} + q_{BH}^{x}\right)\mathbf{\omega}_{BH} \\
\dot{q}_{BH,4} &= -\frac{1}{2}\mathbf{q}_{BH}^{T}\mathbf{\omega}_{BH} \\
\dot{\mathbf{\omega}}_{BH} &= -J^{-1}\omega_{BI}^{x}J\mathbf{\omega}_{BI} - \omega_{0}\omega_{BH}^{x}\left[R_{13},R_{23},R_{33}\right]^{T} + J^{-1}\mathbf{T}
\end{aligned} \tag{115}
$$

5.   Chaser Spacecraft Relative Motion Dynamics

From (94) and (115), the full set of equations describing the relative motion of the chaser spacecraft with respect to the rotating satellite reference frame $\mathcal{H}$ become

$$\dot{\mathbf{r}}_{BH} = \mathbf{v}_{BH}$$

$$\dot{\mathbf{v}}_{BH} = \mathbf{f}\left(\mathbf{r}_{BH}, \mathbf{v}_{BH}\right) + m^{-1}\,{}^{H}R_{B}\mathbf{F}$$

$$\dot{\mathbf{q}}_{BH} = \frac{1}{2}\left(q_{BH,4}I_{3x3} + q_{BH}^{x}\right)\boldsymbol{\omega}_{BH} \tag{116}$$

$$\dot{q}_{BH,4} = -\frac{1}{2}\mathbf{q}_{BH}^{T}\boldsymbol{\omega}_{BH}$$

$$\dot{\boldsymbol{\omega}}_{BH} = -J^{-1}\omega_{BI}^{x}J\boldsymbol{\omega}_{BI} - \omega_{0}\omega_{BH}^{x}\left[R_{13}, R_{23}, R_{33}\right]^{T} + J^{-1}\mathbf{T}$$

with $\mathbf{F}(t) \in \mathbb{R}^{3}, \forall \mathbf{F} = \left[\,{}^{B}F_{1},\,{}^{B}F_{2},\,{}^{B}F_{3}\right]^{T}$ representing the control thrust vector acting on the body-fixed frame $\mathscr{B}$ and $\,{}^{H}R_{B} = \,{}^{B}R_{H}^{T}$ representing the 3x3 rotation matrix that brings $\mathscr{B}$ onto $\mathscr{H}$.

Following Wie (1998, p. 407), the system of concern can be reduced to the twelve dimensional space through substitution of the constraint on the components of the quaternion given by (105) into (108) and (116) to yield

$$\dot{\mathbf{r}}_{BH} = \mathbf{v}_{BH}$$

$$\dot{\mathbf{v}}_{BH} = \mathbf{f}\left(\mathbf{r}_{BH}, \mathbf{v}_{BH}\right) + m^{-1}\,{}^{H}R_{B}\mathbf{F}$$

$$\dot{\mathbf{q}}_{BH} = \frac{1}{2}\left(\pm\sqrt{1 - \left\|\mathbf{q}_{BH}\right\|^{2}}I_{3x3} + q_{BH}^{x}\right)\boldsymbol{\omega}_{BH} \tag{117}$$

$$\dot{\boldsymbol{\omega}}_{BH} = -J^{-1}\omega_{BI}^{x}J\boldsymbol{\omega}_{BI} - \omega_{0}\omega_{BH}^{x}\left[R_{13}, R_{23}, R_{33}\right]^{T} + J^{-1}\mathbf{T}$$

where

$$\,{}^{B}R_{H} = \left(1 - 2\left\|\mathbf{q}_{BH}\right\|^{2}\right)I_{3x3} + 2\mathbf{q}_{BH}\mathbf{q}_{BH}^{T} \mp 2\sqrt{1 - \left\|\mathbf{q}_{BH}\right\|^{2}}\,q_{BH}^{x} \tag{118}$$

By considering a diagonal zed inertia matrix so that (98) simplifies to

$$J = \begin{bmatrix} J_{11} & 0 & 0 \\ 0 & J_{22} & 0 \\ 0 & 0 & J_{33} \end{bmatrix} \tag{119}$$

the relative motion equations described by (117) can be compactly expressed in proper control-affine form as

$$\dot{\mathbf{x}} = \mathbf{f}(\mathbf{x}) + G(\mathbf{x})\mathbf{u} \qquad (120)$$

where $\mathbf{x}(t) \in \mathbb{R}^{12}$ is the 12-dimensional state vector given by

$$\mathbf{x} = \left[x_1, x_2, x_3, ..., x_{12}\right]^T = \left[r_{BH,1}, r_{BH,2}, r_{BH,3}, q_{BH,1}, q_{BH,2}, q_{BH,3}, v_{BH,1}, v_{BH,2}, v_{BH,3}, \omega_{BH,2}, \omega_{BH,3}\right]^T (121)$$

$\mathbf{u}(t) \in \mathrm{U}^6$ is the 6-dimensional control vector given by

$$\mathbf{u} = \left[u_1, u_2, ..., u_6\right]^T = \left[{}^B F_1, {}^B F_2, {}^B F_3, {}^B T_1, {}^B T_2, {}^B T_3\right]^T \qquad (122)$$

the drift vector $\mathbf{f}(\mathbf{x}) \in \mathbb{R}^{12}$ given by

$$\mathbf{f}(\mathbf{x}) = \begin{bmatrix}
x_7 \\
x_8 \\
x_9 \\
-\dfrac{1}{2}x_6\left[x_{11} + \omega_0\left(2\eta x_4 + 2x_5 x_6\right)\right] + \dfrac{1}{2}x_5\left[x_{12} + \omega_0\left(1 - 2x_4^2 - 2x_5^2\right)\right] + \dfrac{1}{2}\eta\left[x_{10} + \omega_0\left(2x_4 x_6 - 2\eta x_5\right)\right] \\
\dfrac{1}{2}x_6\left[x_{10} + \omega_0\left(2x_4 x_6 - 2\eta x_5\right)\right] + \dfrac{1}{2}x_4\left[x_{12} + \omega_0\left(1 - 2x_4^2 - 2x_5^2\right)\right] + \dfrac{1}{2}\eta\left[x_{11} + \omega_0\left(2\eta x_4 + 2x_5 x_6\right)\right] \\
-\dfrac{1}{2}x_5\left[x_{10} + \omega_0\left(2x_4 x_6 - 2\eta x_5\right)\right] + \dfrac{1}{2}x_4\left[x_{11} + \omega_0\left(2\eta x_4 + 2x_5 x_6\right)\right] + \dfrac{1}{2}\eta\left[x_{12} + \omega_0\left(1 - 2x_4^2 - 2x_5^2\right)\right] \\
3\omega_0^2 x_1 + 2\omega_0 x_8 \\
-2\omega_0 x_7 \\
-\omega_0^2 x_3 \\
\dfrac{\left(J_{B,2} - J_{B,3}\right)}{J_{B,1}}\left[x_{12} + \omega_0\left(1 - 2x_4^2 - 2x_5^2\right)\right]\left[x_{11} + \omega_0\left(2\eta x_4 + 2x_5 x_6\right)\right] + \omega_0\left[x_{11}\left(1 - 2x_4^2 - 2x_5^2\right) - x_{12}\left(2\eta x_4 + 2x_5 x_6\right)\right] \\
\dfrac{\left(J_{B,3} - J_{B,1}\right)}{J_{B,2}}\left[x_{12} + \omega_0\left(1 - 2x_4^2 - 2x_5^2\right)\right]\left[x_{10} + \omega_0\left(2x_4 x_6 - 2\eta x_5\right)\right] + \omega_0\left[x_{12}\left(2x_4 x_6 - 2\eta x_5\right) - x_{10}\left(1 - 2x_4^2 - 2x_5^2\right)\right] \\
\dfrac{\left(J_{B,1} - J_{B,2}\right)}{J_{B,3}}\left[x_{11} + \omega_0\left(2\eta x_4 + 2x_5 x_6\right)\right]\left[x_{10} + \omega_0\left(2x_4 x_6 - 2\eta x_5\right)\right] + \omega_0\left[x_{10}\left(2\eta x_4 + 2x_5 x_6\right) - x_{11}\left(2x_4 x_6 - 2\eta x_5\right)\right]
\end{bmatrix}$$

$$(123)$$

where $\eta = \pm\sqrt{1 - \|\mathbf{q}_{BH}\|}$ and the control matrix $G(\mathbf{x}) \in \mathbb{R}^{12 \times 6}$ given by

$$G(\mathbf{x}) = \begin{bmatrix} 0_{6x6} \\ G_1(\mathbf{x}) \end{bmatrix} \tag{124}$$

where $G_1(\mathbf{x}) \in \mathbb{R}^{6x6}$ represents the control distribution matrix given the placement of the control inputs with respect to the spacecraft's mass center. For the ideal case, where each thrust vector is parallel to its corresponding body-fixed axis acting through the spacecraft's mass center and three independent paired thrusters provide torque about their corresponding body-fixed axes, $G_1(\mathbf{x})$ becomes

$$G_1(\mathbf{x}) = \begin{bmatrix} m^{-1}\,{}^H R_B & 0_{3x3} \\ 0_{3x3} & J^{-1} \end{bmatrix} \tag{125}$$

B.   SMALL-TIME LOCAL CONTROLLABILITY CONSIDERATIONS FOR THE PROPOSED 6-DOF SPACECRAFT DESIGN

Small-time local controllability for the 6-DoF nonlinear equations representing the relative motion of a chaser spacecraft given by (120) can be determined following the same methods as presented in Chapter II for the 3-DoF spacecraft simulator. In order to properly deal with the momentum of the drift vector term $\mathbf{f}(\mathbf{x})$, the analysis of small-time local controllability is performed at the equilibrium point corresponding to $\mathbf{f}(\mathbf{p}) = \mathbf{0}$ or

$$\mathbf{p} = [0, x_2, 0, 0, 0, 0, 0, 0, 0, 0, 0, 0]^T \tag{126}$$

By varying the control vector $\mathbf{u}$, the minimum number of control actuators for the system can be gained. In order to consider a general case, the thrust vector in the $\hat{b}_1$ direction is defined as ${}^B F_1$ and is taken to be directed through the spacecraft's mass center so that no torque is imparted on the body; the thrust vector parallel to the $\hat{b}_2$ axis is defined as ${}^B F_{2,rot3}$ and is taken to be a distance L from the spacecraft's mass center along the $\hat{b}_1$ axis so that both a force is imparted in the $\hat{b}_2$ direction as well as a torque about

the $\hat{b}_3$ axis; and the thrust vector parallel to the $\hat{b}_3$ axis is defined as $^BF_{3,rot2}$ and is also

taken to be a distance L from the spacecraft's mass center along the $\hat{b}_1$ axis so that both

a force is imparted in the $\hat{b}_3$ direction as well as a torque about the $\hat{b}_2$ axis. Additionally,

the effects of pure control torques are considered. Each torque is assumed to provide a

pure torque about its corresponding body-fixed axis so that $^BT_1$ represents a torque

about $\hat{b}_1$, $^BT_2$ represents a torque about $\hat{b}_2$, and $^BT_3$ represents a torque about $\hat{b}_3$. In this

manner, a small-time local controllability analysis is conducted on variations of the

control vector $\mathbf{u}(t) \in U^6, \forall \mathbf{u} = \begin{bmatrix} ^BF_1, {}^BF_{2/rot3}, {}^BF_{3/rot2}, {}^BT_1, {}^BT_2, {}^BT_3 \end{bmatrix}$ such that the

corresponding vectors of the associated control distribution matrix $G_1(\mathbf{x})$ are:

$$^BF_1 \rightarrow \mathbf{g}(\mathbf{x}) = \begin{bmatrix} m^{-1}R_{11}, m^{-1}R_{12}, m^{-1}R_{13}, 0, 0, 0 \end{bmatrix}^T \tag{127}$$

$$^BF_{2/rot3} \rightarrow \mathbf{g}(\mathbf{x}) = \begin{bmatrix} m^{-1}R_{21}, m^{-1}R_{22}, m^{-1}R_{23}, 0, 0, LJ_3^{-1} \end{bmatrix}^T \tag{128}$$

$$^BF_{3/rot2} \rightarrow \mathbf{g}(\mathbf{x}) = \begin{bmatrix} m^{-1}R_{31}, m^{-1}R_{32}, m^{-1}R_{33}, 0, LJ_2^{-1}, 0 \end{bmatrix}^T \tag{129}$$

$$^BT_1 \rightarrow \mathbf{g}(\mathbf{x}) = \begin{bmatrix} 0, 0, 0, LJ_1^{-1}, 0, 0 \end{bmatrix}^T \tag{130}$$

$$^BT_2 \rightarrow \mathbf{g}(\mathbf{x}) = \begin{bmatrix} 0, 0, 0, 0, LJ_2^{-1}, 0 \end{bmatrix}^T \tag{131}$$

$$^BT_3 \rightarrow \mathbf{g}(\mathbf{x}) = \begin{bmatrix} 0, 0, 0, 0, 0, LJ_3^{-1} \end{bmatrix}^T \tag{132}$$

The results of this investigation, which are summarized in Table 5, demonstrate

that the minimum number of actuators for small-time local controllability of the relative

motion spacecraft dynamics defined by (117) include one thrust vector acting through the

spacecraft's center of mass and two body-fixed control torques. This combination can be

achieved by considering a total of six control actuators with two fixed thrusters mounted

on opposite faces of the spacecraft with their thrust vectors acting in an opposing manner

along the $\hat{b}_1$ axis through the spacecraft's center of mass and two sets of fixed paired

thrusters acting together to produce pure torque about two of the body-fixed axes. For instance, by considering the control vector $\mathbf{u}(t) \in \mathrm{U}^3, \forall \mathbf{u} = \begin{bmatrix} {}^B F_1, {}^B T_2, {}^B T_3 \end{bmatrix}$ and the corresponding control distribution matrix $G_1(\mathbf{x}) \in \mathbb{R}^{6x3}$

$$G_1(\mathbf{x}) = [\mathbf{g}_1, \mathbf{g}_2, \mathbf{g}_3] = \begin{bmatrix} m^{-1}R_{11} & 0 & 0 \\ m^{-1}R_{12} & 0 & 0 \\ m^{-1}R_{13} & 0 & 0 \\ 0 & 0 & 0 \\ 0 & LJ_{22}^{-1} & 0 \\ 0 & 0 & LJ_{33}^{-1} \end{bmatrix} \tag{133}$$

the Lie Algebra evaluates to:

$$\mathcal{L}(\Delta) = span \left\{ \begin{array}{l} \mathbf{g}_1, \mathbf{g}_2, \mathbf{g}_3, [\mathbf{f}, \mathbf{g}_1], [\mathbf{f}, \mathbf{g}_2], [\mathbf{f}, \mathbf{g}_3], [\mathbf{f}, [\mathbf{f}, \mathbf{g}_1]], [\mathbf{f}, [\mathbf{f}, \mathbf{g}_2]], \\ [\mathbf{g}_1, [\mathbf{f}, \mathbf{g}_2]], [\mathbf{g}_1, [\mathbf{f}, \mathbf{g}_3]], [\mathbf{g}_2, [\mathbf{f}, \mathbf{g}_3]] [\mathbf{f}, [\mathbf{f}, [\mathbf{f}, \mathbf{g}_1]]] \end{array} \right\} \tag{134}$$

However, by considering the vectorable thruster depicted in Figure 13, only two control actuators are required to achieve small-time local controllability of the relative motion spacecraft dynamics given by (117). This can be achieved by placing each hemispherically vectorable thruster a distance L from the spacecraft's center of mass along the $\hat{b}_1$ axis. For this configuration, the control vector $\mathbf{u}(t) \in \mathrm{U}^3, \forall \mathbf{u} = \begin{bmatrix} {}^B F_1, {}^B F_{2/rot3}, {}^B F_{3/rot2} \end{bmatrix}$ is considered with the corresponding control distribution matrix $G_1(\mathbf{x}) \in \mathbb{R}^{6x3}$

$$G_1(\mathbf{x}) = [\mathbf{g}_1, \mathbf{g}_2, \mathbf{g}_3] = \begin{bmatrix} m^{-1}R_{11} & m^{-1}R_{21} & m^{-1}R_{31} \\ m^{-1}R_{12} & m^{-1}R_{22} & m^{-1}R_{32} \\ m^{-1}R_{13} & m^{-1}R_{23} & m^{-1}R_{33} \\ 0 & 0 & 0 \\ 0 & 0 & LJ_{22}^{-1} \\ 0 & LJ_{33}^{-1} & 0 \end{bmatrix} \tag{135}$$

yielding a Lie Algebra for this minimally configured system of

69

$$\mathcal{L}(\Delta) = span \left\{ \begin{matrix} \mathbf{g}_1, \mathbf{g}_2, \mathbf{g}_3, [\mathbf{f}, \mathbf{g}_1], [\mathbf{f}, \mathbf{g}_2], [\mathbf{f}, \mathbf{g}_3], [\mathbf{f}, [\mathbf{f}, \mathbf{g}_1]], [\mathbf{f}, [\mathbf{f}, \mathbf{g}_2]], \\ [\mathbf{g}_1, [\mathbf{f}, \mathbf{g}_3]], [\mathbf{g}_2, [\mathbf{f}, \mathbf{g}_3]], [\mathbf{f}, [\mathbf{g}_1, [\mathbf{f}, \mathbf{g}_3]]], [\mathbf{f}, [\mathbf{g}_2, [\mathbf{f}, \mathbf{g}_3]]] \end{matrix} \right\} \quad (136)$$

Control Inputs	$\dim(\mathcal{L}(\Delta))$	Controllability
${}^B F_1 \; or \; {}^B F_{2/rot3} \; or \; {}^B F_{3/rot2}$	3	Inaccessible
$\left({}^B F_1, {}^B F_{2/rot3} \right), \left({}^B F_1, {}^B F_{3/rot2} \right)$	6	Inaccessible
$\left({}^B F_1, T_1 \right)$	8	Inaccessible
$\left({}^B F_1, T_2 \right), \left({}^B F_1, T_3 \right), \left({}^B F_{3/rot2}, T_2 \right), \left({}^B F_{2/rot3}, T_3 \right),$ $\left({}^B F_{3/rot2}, T_3 \right) or \left({}^B F_{2/rot3}, T_2 \right)$	9	Inaccessible
$\left({}^B F_{2/rot3}, {}^B F_{3/rot2} \right), \left({}^B F_{2/rot3}, T_1 \right) or \left({}^B F_{3/rot2}, T_1 \right)$	10	Inaccessible
$\left({}^B F_1, {}^B T_1, {}^B T_2 \right), \left({}^B F_1, {}^B T_1, {}^B T_3 \right) or \left({}^B F_1, {}^B T_2, {}^B T_3 \right)$	12	STLC
${}^B F_1, {}^B F_{2/rot3}, {}^B F_{3/rot2}$	12	STLC

Table 5.　　　STLC Analysis for the 6-DoF Relative Motion Spacecraft Dynamics

C.　PROPOSED FEEDBACK LINEARIZABLE SPACECRAFT SYSTEM DESIGN WITH MINIMUM NUMBER OF CONTROL ACTUATORS

In the previous section, a full analysis of the small-time controllability for a spacecraft with variations on the control inputs was conducted. This analysis yielded two satisfactory variations in control inputs for small-time local controllability: a set of six control actuators consisting of two opposing fixed thrusters acting through the spacecraft's center aligned with one of the three body-fixed axes and two sets of paired thrusters acting about two of the three body-fixed axes or a set of two control actuators consisting of oppositely mounted hemispherically vectorable thrusters. From this analysis, a unique spacecraft control actuator configuration is proposed that leverages this study to provide a feedback linearizable system as might be necessary in a path or sensor constrained environment. As stated in Section II, in order for a system to be state-feedback linearizable, it must be square so that the number of actuators is equal to the number of observed states. From this, the number of observed states and number of control inputs are assumed to be six and a novel minimally actuated system is proposed consisting of a total of four thrusters. Figure 14 graphically depicts the forces acting

upon the body-fixed frame $\mathscr{B}$ through two hemispherically vectorable oppositely mounted thrust vectors $\mathbf{F}_a \in \mathbb{R}^3$ and $\mathbf{F}_b \in \mathbb{R}^3$ and a set of paired thrusters acting about the $\hat{b}_1$ axis to impart the torque $T_c \in \mathbb{R}$.
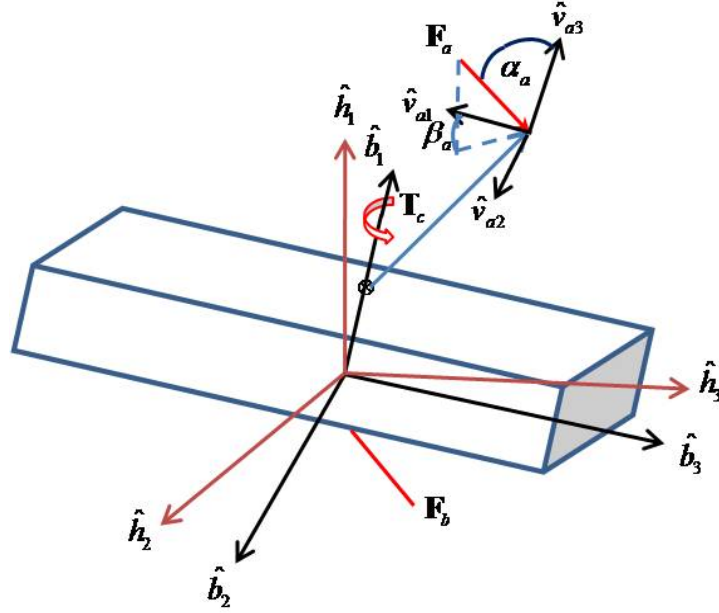
Figure 14.   6-DoF Minimally Actuated Feedback Linearizable Spacecraft
Configuration

In order to properly resolve $\mathbf{F}_a$ and $\mathbf{F}_b$ into $\mathscr{B}$, the vectorable thruster frame $\mathscr{V}_i$ is established with orthogonal axes defined by the set of unit vectors $\{\hat{v}_{i1}, \hat{v}_{i2}, \hat{v}_{i3}\}$ where $i = a, b$ corresponding to either $\mathbf{F}_a$ or $\mathbf{F}_b$. Both axes $\hat{v}_{a2}$ and $\hat{v}_{a2}$ are taken to be collinear with the $\hat{b}_2$ axis. Additionally, the $\hat{v}_{a3}$ axis is taken to be aligned with the $\hat{b}_1$ axis with $\hat{v}_{a3} = \hat{b}_1$ while the $\hat{v}_{b3}$ axis is taken to be aligned with $\hat{b}_1$ with $\hat{v}_{b3} = -\hat{b}_1$. The coordinates of the imparted force vector, as depicted in Figure 14, is defined in the thruster frame through two angles α_i and β_i, referred to as the polar and azimuthal angles, respectively. The azimuthal angle α_i is the angle between the axis of the imparted thrust vector and the $\hat{v}_{i3}$ unit vector and is limited to the range $[0, \pi/2]$. The

polar angle is defined as the angle between the $\hat{v}_{i1}$ and the projection of the thrust vector $\mathbf{F}_i$ onto the $\{\hat{v}_{i1}, \hat{v}_{i2}\}$ plane. In this manner,

$$^{V}\mathbf{F}_{a} = -F_{a}\left[\sin\alpha_{a}\cos\beta_{a}, \sin\alpha_{a}\sin\beta_{a}, \cos\alpha_{a}\right]^{T} \tag{137}$$

and

$$^{V}\mathbf{F}_{b} = -F_{b}\left[\sin\alpha_{b}\cos\beta_{b}, \sin\alpha_{b}\sin\beta_{b}, \cos\alpha_{b}\right]^{T} \tag{138}$$

The 3x3 rotation matrices that bring $\mathcal{V}_i$ onto $\mathcal{B}$ are then

$$^{B}R_{V_{a}} = \begin{bmatrix} 0 & 0 & 1 \\ 0 & 1 & 0 \\ -1 & 0 & 0 \end{bmatrix} \tag{139}$$

and

$$^{B}R_{V_{b}} = \begin{bmatrix} 0 & 0 & -1 \\ 0 & 1 & 0 \\ 1 & 0 & 0 \end{bmatrix} \tag{140}$$

In this manner, the hemispherically vectorable thrust vectors can be expressed in the body-fixed frame $\mathcal{B}$ as

$$^{B}\mathbf{F}_{a} = -F_{a}\left[\cos\alpha_{a}, \sin\alpha_{a}\sin\beta_{a}, -\sin\alpha_{a}\cos\beta_{a}\right]^{T} \tag{141}$$

and

$$^{B}\mathbf{F}_{b} = -F_{b}\left[-\cos\alpha_{b}, \sin\alpha_{b}\sin\beta_{b}, \sin\alpha_{b}\cos\beta_{b}\right]^{T} \tag{142}$$

yielding the thrust vector given in (117) by $\mathbf{F}(t) \in \mathbb{R}^{3}, \forall \mathbf{F} = {}^{B}\mathbf{F}_{a} + {}^{B}\mathbf{F}_{b}$.

The torque vector in (117) given by $\mathbf{T} \in \mathbb{R}^{3}$ can be resolved as

$$\mathbf{T} = \begin{bmatrix} T_c \\ -F_a \sin\alpha_a \cos\beta_a - F_b \sin\alpha_b \cos\beta_b \\ -F_a \sin\alpha_a \sin\beta_a + F_b \sin\alpha_b \sin\beta_b \end{bmatrix} \tag{143}$$

Defining the control inputs as such yields the control vector $\mathbf{u}(t) \in \mathrm{U}^6, \forall \mathbf{u} = \begin{bmatrix} {}^B F_1, {}^B F_{2/rot3}, {}^B F_{3/rot2}, {}^B T_1, {}^B T_2, {}^B T_3 \end{bmatrix}$ and corresponding control distribution matrix $G_1(\mathbf{x}) \in \mathbb{R}^{6x6}$

$$G_1(\mathbf{x}) = \begin{bmatrix} m^{-1}R_{11} & m^{-1}R_{21} & m^{-1}R_{31} & 0 & m^{-1}R_{31} & m^{-1}R_{21} \\ m^{-1}R_{12} & m^{-1}R_{22} & m^{-1}R_{32} & 0 & m^{-1}R_{32} & m^{-1}R_{22} \\ m^{-1}R_{13} & m^{-1}R_{23} & m^{-1}R_{33} & 0 & m^{-1}R_{33} & m^{-1}R_{23} \\ 0 & 0 & 0 & dJ_{11}^{-1} & 0 & 0 \\ 0 & 0 & dJ_{22}^{-1} & 0 & -dJ_{22}^{-1} & 0 \\ 0 & -dJ_{33}^{-1} & 0 & 0 & 0 & dJ_{33}^{-1} \end{bmatrix} \tag{144}$$

The components R_{ij} represent the entries in the corresponding i-th row and j-th column of ${}^H R_B$ as defined by (109) and the variable d is defined similar to what is proposed for the 3-DoF spacecraft simulator presented in Chapter II whereby the control variables are defined given a desired control input to the system with respect to $\hat{b}_1$. Thus if

$$
\begin{aligned}
{}^B U_1 \le 0 \to &\begin{cases} d = -L \\ {}^B F_1 = -F_a \cos\alpha_a, \; {}^B F_{2/rot3} = -F_a \sin\alpha_a \sin\beta_a, \; {}^B F_{3/rot2} = F_a \sin\alpha_a \cos\beta_a \\ {}^B T_1 = T_c, \; {}^B T_2 = -F_b \sin\alpha_b \cos\beta_b, \; {}^B T_3 = -F_b \sin\alpha_b \sin\beta_b \end{cases} \\
{}^B U_1 > 0 \to &\begin{cases} d = L \\ {}^B F_1 = F_b \cos\alpha_b, \; {}^B F_{2/rot3} = -F_b \sin\alpha_b \sin\beta_b, \; {}^B F_{3/rot2} = -F_b \sin\alpha_b \cos\beta_b \\ {}^B T_1 = -T_c, \; {}^B T_2 = F_a \sin\alpha_a \cos\beta_a, \; {}^B T_3 = -F_a \sin\alpha_a \sin\beta_a \end{cases}
\end{aligned} \tag{145}
$$

1.   Smooth Feedback Control via State Feedback Linearization

The methodology presented in (62) through (65) can be used to demonstrate that the nonlinear relative motion dynamics given by (117) are state feedback linearizable. With the nonlinear relative motion dynamics expressed in control-affine form given by

(120) with $G_1(\mathbf{x})$ defined by (144), the matrix $E(\mathbf{x})$ as defined by (63) is invertible and the relative degree of the system at the equilibrium point $\mathbf{p}$ is $(r_1, r_2, r_3, r_4, r_5, r_6) = (2, 2, 2, 2, 2, 2)$. Therefore, the total relative degree of the system is twelve. Given that the total relative degree of the system is equal to the number of states, the nonlinear system can be fully linearized by state feedback to yield smooth feedback control. If we choose

$$\mathbf{h}(\mathbf{x}) = \left[\mathbf{h}_1(\mathbf{x}), \mathbf{h}_2(\mathbf{x})\right]^T = \left[\left[x_1, x_2, x_3\right], \left[x_4, x_5, x_6\right]\right]^T = \left[\mathbf{r}_{BH}, \mathbf{q}_{BH}\right]^T \tag{146}$$

the state transformation can be chosen as

$$\begin{aligned}
\mathbf{z} &= \left[\mathbf{h}_1(\mathbf{x}), \mathbf{h}_2(\mathbf{x}), L_\mathbf{f}\mathbf{h}_1(\mathbf{x}), L_\mathbf{f}\mathbf{h}_2(\mathbf{x})\right]^T \\
&= \left[\mathbf{r}_{BH}, \mathbf{q}_{BH}, \mathbf{v}_{BH}, \frac{1}{2}\left(\pm\sqrt{1 - \|\mathbf{q}_{BH}\|^2}\, I_{3x3} + q_{BH}^x\right)\boldsymbol{\omega}_{BH}\right]^T
\end{aligned} \tag{147}$$

That is

$$\begin{aligned}
\mathbf{r}_{BH} &= \mathbf{z}_1 \\
\mathbf{q}_{BH} &= \mathbf{z}_2 \\
\mathbf{v}_{BH} &= \mathbf{z}_3 \\
\boldsymbol{\omega}_{BH} &= Q^{-1}\mathbf{z}_4 \\
\boldsymbol{\omega}_{BI} &= Q^{-1}\mathbf{z}_4 + {}^B R_H \left[0, 0, \omega_0\right]^T
\end{aligned} \tag{148}$$

where $\mathbf{z}_1 \in \mathbb{R}^3, \mathbf{z}_2 \in \mathbb{R}^3, \mathbf{z}_3 \in \mathbb{R}^3, \mathbf{z}_4 \in \mathbb{R}^3$ are new state variables and $Q \in \mathbb{R}^{3x3}$ is given by

$$Q = \left[\frac{1}{2}\left(\pm\sqrt{1 - \|\mathbf{q}_{BH}\|^2}\, I_{3x3} + q_{BH}^x\right)\right] \tag{149}$$

and the system is transformed into

$$\dot{\mathbf{z}}_1 = \mathbf{z}_3$$

$$\dot{\mathbf{z}}_2 = \mathbf{z}_4$$

$$\dot{\mathbf{z}}_3 = \mathbf{f}(\mathbf{z}_1, \mathbf{z}_3) + {}^H R_B \mathbf{F}$$

$$\dot{\mathbf{z}}_4 = \dot{Q} Q^{-1} \mathbf{z}_4 + Q \left\{ \begin{array}{l} J^{-1} S\left(Q^{-1}\mathbf{z}_4 + {}^B R_H \left[0,0,\omega_0\right]^T\right) J\left(Q^{-1}\mathbf{z}_4 + {}^B R_H \left[0,0,\omega_0\right]^T\right) + \\ S\left(Q^{-1}\mathbf{z}_4\right) {}^B R_H \left[0,0,\omega_0\right]^T + J^{-1}\mathbf{T} \end{array} \right\}$$

(150)

where $S(\bullet)$ represents the skew-symmetric matrix of $\bullet$.

The relative motion dynamics given by (117) can now be transformed via (150) and the state feedback control law

$$\left[\mathbf{F}, \mathbf{T}\right]^T = E(\mathbf{x})^{-1}(\mathbf{v} - \mathbf{b})$$

(151)

into the linear system

$$\dot{\mathbf{z}} = \begin{bmatrix} 0_{6x6} & I_{6x6} \\ 0_{6x6} & 0_{6x6} \end{bmatrix} \mathbf{z} + \begin{bmatrix} 0_{6x6} \\ I_{6x6} \end{bmatrix} \mathbf{v}$$

(152)

where $E(\mathbf{x}) \in \mathbb{R}^{6x6} = L_G L_f \mathbf{h}(\mathbf{x}), \mathbf{b} \in \mathbb{R}^6 = L_f^2 \mathbf{h}(\mathbf{x})$ and $\mathbf{v}(t) \in \mathbb{R}^6, \forall \mathbf{v} = \left[\mathbf{v}_1, \mathbf{v}_2\right]^T$.

With the system now in linear form, traditional linear control techniques such as the linear quadratic regulator as presented in Chapter II can be used to stabilize it to a desired state.

2. Determination of the Commanded Azimuthal and Polar Thruster Angles

Using the decoupling law as expressed in (151), the commanded azimuthal and polar angles for the hemispherically vectorable thrusters and the required torque for the paired thrusters can be determined. For example, if ${}^B U_1 > 0$ with the azimuthal angle $0 \le \alpha_b \le \pi/2$ and the polar angle $0 \le \beta_b \le 2\pi$, the angles to slew thruster b can be resolved as

$$\alpha_b = \tan^{-1}\left(\frac{{}^B F_1}{\sqrt{{}^B F_{2/rot3}^2 + {}^B F_{3/rot2}^2}}\right) \tag{153}$$

$$\beta_b = \text{atan2}\left({}^B F_{2/rot3}, {}^B F_{3/rot2}\right) \tag{154}$$

and the required thrust as

$$^B F_b = \sqrt{{}^B F_1^2 + {}^B F_{2/rot3}^2 + {}^B F_{3/rot2}^2} \tag{155}$$

The angles to slew thruster a can be resolved as

$$\alpha_a = \frac{\pi}{2} \tag{156}$$

$$\beta_a = \text{atan2}\left({}^B T_3, {}^B T_2\right) \tag{157}$$

and the required thrust as

$$^B F_a = \sqrt{{}^B T_2^2 + {}^B T_3^2} \tag{158}$$

Likewise, for the case where ${}^B U_1 \leq 0$ with the azimuthal angle $0 \leq \alpha_b \leq \pi/2$ and the polar angle $0 \leq \beta_b \leq 2\pi$, the angles to slew thruster a can be resolved as

$$\alpha_a = \tan^{-1}\left(\frac{-{}^B F_1}{\sqrt{{}^B F_{2/rot3}^2 + {}^B F_{3/rot2}^2}}\right) \tag{159}$$

$$\beta_b = \text{atan2}\left({}^B F_{2/rot3}, -{}^B F_{3/rot2}\right) \tag{160}$$

and the required thrust as

$$^B F_b = \sqrt{{}^B F_1^2 + {}^B F_{2/rot3}^2 + {}^B F_{3/rot2}^2} \tag{161}$$

The angles to slew thruster b can be resolved as

$$\alpha_b = \frac{\pi}{2} \tag{162}$$

$$\beta_a = \text{atan2}\left({}^BT_3, {}^BT_2\right) \tag{163}$$

and the required thrust as

$$^BF_b = \sqrt{{}^BT_2^2 + {}^BT_3^2} \tag{164}$$

THIS PAGE INTENTIONALLY LEFT BLANK

IV. QUATERNION FEEDBACK ATTITUDE REGULATION OF UNDERACTUATED RIGID SPACECRAFT

Methods of providing three-axis stabilization via two body-fixed control torques are introduced in this chapter. The current state-of-the-art in three-axis stabilization for a rigid spacecraft with arbitrary inertia via two body-fixed control torques is limited to rate stabilization followed by three sequential Euler angle rotations or time-varying attitude control based on a variety of switching logics. Byrnes and Isidori (1991) demonstrated that for the full underactuated rigid spacecraft system of angular motion equations, a smooth, time-invariant state feedback control can be designed to locally stabilize the spacecraft with a revolute motion about the unactuated axis. Without violating their assertion, this chapter introduces a novel, time-invariant smooth state feedback controller based on generalized inverse methods and quaternion kinematics to obtain simultaneous attitude stabilization to an arbitrarily small region of the zero error state with two bounded body-fixed control torques for an asymmetric spacecraft. This smooth state feedback controller will be shown to be most naturally suited to either rest to rest reorientation maneuvers or detumbling and reorientation maneuvers. It is not applicable for attitude mainentenance for attitude tracking or in the presence of large disturbance torques as a perturbation is imparted about the unactuated axis through the interactions between the two actuated axes to stabilize the attitude to a desired orientation. This chapter provides two key contributions: First, the method of generalized inverse control is extended from a study of only the dynamics as considered by Bajodah (2009b) to the full system of dynamic and kinematic equations. Second, two separate null-control vector designs are derived for the proposed quaternion feedback regulator which capitalize on the generalized inverse control methodology. The first design is Lyapunov function based and is conjectured to yield global stability but results in significant control effort noise near an inherent singularity in the null-control vector. The second design is based on perturbed feedback linearization and provides local stability while keeping the control effort to low levels. In addition to formal proofs for each control design, simulation results are provided to demonstrate the capabilities of these novel controllers.

79

A. UNDERACTUATED RIGID SPACECRAFT REORIENTATION THROUGH QUATERNION FEEDBACK

In this section, the general case of an underactuated rigid spacecraft being rotated by two body-fixed control torques is considered. In order to simplify the problem, an ideal control torque is assumed. The rotational motion and quaternion kinematic representation of the orientation of the rigid body remain as developed in Section III for the general case of the body-fixed frame $\mathcal{B}$ with respect to an inertial frame $\mathcal{I}$. In summary, these are:

$$
\begin{aligned}
\dot{\boldsymbol{\omega}}_{BI} &= -J^{-1}\omega_{BI}^{x}J\boldsymbol{\omega}_{BI} + J^{-1}\mathbf{T} \\
\dot{\mathbf{q}}_{BI} &= \frac{1}{2}\left(q_{BI,4}I_{3x3} + q_{BI}^{x}\right)\boldsymbol{\omega}_{BI} \\
\dot{q}_{BI,4} &= -\frac{1}{2}\mathbf{q}_{BI}^{T}\boldsymbol{\omega}_{BI}
\end{aligned}
\tag{165}
$$

1. Attitude Error Parameterization via Quaternions

The 3x3 rotation matrix that brings $\mathcal{I}$ onto $\mathcal{B}$ is given by

$$
{}^{B}R_{I} = \left(q_{BI,4}^{2} - \mathbf{q}_{BI}^{T}\mathbf{q}_{BI}\right)I_{3x3} + 2\mathbf{q}_{BI}\mathbf{q}_{BI}^{T} - 2q_{BI4}q_{BI}^{x}
\tag{166}
$$

Similarly, the desired attitude of the spacecraft can be described by a desired, body-fixed frame $\mathcal{B}_d$ with respect to $\mathcal{I}$. In this manner, the attitude is parameterized by considering a desired unit quaternion $\hat{\mathbf{q}}_{B_dI}(t) = \left\{\mathbf{q}_{B_dI}(t), q_{B_d1,4}(t)\right\} \in \mathbb{R}^{3}x\mathbb{R}$ where the constraint of (105) holds. Therefore, the 3x3 rotation matrix that brings $\mathcal{I}$ onto $\mathcal{B}_d$ can be defined as

$$
{}^{B_d}R_{I} = \left(q_{B_dI,4}^{2} - \mathbf{q}_{B_dI}^{T}\mathbf{q}_{B_dI}\right)I_{3x3} + 2\mathbf{q}_{B_dI}\mathbf{q}_{B_dI}^{T} - 2q_{B_dI,4}q_{B_dI}^{x}
\tag{167}
$$

and from (108) and (167), the 3x3 rotation matrix that brings $\mathcal{B}_d$ onto $\mathcal{B}$ is therefore

$$
{}^{B}R_{B_d} = {}^{B}R_{I}\,{}^{B_d}R_{I}^{T} = \left(q_{B_dB,4}^{2} - \mathbf{q}_{B_dB}^{T}\mathbf{q}_{B_dB}\right)I_{3x3} + 2\mathbf{q}_{B_dB}\mathbf{q}_{B_dB}^{T} - 2q_{B_dB,4}q_{B_dB}^{x}
\tag{168}
$$

where the quaternion error vector $\hat{\mathbf{q}}_{B_dB}(t) = \{\mathbf{q}_{B_dB}(t), q_{B_dB,4}(t)\} \in \mathbb{R}^3 x\mathbb{R}$ is defined by Behal et al. (2002) as

$$\mathbf{q}_{B_dB} = q_{B_dI,4}\mathbf{q}_{BI} - q_{B_dI,4}\mathbf{q}_{B_dI} + q_{BI}^x\mathbf{q}_{B_dI}$$
$$q_{B_dB} = q_{BI,4}q_{B_dI,4} + \mathbf{q}_{BI}^T\mathbf{q}_{B_dI} \tag{169}$$

The error quaternion kinematic differential equation then becomes

$$\dot{\mathbf{q}}_{B_dB} = \frac{1}{2}\left(q_{B_dB,4}I_{3x3} + q_{B_dB}^x\right)\boldsymbol{\omega}_{BI}$$
$$\dot{q}_{B_dB} = -\frac{1}{2}\mathbf{q}_{B_dB}^T\boldsymbol{\omega}_{BI} \tag{170}$$

with $\boldsymbol{\omega}_{BI} = \boldsymbol{\omega}_{B_dB}$ considering a rest-to-rest maneuver where $\boldsymbol{\omega}_{B_dI} = \mathbf{0}_{3x1}$. For simplicity, the components of $\hat{\mathbf{q}}_{B_dB}$ will be referred to as $\hat{\mathbf{q}}_{B_dB} = \{q_1, q_2, q_3, q_4\}$ for the remainder of this chapter. The full rigid spacecraft system of angular motion equations considering the error quaternion kinematics can be expressed as

$$\dot{\mathbf{q}}_{B_dB} = \frac{1}{2}\left(q_{B_dB,4}I_{3x3} + q_{B_dB}^x\right)\boldsymbol{\omega}_{BI}$$
$$\dot{q}_{B_dB} = -\frac{1}{2}\mathbf{q}_{B_dB}^T\boldsymbol{\omega}_{BI} \tag{171}$$
$$\dot{\boldsymbol{\omega}}_{BI} = -J^{-1}\omega_{BI}^x J\boldsymbol{\omega}_{BI} + J^{-1}\mathbf{T}$$

2. Underactuated Rigid Spacecraft with Two Control Torques

In considering an underactuated rigid spacecraft with only two independent control torques, the unactuated axis can be taken to be $\mathscr{B}_1$ without loss of generality and (96) can be rewritten as

$$\dot{\boldsymbol{\omega}}_{BI} = F(\boldsymbol{\omega}_{BI})\boldsymbol{\omega}_{BI} + \boldsymbol{\tau} \tag{172}$$

where $\boldsymbol{\tau}(t) \in \mathbb{R}^3, \forall \boldsymbol{\tau} = J^{-1}\mathbf{T} = [0, \mathbf{u}]^T$ is the scaled control vector with $\mathbf{u}(t) \in \mathrm{U}^2, \forall \mathbf{u} = [u_2, u_3]^T$ and $F(\boldsymbol{\omega}) \in \mathbb{R}^{3x3}$ denotes the drift matrix

$$F\left(\boldsymbol{\omega}_{BI}\right) = -J^{-1}\omega_{BI}^{x}J \tag{173}$$

In this manner, the full underactuated rigid spacecraft system of angular motion equations become

$$\dot{\mathbf{q}}_{B_dB} = \frac{1}{2}\left(q_{B_dB,4}I_{3x3} + q_{B_dB}^{x}\right)\boldsymbol{\omega}_{BI}$$

$$\dot{q}_{B_dB} = -\frac{1}{2}\mathbf{q}_{B_dB}^{T}\boldsymbol{\omega}_{BI} \tag{174}$$

$$\dot{\boldsymbol{\omega}}_{BI} = F\left(\boldsymbol{\omega}_{BI}\right)\boldsymbol{\omega}_{BI} + \boldsymbol{\tau}$$

(174) can be written in control-affine form as

$$\dot{\mathbf{x}} = f\left(\mathbf{x}\right) + G\left(\mathbf{x}\right)\mathbf{u} = F\left(\mathbf{x}\right)\boldsymbol{\omega}_{BI} + G\mathbf{u} \tag{175}$$

with state vector $\mathbf{x}(t) \in \mathbb{R}^6 x\mathbb{R}$, $\forall \mathbf{x} = \left[q_1, q_2, q_3, q_4, \omega_1, \omega_2, \omega_3\right]^T$, control vector $\mathbf{u}(t) \in \mathbb{R}^2$, $\forall \mathbf{u} = \left[u_1, u_2\right]^T$, drift matrix $F\left(\mathbf{x}\right) \in \mathbb{R}^{7x3}$ given by

$$F\left(\mathbf{x}\right) = \begin{bmatrix} \frac{1}{2}\left(q_4 I_{3x3} + q_{B_dB}^{x}\right) \\ -\frac{1}{2}\mathbf{q}_{B_dB}^{T} \\ -J^{-1}\omega_{BI}^{x}J \end{bmatrix} \tag{176}$$

and control matrix $G \in \mathbb{R}^{7x2}$ given by

$$G = \begin{bmatrix} 0_{5x2} \\ I_{2x2} \end{bmatrix} \tag{177}$$

Furthermore, (175) can be split into two coupled differential subsystems of concern; the first coupled subsystem combines the unactuated dynamics with the unactuated quaternion kinematic component, while the second considers the remaining two quaternion kinematic components. Both of these systems are indirectly controlled through the action of the angular velocity components about the actuated body-fixed

82

axes. The third subsystem considers the actuated dynamics. In fact, although global asymptotic stability cannot be achieved without unbounded control, the full system of underactuated rigid spacecraft equations of angular motion can be stabilizable to an arbitrarily small region about the equilibrium of the system via time-invariant smooth state feedback control by considering a damping coefficient to ensure the generalized inverse of the controls coefficient in the proposed control law does not go unbounded at times during the maneuver. This concept will be discussed in detail in subsequent sections.

In order to compactly view the three subsystems of concern, it is useful to first partitioning (173) as done by Bajodah (2009b) where

$$F\left(\mathbf{\omega}_{BI}\right) = \begin{bmatrix} F_{11}\left(\mathbf{\omega}_{BI}\right) & F_{12}\left(\mathbf{\omega}_{BI}\right) \\ F_{21}\left(\mathbf{\omega}_{BI}\right) & F_{22}\left(\mathbf{\omega}_{BI}\right) \end{bmatrix} \tag{178}$$

with $F_{11}\left(\mathbf{\omega}_{BI}\right) \in \mathbb{R}^{1x1}, F_{12}\left(\mathbf{\omega}_{BI}\right) \in \mathbb{R}^{1x2}, F_{21}\left(\mathbf{\omega}_{BI}\right) \in \mathbb{R}^{2x1}, F_{22}\left(\mathbf{\omega}_{BI}\right) \in \mathbb{R}^{2x2}$, and then consider the drift matrix associated with the vector differential equations of (170) as

$$F\left(\hat{\mathbf{q}}_{B_dB}\right) = \frac{1}{2}\left(q_4 I_{3x3} + q^x\right) = \begin{bmatrix} F_{11}\left(\hat{\mathbf{q}}_{B_dB}\right) & F_{12}\left(\hat{\mathbf{q}}_{B_dB}\right) \\ F_{21}\left(\hat{\mathbf{q}}_{B_dB}\right) & F_{22}\left(\hat{\mathbf{q}}_{B_dB}\right) \end{bmatrix} \tag{179}$$

where $F_{11}\left(\hat{\mathbf{q}}_{B_dB}\right) \in \mathbb{R}^{1x1}, F_{12}\left(\hat{\mathbf{q}}_{B_dB}\right) \in \mathbb{R}^{1x2}, F_{21}\left(\hat{\mathbf{q}}_{B_dB}\right) \in \mathbb{R}^{2x1}, F_{22}\left(\hat{\mathbf{q}}_{B_dB}\right) \in \mathbb{R}^{2x2}$. Now, by taking the unactuated state vector to be $\mathbf{x}_u\left(t\right) \in \mathbb{R}^2, \forall \mathbf{x}_u = \left[q_u, \omega_u\right]^T$ where $q_u = q_1$ and $\omega_u = \omega_1$, and the actuated angular velocity vector to be $\mathbf{\omega}_a\left(t\right) \in \mathbb{R}^2, \forall \mathbf{\omega}_a = \left[\omega_2, \omega_3\right]^T$, the unactuated system becomes

$$\dot{\mathbf{x}}_u = \begin{bmatrix} 0 & F_{11}\left(\hat{\mathbf{q}}_{B_dB}\right) \\ 0 & F_{11}\left(\mathbf{\omega}_{BI}\right) \end{bmatrix} \mathbf{x}_u + \begin{bmatrix} F_{12}\left(\hat{\mathbf{q}}_{B_dB}\right) \\ F_{12}\left(\mathbf{\omega}_{BI}\right) \end{bmatrix} \mathbf{\omega}_a \tag{180}$$

By considering the two remaining components of the error quaternion to be pseudo-actuated, the pseudo-actuated error quaternion vector can be taken to be $\mathbf{q}_p(t) \in \mathbb{R}^2, \forall \mathbf{q}_p = [q_2, q_3]^T$ and the actuated error quaternion subsystem then becomes

$$\dot{\mathbf{q}}_p = \begin{bmatrix} \mathbf{0}_{2x1} & F_{21}(\hat{\mathbf{q}}_{B_dB}) \end{bmatrix} \mathbf{x}_u + F_{22}(\hat{\mathbf{q}}_{B_dB})\boldsymbol{\omega}_a \tag{181}$$

The third and final coupled subsystem which considers the actuated dynamics and explicitly contains the control vector $\mathbf{u}$ is therefore

$$\dot{\boldsymbol{\omega}}_a = \begin{bmatrix} \mathbf{0}_{2x1} & F_{21}(\boldsymbol{\omega}_{BI}) \end{bmatrix} \mathbf{x}_u + F_{22}(\boldsymbol{\omega}_{BI})\boldsymbol{\omega}_a + \mathbf{u} \tag{182}$$

B.   LINEAR PARAMETERIZATION OF THE UNDERACTUATED RIGID SPACECRAFT SUBSYSTEM

As mentioned previously, the unactuated subsystem given in (180) can be seen to be indirectly affected by the control vector $\mathbf{u}$ through $\boldsymbol{\omega}_a$. By defining the scalar function $\phi(\mathbf{x}_u): \mathbb{R}^2 \rightarrow \mathbb{R}$ as

$$\phi(\mathbf{x}_u) = \omega_u + \alpha q_u \tag{183}$$

where $\alpha > 0$ represents a scalar on q_u and $\phi(\mathbf{x}_u)$ is a continuous twice differentiable function satisfying

$$\phi(\mathbf{x}_u) = 0 \Leftrightarrow \omega_u = -\alpha q_u \tag{184}$$

the unactuated subsystem (180) can now be transformed into a stable, linear, second-order dynamic system similar to what is proposed in Bajodah (2009a and 2009b) where

$$\ddot{\phi}(\mathbf{x}_u) + 2\gamma\dot{\phi}(\mathbf{x}_u) + \gamma^2\phi(\mathbf{x}_u) = 0 \tag{185}$$

with the coefficient γ chosen such that (185) is stable, i.e., the characteristic equation

$$s^2 + 2\gamma s + \gamma^2 = 0 \tag{186}$$

has strictly negative-real part roots thus implying that $\gamma > 0$.

The first time derivative of $\phi(\mathbf{x}_u)$ along solution trajectories of the underactuated rigid spacecraft angular motion equations given by (175) considering the control vector $\mathbf{u}$, the control matrix G given by (177) and $\mathbf{f}(\mathbf{x}) = F(\mathbf{x})\boldsymbol{\omega}_{BI}$ is:

$$\dot{\phi}(\mathbf{x}_u) = \frac{\partial \phi(\mathbf{x}_u)}{\partial \mathbf{x}}\dot{\mathbf{x}} = \frac{\partial \phi(\mathbf{x}_u)}{\partial \mathbf{x}}\left(\mathbf{f}(\mathbf{x}) + G\mathbf{u}\right) = L_{\mathbf{f}}\phi(\mathbf{x}_u) + L_G\phi(\mathbf{x}_u)\mathbf{u} \qquad (187)$$

where $L_G\phi(\mathbf{x}_u)$ evaluates to the 2x1 null vector. Likewise, the second time derivative of $\phi(\mathbf{x}_u)$ along the solution trajectories of the underactuated rigid spacecraft angular motion equations:

$$\ddot{\phi}(\mathbf{x}_u) = \frac{\partial L_{\mathbf{f}}\phi(x_u)}{\partial \mathbf{x}}\dot{\mathbf{x}} = \frac{\partial L_{\mathbf{f}}\phi(\mathbf{x}_u)}{\partial \mathbf{x}}\left(\mathbf{f}(\mathbf{x}) + G\mathbf{u}\right) = L_{\mathbf{f}}^2\phi(\mathbf{x}_u) + L_G L_{\mathbf{f}}\phi(\mathbf{x}_u)\mathbf{u} \qquad (188)$$

where $L_{\mathbf{f}}\phi(\mathbf{x}_u)$, $L_{\mathbf{f}}^2\phi(\mathbf{x}_u)$ and $L_G L_{\mathbf{f}}\phi(\mathbf{x}_u)$ represent the Lie derivatives, or directional derivatives of $\phi(\mathbf{x}_u)$ along the direction of the vector fields defined by $\mathbf{f}(\mathbf{x})$ and G (Slotine 1991). With $\dot{\phi}$ and $\ddot{\phi}$ given by (187) and (188), (185) can then be expressed as the point-wise linear form

$$\mathbf{a}^T(\mathbf{x})\mathbf{u} = b(\mathbf{x}) \qquad (189)$$

where the controls coefficient $\mathbf{a}(\mathbf{x}) \in \mathbb{R}^{2x1}$ is given by

$$\mathbf{a}(\mathbf{x}) = \left[L_G L_{\mathbf{f}}\phi(\mathbf{x}_u)\right]^T \qquad (190)$$

and the scalar controls load $b(\mathbf{x})$ is given by

$$b(\mathbf{x}) = -L_{\mathbf{f}}^2\phi(\mathbf{x}_u) - 2\gamma L_{\mathbf{f}}\phi(\mathbf{x}_u) - \gamma^2\phi(\mathbf{x}_u) \qquad (191)$$

The following definitions, propositions and theorem include only minor changes from Bajodah (2009b) to further expand them to include the full state $\mathbf{x}$ containing both

the dynamics and kinematics of the system. The proofs of these flow directly from those presented in Bajodah (2009b) due to the cascading nature of the controls.

Definition 1: *The desired linear unactuated dynamics given by (185) is said to be realizable by the rigid spacecraft angular motion equations (174) at specific values of* $\mathbf{x}(t)$ *if there exists a control vector* $\mathbf{u}(t)$ *that solves (189) for these values of* $\mathbf{x}(t)$. *If this is true for all* $\mathbf{x}(t)$ *such that* $\mathbf{x}_u(t) \neq \mathbf{0}_{2x1}$, *then the linear unactuated dynamics given by (185) is said to be globally realizable by (174).*

Proposition 1: *By letting (190) be the controls coefficient relative to (183) along* $f(\mathbf{x})$ *for the linear dynamics given by (185) that is globally realizable by (174), then*

$$\mathbf{a}(\mathbf{x}) = \mathbf{0}_{2x1} \Leftrightarrow \phi(\mathbf{x}_u, t) = \mathbf{0}_{2x1} \tag{192}$$

Proof: For a vector $\mathbf{u}$ to exist that solves (189) at specific values of $\mathbf{x}$, $b(\mathbf{x})$ must be in the range space of $\mathbf{a}^T(\mathbf{x})$ at that value of $\mathbf{x}$. This is possible for any value of $b(\mathbf{x})$ only if (189) is consistent. That is to say that not all elements of $\mathbf{a}^T(\mathbf{x})$ vanish at that value of $\mathbf{x}$. Therefore, the existence of a vector $\mathbf{x}^* \neq \mathbf{0}$ such that $\mathbf{a}(\mathbf{x}^*) = \mathbf{0}_{2x1}$ implies that the desired linear dynamics of (185) are not realizable at $\mathbf{x}^*$, which in turn violates global realizability of these desired linear dynamics and thus proves sufficiency. Necessity flows from the fact that the elements of the drift vector $\mathbf{f}(\mathbf{x})$ are multivariable polynomials with only quadratic elements in the components of $\mathbf{x}$ and that $\phi(\mathbf{x}_u)$ has a bounded $\mathbf{x}_u$ gradient, so that $\mathbf{a}(\mathbf{0}_{6x1}) = \mathbf{0}_{2x1}$.

Definition 2: *The zero actuated full-state Jacobian of the controls coefficient* $\mathcal{J}_0(\mathbf{x})$ *is the square matrix that results by partially differentiating the controls coefficient with respect to the actuated angular rates* $\boldsymbol{\omega}_a$ *evaluated at* $\boldsymbol{\omega}_a = 0_{2x1}$.

$$\mathcal{J}_0(\mathbf{x}) = \left[\frac{\partial \mathbf{a}^T(\mathbf{x})}{\partial \boldsymbol{\omega}_a} \right]_{\boldsymbol{\omega}_a = \mathbf{0}_{2x1}} \tag{193}$$

86

Proposition 2: *The unactuated linear dynamics given by (185) is globally realizable by the rigid spacecraft angular motion equations given in (174) if and only if*

$$\det\left[\mathcal{J}_0(\mathbf{x})\right] \neq 0 \tag{194}$$

Proof: The partial derivative of (189) with respect to $\boldsymbol{\omega}_a$ and evaluating the resulting equation at $\boldsymbol{\omega}_a = \mathbf{0}$ yields

$$\mathcal{J}_0(\mathbf{x})\mathbf{u} = \left[\frac{\partial b(\mathbf{x})}{\partial \boldsymbol{\omega}_a}\right]_{\boldsymbol{\omega}_a = \mathbf{0}_{2x1}} \tag{195}$$

Invertibility of the zero actuated state Jacobian of the controls coefficient implies that a control law $\mathbf{u}$ can be derived for global realizability of the desired linear dynamics of (185) as

$$\mathbf{u} = \mathcal{J}_0^{-1}(\mathbf{x})\left[\frac{\partial b(\mathbf{x})}{\partial \boldsymbol{\omega}_a}\right]_{\boldsymbol{\omega}_a = \mathbf{0}_{2x1}} \tag{196}$$

which proves necessity. Consider the non-linear time-varying system given by the equations

$$\dot{\mathbf{z}}_0 = \mathbf{a}(\mathbf{z}_0) \tag{197}$$

where $\mathbf{z}_0 = \left[z_u, \mathbf{z}_a\right]^T, \forall z_u \in \mathbb{R}, \forall z_a \in \mathbb{R}^{2x1}$. From Proposition 1, global realizability of the desired linear dynamics of (185) implies that the origin $\mathbf{z}_a = \mathbf{0}_{2x1}$ is the unique equilibrium point of (197) at $z_u = 0$. Furthermore, since $\mathbf{a}(\mathbf{z}_0)$ is a smooth vector field, it follows from Milnor's theorem (Bajodah 2006b) that it is also a global diffeomorphism on $\mathbb{R}^{6x1}$, i.e. that it has continuous partial derivatives and an invertible zero actuated state Jacobian and thus sufficiency is obtained.

Theorem 1: *Given a non-singular zero actuated state Jacobian $\mathcal{J}_0(\mathbf{x})$ of the controls coefficient $\mathbf{a}(\mathbf{x}) = \mathbf{0}_{2x1}$ along $f(\mathbf{x}) = F(\mathbf{x})\boldsymbol{\omega}$ for all $\mathbf{x}(t) \in \mathbb{R}^6$, the infinite set of*

control laws that globally realize the unactuated dynamics by the underactuated rigid spacecraft angular motion equations given by (174) is given by

$$\mathbf{u} = \bar{\mathbf{u}} + P(\mathbf{x})\mathbf{y} \tag{198}$$

where $\bar{\mathbf{u}} \in \mathbb{R}^2$ is

$$\bar{\mathbf{u}} = \mathbf{a}^+(\mathbf{x})b(\mathbf{x}) \tag{199}$$

and $\mathbf{a}^+(\mathbf{x}) \in \mathbb{R}^{2x1}$ represents the Moore-Penrose or generalized inverse of the controls coefficient $\mathbf{a}(\mathbf{x}) \in \mathbb{R}^{2x1}$ so that

$$\mathbf{a}^+(\mathbf{x}) = \begin{cases} \dfrac{\mathbf{a}(\mathbf{x})}{\|\mathbf{a}(\mathbf{x})\|^2} & \|\mathbf{a}(\mathbf{x})\| \neq 0 \\ \mathbf{0}_{2x1} & \|\mathbf{a}(\mathbf{x})\| = 0 \end{cases} \tag{200}$$

and $P(\mathbf{x}) \in \mathbb{R}^{2x2}$ represents the null-space projection matrix of $\mathbf{a}(\mathbf{x})$ such that

$$P(\mathbf{x}) = I_{2x2} + \mathbf{a}^+(\mathbf{x})\mathbf{a}^T(\mathbf{x}) \tag{201}$$

and $\mathbf{y} \in \mathbb{R}^{2x1}$ is an arbitrarily selected null-control vector.

Proof: Satisfaction of condition (194) implies that the desired linear dynamics of (185) are globally realizable by the underactuated rigid spacecraft system of angular motion equations. From Proposition 1, this global realizability further implies that $\mathbf{a}(\mathbf{x}) \neq \mathbf{0}_{2x1}$ at which infinite number of solutions for the point-wise linear relation (189) exist. Multiplying both sides of (198) by $\mathbf{a}^T(\mathbf{x})$ yields

$$\begin{aligned} \mathbf{a}^T(\mathbf{x})\mathbf{u} &= \mathbf{a}^T(\mathbf{x})\mathbf{a}^+(\mathbf{x})b(\mathbf{x}) + \mathbf{a}^T(\mathbf{x})P(\mathbf{x})\mathbf{y} \\ &= b(\mathbf{x}) \end{aligned} \tag{202}$$

and thus (189) is recovered. Therefore, the control vector $\mathbf{u}$ given by (198) linearly parameterizes all solutions of (189) by the null-control vector $\mathbf{y}$. $\square$

In this manner, the infinite set of closed-loop full underactuated rigid spacecraft system of angular motion equations in partitioned form become

$$\dot{\mathbf{x}}_u = \begin{bmatrix} 0 & F_{11}\left(\hat{\mathbf{q}}_{B_dB}\right) \\ 0 & F_{11}\left(\boldsymbol{\omega}_{BI}\right) \end{bmatrix} \mathbf{x}_u + \begin{bmatrix} F_{12}\left(\hat{\mathbf{q}}_{B_dB}\right) \\ F_{12}\left(\boldsymbol{\omega}_{BI}\right) \end{bmatrix} \boldsymbol{\omega}_a \tag{203}$$

$$\dot{\mathbf{q}}_p = \begin{bmatrix} \mathbf{0}_{2x1} & F_{21}\left(\hat{\mathbf{q}}_{B_dB}\right) \end{bmatrix} \mathbf{x}_u + F_{22}\left(\hat{\mathbf{q}}_{B_dB}\right) \boldsymbol{\omega}_a \tag{204}$$

$$\dot{q}_4 = \begin{bmatrix} 0 & -\frac{1}{2}q_u \end{bmatrix} \mathbf{x}_u + \mathbf{q}_p^T \boldsymbol{\omega}_a \tag{205}$$

$$\dot{\boldsymbol{\omega}}_a = \begin{bmatrix} \mathbf{0}_{2x1} & F_{21}\left(\boldsymbol{\omega}_{BI}\right) \end{bmatrix} \mathbf{x}_u + F_{22}\left(\boldsymbol{\omega}_{BI}\right) \boldsymbol{\omega}_a + \mathbf{u} \tag{206}$$

(198) consists of two parts. The first part, given by $\bar{\mathbf{u}}$, is termed the particular solution and acts specifically on the range-space of the generalized inverse of the controls coefficient $\mathbf{a}^+(\mathbf{x})$. The second part, given by $P(\mathbf{x})\mathbf{y}$, is termed the auxiliary solution and resides in the orthogonal complement subspace, or the null-space of the controls coefficient in $\mathbb{R}^3$ with the null-control vector $\mathbf{y}$ being projected onto this space by means of the projection matrix $P(\mathbf{x})$.

As discussed in Bajodah (2009b), the null-control vector $\mathbf{y} \in \mathbb{R}^{2x1}$ is not fully arbitrary and should be chosen to yield stability of the closed loop system of equations given in (203) through (206). Two such null-control vectors will be presented in the following sections, the first is Lyapunov function based to yield global stability for the system given established bounds on the control and the second is perturbed feedback-linearizing to yield local stability and guaranteed boundedness. The development of these null-control vectors and their subsequent proofs of stability provide a key contribution to the body of knowledge with respect to underactuated rigid body attitude control.

C. DEVELOPMENT OF THE QUATERNION FEEDBACK REGULATOR AND STABILITY ANALYSIS

In this section, the stability of the closed-loop system of equations given by (203) through (206) is addressed for two derived null-control vectors. From the definition of the generalized inverse of $\mathbf{a}(\mathbf{x})$ given by (200),

$$\lim_{\mathbf{a}(\mathbf{x})\to\mathbf{0}_{2x1}} \mathbf{a}^+(\mathbf{x}) = \infty_{2x1} \tag{207}$$

which implies a singularity on the closed-loop stability of the system. Similarly from Proposition 1, if the linear unactuated dynamics (185) are globally realizable by the underactuated rigid spacecraft system of angular motion equations given in (175), then

$$\lim_{\phi(\mathbf{x}_u)\to0} \mathbf{a}(\mathbf{x}) = \mathbf{0}_{2x1} \tag{208}$$

In order to properly bound the control input to allow for the control law derivations that follow, the damped generalized inverse and its corresponding damped controls coefficient null-projector are used as presented in Bajodah (2009a). The damped controls coefficient generalized inverse is formulated by considering an arbitrarily small damping coefficient β_1 to provide a bound on the generalized inverse as the squared Euclidean norm of the controls coefficient tends to zero. Thus, the damped generalized inverse of the controls coefficient $\mathbf{a}_d^+(\mathbf{x}) \in \mathbb{R}^{2x1}$ is

$$\mathbf{a}_d^+(\mathbf{x}) = \begin{cases} \dfrac{\mathbf{a}(\mathbf{x})}{\|\mathbf{a}(\mathbf{x})\|^2} & \|\mathbf{a}(\mathbf{x})\| \geq \beta_1 \\[3mm] \dfrac{\mathbf{a}(\mathbf{x})}{\beta_1^2} & \|\mathbf{a}(\mathbf{x})\| < \beta_1 \end{cases} \tag{209}$$

where scalar β_1 is a positive damping coefficient. Bounding the generalized inverse of $\mathbf{a}(\mathbf{x})$ given by (200) in this manner smoothes the infinite set of control laws presented in Theorem 1. Furthermore,

$$\left\| \mathbf{a}_d^+ \left(\mathbf{x} \right) \right\| \le \frac{1}{\beta_1} \tag{210}$$

and

$$\lim_{\phi(\mathbf{x}_u) \to \mathbf{0}_{2x1}} \left\| \mathbf{a}_d^+ \left(\mathbf{x} \right) \right\| = 0 \tag{211}$$

and $\mathbf{a}_d^+ \left(\mathbf{x} \right)$ pointwise converges to $\mathbf{a}^+ \left(\mathbf{x} \right)$ as β_1 vanishes (Bajodah 2009a).

Likewise, the damped null-projection matrix of $\mathbf{a} \left(\mathbf{x} \right)$ is modified from (209) such that

$$P_d \left(\mathbf{x} \right) = I_{2x2} - \mathbf{a}_d^+ \left(\mathbf{x} \right) \mathbf{a}^T \left(\mathbf{x} \right) \tag{212}$$

(209) and (212) imply that

$$P_d \left(\mathbf{x} \right) = \begin{cases} I_{2x2} - \dfrac{\mathbf{a}(\mathbf{x}) \mathbf{a}^T (\mathbf{x})}{\left\| \mathbf{a}(\mathbf{x}) \right\|^2} & \left\| \mathbf{a}(\mathbf{x}) \right\| \ge \beta_1 \\[4mm] I_{2x2} - \dfrac{\mathbf{a}(\mathbf{x}) \mathbf{a}^T (\mathbf{x})}{\beta_1^2} & \left\| \mathbf{a}(\mathbf{x}) \right\| < \beta_1 \end{cases} \tag{213}$$

and from (208), during the steady-state phase of response the damped null-projection matrix of $\mathbf{a} \left(\mathbf{x} \right)$ becomes

$$\lim_{\phi(\mathbf{x}_u) \to 0} P_d \left(\mathbf{x} \right) = I_{2x2} \tag{214}$$

such that the auxiliary part of the infinite set of control laws expressed in (198) converge to the null-control vector $\mathbf{y}$. Construction of these control laws with (209) and (212) yields the damped control vector $\mathbf{u}_d$ defined as

$$\mathbf{u}_d = \overline{\mathbf{u}}_d + P_d \left(\mathbf{x} \right) \mathbf{y} \tag{215}$$

where $\overline{\mathbf{u}}_d \in \mathbb{R}^{2x1}$ is given by

91

$$\bar{\mathbf{u}}_d = \mathbf{a}_d^+(\mathbf{x})b(\mathbf{x}) \tag{216}$$

Furthermore, the damped control vector yields the closed-loop full underactuated rigid spacecraft system of angular motion equations

$$\dot{\mathbf{x}}_u = \begin{bmatrix} 0 & F_{11}(\hat{\mathbf{q}}_{B_dB}) \\ 0 & F_{11}(\boldsymbol{\omega}_{BI}) \end{bmatrix}\mathbf{x}_u + \begin{bmatrix} F_{12}(\hat{\mathbf{q}}_{B_dB}) \\ F_{12}(\boldsymbol{\omega}_{BI}) \end{bmatrix}\boldsymbol{\omega}_a \tag{217}$$

$$\dot{\mathbf{q}}_p = \begin{bmatrix} \mathbf{0}_{2x1} & F_{21}(\hat{\mathbf{q}}_{B_dB}) \end{bmatrix}\mathbf{x}_u + F_{22}(\hat{\mathbf{q}}_{B_dB})\boldsymbol{\omega}_a \tag{218}$$

$$\dot{q}_4 = \begin{bmatrix} 0 & -\frac{1}{2}q_u \end{bmatrix}\mathbf{x}_u + \mathbf{q}_p^T\boldsymbol{\omega}_a \tag{219}$$

$$\dot{\boldsymbol{\omega}}_a = \begin{bmatrix} \mathbf{0}_{2x1} & F_{21}(\boldsymbol{\omega}_{BI}) \end{bmatrix}\mathbf{x}_u + F_{22}(\boldsymbol{\omega}_{BI})\boldsymbol{\omega}_a + \bar{\mathbf{u}}_d + P_d(\mathbf{x})\mathbf{y} \tag{220}$$

D. LYAPUNOV FUNCTION-BASED QUATERNION FEEDBACK REGULATOR

Let the null-control vector $\mathbf{y}$ be chosen as

$$\mathbf{y} = \boldsymbol{\eta}_d^+(\mathbf{x})\Big[-\boldsymbol{\omega}_a^T F_{21}(\boldsymbol{\omega}_{BI})\omega_u - \boldsymbol{\omega}_a^T F_{22}(\boldsymbol{\omega}_{BI})\boldsymbol{\omega}_a - \boldsymbol{\omega}_a^T\bar{\mathbf{u}}_d - k\mathbf{q}_{B_dB}^T\boldsymbol{\omega}\Big] - d\boldsymbol{\omega}_a \tag{221}$$

where k, d are positive scalar gains and the damped actuated dynamics projector $\boldsymbol{\eta}_d^+(\mathbf{x}) \in \mathbb{R}^2$ is defined as

$$\boldsymbol{\eta}_d^+(\mathbf{x}) = \begin{cases} \dfrac{\boldsymbol{\omega}_a}{\boldsymbol{\omega}_a^T P_d(\mathbf{x})\boldsymbol{\omega}_a} & \boldsymbol{\omega}_a^T P_d(\mathbf{x})\boldsymbol{\omega}_a \geq \beta_2 \\[3mm] \dfrac{\boldsymbol{\omega}_a}{\beta_2} & \boldsymbol{\omega}_a^T P_d(\mathbf{x})\boldsymbol{\omega}_a < \beta_2 \end{cases} \tag{222}$$

where β_2 is a positive damping coefficient on $\boldsymbol{\eta}(\mathbf{x})$. In this manner, substitution of (221) into (212) yields the class of control laws

$$\mathbf{u}_d = \bar{\mathbf{u}}_d + P_d(\mathbf{x})\Big\{\boldsymbol{\eta}_d^+(\mathbf{x})\Big[-\boldsymbol{\omega}_a^T F_{21}(\boldsymbol{\omega}_{BI})\omega_u - \boldsymbol{\omega}_a^T F_{22}(\boldsymbol{\omega}_{BI})\boldsymbol{\omega}_a - \boldsymbol{\omega}_a^T\bar{\mathbf{u}} - k\mathbf{q}_{B_dB}^T\boldsymbol{\omega}\Big] - d\boldsymbol{\omega}_a\Big\} \tag{223}$$

which yield the closed-loop dynamical actuated subsystem

$$\dot{\boldsymbol{\omega}}_a = F_{21}\left(\boldsymbol{\omega}_{BI}\right)\omega_u + F_{22}\left(\boldsymbol{\omega}_{BI}\right)\boldsymbol{\omega}_a + \overline{\mathbf{u}}_d$$
$$+ P_d\left(\mathbf{x}\right)\left\{\boldsymbol{\eta}_d^+\left(\mathbf{x}\right)\begin{bmatrix} -\boldsymbol{\omega}_a^T F_{21}\left(\boldsymbol{\omega}_{BI}\right)\omega_u - \boldsymbol{\omega}_a^T F_{22}\left(\boldsymbol{\omega}_{BI}\right)\boldsymbol{\omega}_a \\ -\boldsymbol{\omega}_a^T\overline{\mathbf{u}} - k\mathbf{q}_{B_dB}^T\boldsymbol{\omega}_{BI} \end{bmatrix} - d\boldsymbol{\omega}_a\right\} \tag{224}$$

Conjecture 1. *Let the function $\phi\left(\mathbf{x}_u\right)$ be globally twice continuously differentiable and satisfy the condition given by (184), the controls coefficient $\mathbf{a}\left(\mathbf{x}\right)$ given by (190) and controls load $b\left(\mathbf{x}\right)$ given by (191) relative to $\phi\left(\mathbf{x}_u\right)$ of the linear unactuated second-order dynamics given by (185) along the drift vector $\mathbf{f}\left(\mathbf{x}\right) = F\left(\mathbf{x}\right)\boldsymbol{\omega}_{BI}$ of the underactuated rigid spacecraft system of angular motion equations given by (175). Furthermore, let the damped generalized inverse of the controls coefficient $\mathbf{a}_d^+\left(\mathbf{x}\right)$ be given by (209), the damped null-projector of the controls coefficient $P_d\left(\mathbf{x}\right)$ be given by (212), and the null-control vector $\mathbf{y}$ be given by (221) with damped actuated dynamics projector $\boldsymbol{\eta}_d^+\left(\mathbf{x}\right)$ be given by (222). If the zero-actuated state Jacobian $J_0\left(\mathbf{x}\right)$ given by (193) is non-singular, then the positive scalar feedback gains $k, d \in \mathbb{R}$ can be chosen to globally stabilize the closed-loop underactuated rigid spacecraft system of angular motion equations given by (217) through (220) by bounded, smooth, time-invariant state feedback to an arbitrarily small vicinity of the equilibrium of the system defined by the damping coefficients β_1 and β_2.*

Proof. Let the scalar function $e\left(\mathbf{x}\right)$ be defined as

$$e\left(\mathbf{x}\right) = \dot{\phi}\left(\mathbf{x}_u\right) + \gamma\phi\left(\mathbf{x}_u\right) \tag{225}$$

where γ is as defined for (186). Given (189) and (225), $\dot{e}\left(\mathbf{x}\right)$ therefore evaluates to

$$\dot{e}\left(\mathbf{x}\right) = \ddot{\phi}\left(\mathbf{x}_u\right) + \gamma\dot{\phi}\left(\mathbf{x}_u\right) = -\gamma e\left(\mathbf{x}\right) - b\left(\mathbf{x}\right) + \mathbf{a}^T\left(\mathbf{x}\right)\mathbf{u} \tag{226}$$

Let the Lyapunov control function be defined as

93

$$V = \frac{1}{2}e^2(\mathbf{x}) + \frac{1}{2}k^{-1}\boldsymbol{\omega}_a^T\boldsymbol{\omega}_a + q_1^2 + q_2^2 + q_3^2 + (q_4 - 1)^2$$
$$= \frac{1}{2}e^2(\mathbf{x}) + \frac{1}{2}k^{-1}\boldsymbol{\omega}_a^T\boldsymbol{\omega}_a + 2(1 - q_4)$$

(227)

Note that V is positive definite and asymptotically unbounded in $e(\mathbf{x})$ and $\boldsymbol{\omega}_a$. Furthermore, V can be partitioned into two positive definite functions such that $V = V_1 + V_2$ where

$$V_1 = \frac{1}{2}e^2(\mathbf{x})$$

(228)

$$V_2 = \frac{1}{2}k^{-1}\boldsymbol{\omega}_a^T\boldsymbol{\omega}_a + 2(1 - q_4)$$

(229)

where $k^{-1} \in \mathbb{R}$ is a positive scalar constant gain.

The corresponding time-derivative of V_1 is given by

$$\dot{V}_1 = e(\mathbf{x})\dot{e}(\mathbf{x}) = -e(\mathbf{x})b(\mathbf{x}) - \gamma e^2(\mathbf{x}) + e(\mathbf{x})\mathbf{a}^T(\mathbf{x})\mathbf{u}$$

(230)

which by is reduced by substitution of (226) given that $\mathbf{a}^T(\mathbf{x})P_d(\mathbf{x}) = 0$ by definition to

$$\dot{V}_1 = -\gamma e^2(\mathbf{x})$$

(231)

Note that (231) is guaranteed to be negative definite independent of the choice on the null-control vector $\mathbf{y}$ with proper selection of γ.

Given that the null-control vector $\mathbf{y}$ can be arbitrarily chosen, it can be selected to ensure $\dot{V}_2 \leq 0$ which, when combined with (231), ensures that $\dot{V}$ is negative definite and global asymptotic stability of the underactuated rigid spacecraft system is guaranteed. The corresponding time-derivative of V_2 is

$$\dot{V}_2 = k^{-1}\boldsymbol{\omega}_a^T\dot{\boldsymbol{\omega}}_a - 2\dot{q}_4$$
$$= k^{-1}\boldsymbol{\omega}_a^T F_{21}(\boldsymbol{\omega})\boldsymbol{\omega}_u + k^{-1}\boldsymbol{\omega}_a^T F_{22}(\boldsymbol{\omega})\boldsymbol{\omega}_a + k^{-1}\boldsymbol{\omega}_a^T\bar{\mathbf{u}} + k^{-1}\boldsymbol{\omega}_a^T P_d(\mathbf{x})\mathbf{y} + \mathbf{q}_e^T\boldsymbol{\omega}$$

(232)

94

Let the null-control vector $\mathbf{y}$ be defined as

$$\mathbf{y} = \mathbf{\eta}_d^+(\mathbf{x})\left[-\boldsymbol{\omega}_a^T F_{21}(\boldsymbol{\omega})\omega_u - \boldsymbol{\omega}_a^T F_{22}(\boldsymbol{\omega})\boldsymbol{\omega}_a - \boldsymbol{\omega}_a^T \bar{\mathbf{u}} - k\mathbf{q}_e^T \boldsymbol{\omega}\right] - d\boldsymbol{\omega}_a \qquad (233)$$

with a positive scalar gain $d \in \mathbb{R}$. Similar to the damping of the control coefficient generalized inverse, the damped actuated dynamics generalized inverse $\mathbf{\eta}_d^+(\mathbf{x})$ given by (222) implies that

$$\left\|\mathbf{\eta}_d^+(\mathbf{x})\right\| \le \frac{1}{\beta_2} \qquad (234)$$

and that

$$\lim_{\boldsymbol{\omega}_a \to \mathbf{0}_{2x1}} \left\|\mathbf{\eta}_d^+(\mathbf{x})\right\| = 0 \qquad (235)$$

and that $\mathbf{\eta}_d^+(\mathbf{x})$ pointwise converges to $\mathbf{\eta}_d^+(\mathbf{x})$ as β_2 vanishes.

In the condition where $\boldsymbol{\omega}_a^T P_d(\mathbf{x}) = \mathbf{0}_{1x2}$, the null-control vector can be seen to not affect the stability of the system in a Lyapunov sense from (232). However, do to the arbitrarily small nature of this region by selection of the damping coefficient β_2, it is conjectured that the system is globally stable to this arbitrarily small region defined by the damping coefficients β_1 and β_2 with the feedback control law

$$\mathbf{u} = \mathbf{a}_d^+(\mathbf{x})b(\mathbf{x}) + P_d(\mathbf{x})\mathbf{y} \qquad (236)$$

where $\mathbf{y}$ is given by (233).

E.   FEEDBACK-LINEARIZING QUATERNION FEEDBACK REGULATOR

Let the null-control vector **y** be chosen as

$$\mathbf{y} = -F_{21}(\boldsymbol{\omega})\omega_u - F_{22}(\boldsymbol{\omega})\boldsymbol{\omega}_a - d\boldsymbol{\omega}_a - k\mathbf{q}_p \tag{237}$$

where d, k are positive scalar gains to be determined. In this manner, substitution of (237) into (212) yields the class of control laws

$$\mathbf{u}_d = \bar{\mathbf{u}}_d + P_d(\mathbf{x})\left[-F_{21}(\boldsymbol{\omega})\omega_u - F_{22}(\boldsymbol{\omega})\boldsymbol{\omega}_a - d\boldsymbol{\omega}_a - k\mathbf{q}_p\right] \tag{238}$$

The close-loop actuated dynamical subsystem becomes

$$\dot{\boldsymbol{\omega}}_a = F_{21}(\boldsymbol{\omega})\omega_u + F_{22}(\boldsymbol{\omega})\boldsymbol{\omega}_a + \bar{\mathbf{u}}_d + P_d(\mathbf{x})\left[-F_{21}(\boldsymbol{\omega})\omega_u - F_{22}(\boldsymbol{\omega})\boldsymbol{\omega}_a - d\boldsymbol{\omega}_a - k\mathbf{q}_p\right] \tag{239}$$

which converges by (210) and (214) to the linear dynamical system (Bajodah 2009a)

$$\dot{\boldsymbol{\omega}}_a = -d\boldsymbol{\omega}_a - k\mathbf{q}_p \tag{240}$$

Furthermore, the linear dynamical system given by (240) is upper bounded by selection of the damping coefficient β_1 forming a domain of attraction in **x** whereby $\|\mathbf{a}(\mathbf{x})\| \geq \beta_1$ due to the damped controls coefficient generalized inverse defined by (209). Therefore, the dynamical system given by (240) coupled with the remaining equations of motion given by (217) through (219) form a feedback linearizing transformation from the underactuated rigid spacecraft angular motion equations given by (175) over a domain of attraction in **x**.

Conjecture 2. *Let the function $\phi(\mathbf{x}_u)$ be globally twice continuously differentiable and satisfy the condition given by (184), the controls coefficient $\mathbf{a}(\mathbf{x})$ given by (190) and controls load $b(\mathbf{x})$ given by (191) relative to $\phi(\mathbf{x}_u)$ of the linear unactuated second-order dynamics given by (185) along the drift vector $f(\mathbf{x}) = F(\mathbf{x})\boldsymbol{\omega}_{BI}$ of the underactuated rigid spacecraft system of angular motion equations given by (175)*

96

Furthermore, let the damped generalized inverse of the controls coefficient $\mathbf{a}_d^+(\mathbf{x})$ *be given by (209), the damped null-projector of the controls coefficient* $P_d(\mathbf{x})$ *be given by (212), and the null-control vector* $\mathbf{y}$ *be given by (221). If the zero-actuated state Jacobian* $\mathcal{J}_0(\mathbf{x})$ *given by (193) is nonsingular, then the positive scalar feedback gains* $k, d \in \mathbb{R}$ *can be chosen to stabilize the closed-loop underactuated rigid spacecraft system of angular motion equations given by (217) through (220) by bounded, smooth, time-invariant state feedback control to an arbitrarily small vicinity of the equilibrium of the system defined by the damping coefficients* β_1 *within a domain of attraction in* $\mathbf{x}(t)$.

Proof: Assuming the inverse damping gain $k^{-1} \in \mathbb{R}$ exists and is positive definite, consider the control Lyapunov function

$$
\begin{aligned}
V &= \frac{1}{2} \boldsymbol{\omega}_a^T k^{-1} \boldsymbol{\omega}_a + q_1^2 + q_2^2 + q_3^2 + (q_4 - 1)^2 \\
&= \frac{1}{2} \boldsymbol{\omega}_a^T k^{-1} \boldsymbol{\omega}_a + 2(1 - q_4)
\end{aligned}
\tag{241}
$$

Note that V is positive definite. This particular Lyapunov function is well known for spacecraft attitude dynamics appearing in Wie and Barba (1985); Wie, Weiss and Arapostathis (1989); and Cristi and Burl (1993) among others.

Differentiating V along the trajectories of the underactuated system given by (175) yields

$$
\begin{aligned}
\dot{V} &= \boldsymbol{\omega}_a^T k^{-1} \dot{\boldsymbol{\omega}}_a - 2\dot{q}_4 \\
&= -\boldsymbol{\omega}_a^T k^{-1} d\boldsymbol{\omega}_a + q_u \omega_u
\end{aligned}
\tag{242}
$$

(241) can be rewritten as

$$
V = \frac{1}{2} k \|\boldsymbol{\omega}_a\|^2 + 2(1 - q_4)
\tag{243}
$$

and (242) can be rewritten as

$$\dot{V} = -kd \left\| \boldsymbol{\omega}_a \right\|^2 + q_u \omega_u \tag{244}$$

Given $\phi(\mathbf{x}_u)$ defined by (183) such that

$$\phi(\mathbf{x}_u) = \omega_u + \alpha q_u \tag{245}$$

(244) can be rewritten as

$$\dot{V} = q_u \phi(\mathbf{x}_u) - \alpha q_u^2 - kd \left\| \boldsymbol{\omega}_a \right\|^2 \tag{246}$$

From Lemma 1 in Appendix B, $\left\| \boldsymbol{\omega}_a(t) \right\|$ is uniformly bounded, i.e., $\left\| \boldsymbol{\omega}_a(t) \right\| \le c \ \forall t$. By defining $f(t) \in \mathbb{R}$ to be the scalar function described by

$$f(t) = \int_0^t \left\| \boldsymbol{\omega}_a(\tau) \right\|^2 d\tau \tag{247}$$

and given the designed dynamics in (185), $\phi(\mathbf{x}_u)(t) \to 0$ exponentially, application of Lemma 2 in Appendix B yields

$$\lim_{t \to +\infty} f(t) = f(\infty) < +\infty \tag{248}$$

and

$$f(t) = \int_0^t \left\| \boldsymbol{\omega}_a(\tau) \right\|^2 d\tau \le c \ \forall t \tag{249}$$

Furthermore, with (247) and (249) defined, Barbalat's Lemma (Slotine and Li 1991) can be applied by conjecture given an arbitrarily small selection of the damping coefficient β_1 on the controls coefficient generalized inverse to yield

$$\lim_{t \to +\infty} \dot{f}(t) = \lim_{t \to +\infty} \left\| \boldsymbol{\omega}_a(t) \right\| = 0 \tag{250}$$

From Lemma 3 in Appendix B,

$$\lim_{t \to \infty} \left\| \mathbf{x}_u \left(t \right) \right\| = 0 \tag{251}$$

and given Lemma 4 in Appendix B, (250) and (251) yield

$$\lim_{t \to \infty} \left\| \mathbf{q}_p \left(t \right) \right\| = 0 \tag{252}$$

Thus, the closed-loop equations of motion given by (217) through (220) are stable within a domain of attraction in $\mathbf{x}(t)$.

F. DESIGN EXAMPLE

In order to demonstrate the effectiveness of the presented quaternion feedback regulators with both null-control vector selections for underactuated spacecraft, a control design example is presented that considers an asymmetric rigid spacecraft with principal moments of inertia (in kgm^2) of $J_{11} = 32.5, J_{22} = 25$ and $J_{33} = 12.5$. These selections of moments of inertia correspond to a 30 kg rigid rectangular spacecraft with uniform mass distribution and sides of length 1x2x3 m. For purposes of representing real-world spacecraft torqueing capabilities, the maximum available torque about each control axis is limited to 1 Nm.

From (190), the control coefficient $\mathbf{a}(\mathbf{x})$ relative to the feedback linearizing transformation $\phi(\mathbf{x}_u)$ given by (183) is

$$\mathbf{a}(\mathbf{x}) = \begin{bmatrix} -\dfrac{1}{2} q_{3e} + \dfrac{(J_{22} - J_{33})}{J_{11}} \omega_3 \\ \dfrac{1}{2} q_{2e} + \dfrac{(J_{22} - J_{33})}{J_{11}} \omega_2 \end{bmatrix} \tag{253}$$

The determinant of the associated $\mathcal{J}_0(\mathbf{x})$ as defined by (193) is

$$\det\left[\frac{\partial \mathbf{a}^T(\mathbf{x})}{\partial \boldsymbol{\omega}_a}\right]_{\boldsymbol{\omega}_a=\mathbf{0}_{2x1}} = \det\begin{bmatrix} 0 & \dfrac{(J_{22}-J_{33})}{J_{11}} \\ \dfrac{(J_{22}-J_{33})}{J_{11}} & 0 \end{bmatrix}_{\boldsymbol{\omega}_a=\mathbf{0}_{2x1}} \quad (254)$$

which is non-zero for all $\mathbf{x}(t) \in \mathbb{R}^{7x1}$.

For the numerical simulations that follow, a fourth-order Runge-Kutta numerical integration scheme is used to integrate (217) through (220) with a fixed time step of .1s. Appendix C provides the code for the algorithm implemented via an Embedded MATLAB® function. In order to accommodate exact zero initial conditions on $\boldsymbol{\omega}$ and $\mathbf{q}_e$ without failure of the regulator, the measured state is perturbed to $1x10^{-4}$ in these situations.

1. Numerical Simulations using Lyapunov Function-Based Quaternion Feedback Regulator

a. Rest to Rest Reorientation from Large Initial Angle Offset Given Low Available Control Torque

A large-angle rest-to-rest reorientation maneuver is considered. The quaternion describing the initial orientation (t_0) of $\mathcal{B}_d$ with respect to $\mathcal{J}$ is taken to be $\hat{\mathbf{q}}(t_0) = [.57,.57,.57,.159]^T$ which, by considering a 3-2-1 sequence of rotations, corresponds to initial Euler angles of $\left[\alpha_1(t_0),\alpha_2(t_0),\alpha_3(t_0)\right] = [109.8,-27.9,109.8]\deg$. The final orientation is taken to be $\hat{\mathbf{q}}(t_f) = [0,0,0,1]^T$. The initial and final angular velocity vector is $\boldsymbol{\omega}(t_0) = \boldsymbol{\omega}(t_f) = [0,0,0]^T$. This reorientation maneuver is chosen in order to compare against the fully actuated quaternion feedback controller presented in Wie and Barba (1985). The chosen gains are

$$\gamma = .70, \alpha = 1.25, d = 7.5, k = 2.25, \beta_1, \beta_2 = 1x10^{-4}$$

100

Figure 15 shows the time histories of the Euler angles and angular rates and demonstrates smooth attitude stabilization within 90 s. Figure 16 shows the time histories of the control torques. The control noise near the inherent singularity in the null-control vector given by (233) is evident throughout the maneuver until the stabilization region is reached.

Figure 15. Time Histories of the Euler Angles and Angular Velocities for a Rest to Rest Reorientation Manuever from Large Initial Angle Offset Using the Lyapunov-Function Based Control Law and Nominal Available Control Torque
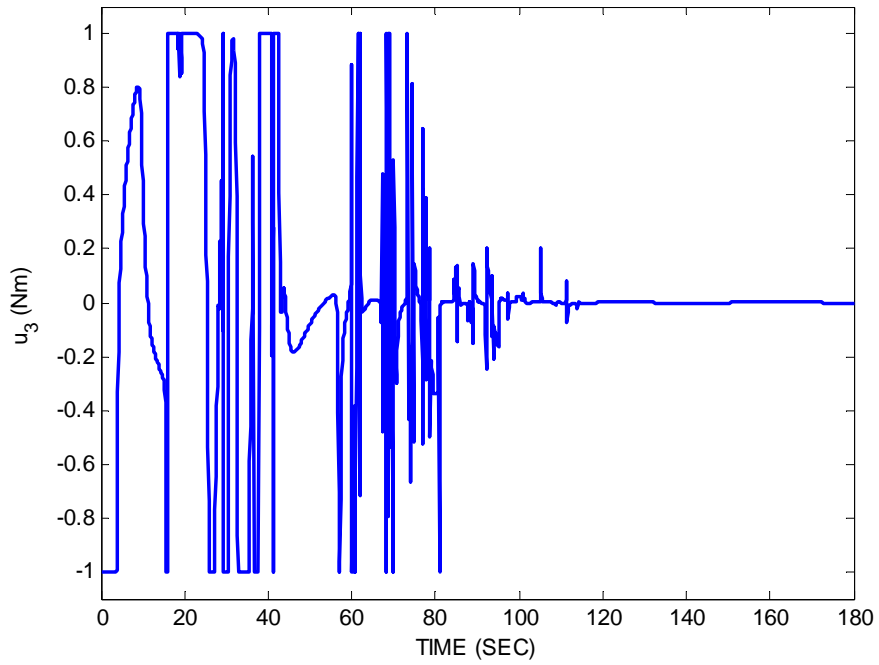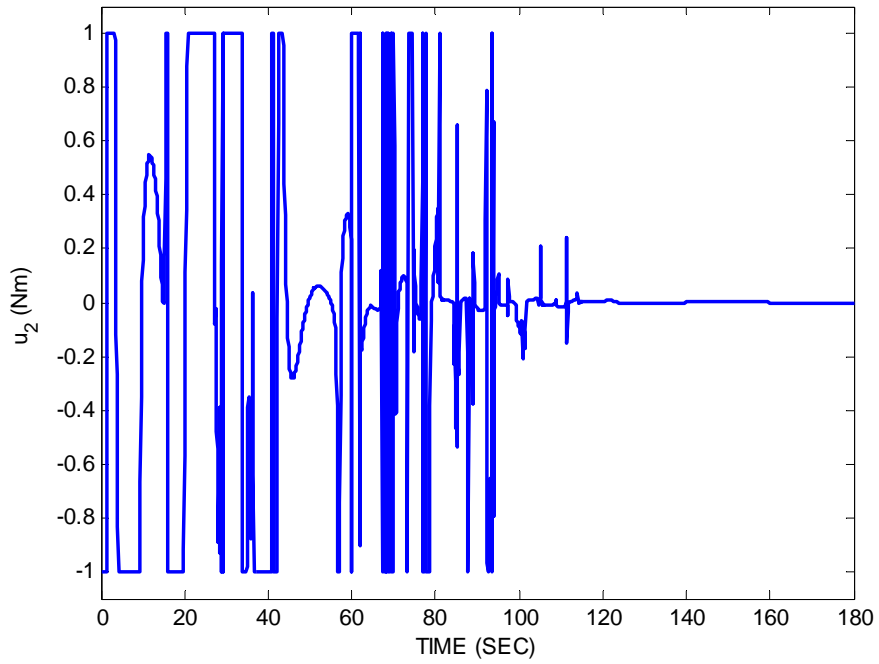
Figure 16.   Time Histories of the Control Torques for a Rest to Rest Reorientation
Manuever from Large Initial Angle Offset Using the Lyapunov-Function Based Control
Law and Nominal Available Control Torque

b. *Large Initial Angular Rate to Rest Stabilization and Reorientation Given Low Available Control Torque*

A three-axis detumbling and reorientation maneuver is considered. The quaternions describing the initial and final orientation of $\mathcal{B}_d$ with respect to $\mathcal{I}$ are $\hat{\mathbf{q}}(t_f) = \hat{\mathbf{q}}(t_0) = [0,0,0,1]^T$ and the initial angular velocity vector is taken to be $\boldsymbol{\omega}(t_0) = [1,-1,1] \, rad/s^2$. The final angular velocity vector is $\boldsymbol{\omega}(t_f) = [0,0,0]^T$. By assuming the same choice of parameters given above, Figure 17 depicts the time histories of the Euler angles and angular rates and demonstrates attitude stabilization within 300 s. The failure to smoothly converge to the origin is due to the limited control torque. Figure 18 shows the time histories of the control torques and again shows significant control effort noise during the maneuver until the stabilization region is reached.
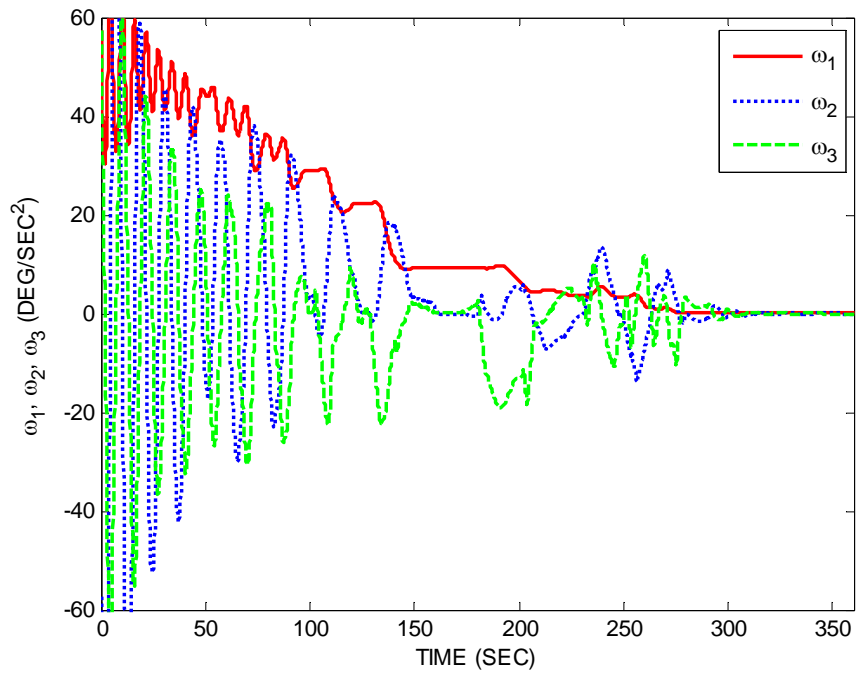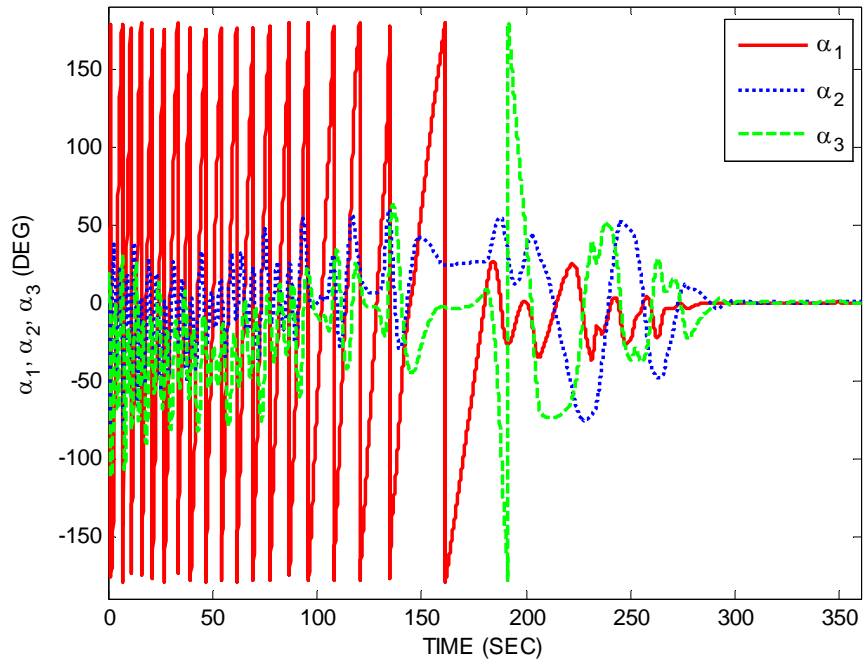
Figure 17. Time Histories of the Euler Angles and Angular Velocities for a Large Initial Angular Rate to Rest Reorientation Manuever Using the Lyapunov-Function Based Control Law and Nominal Available Control Torque

105
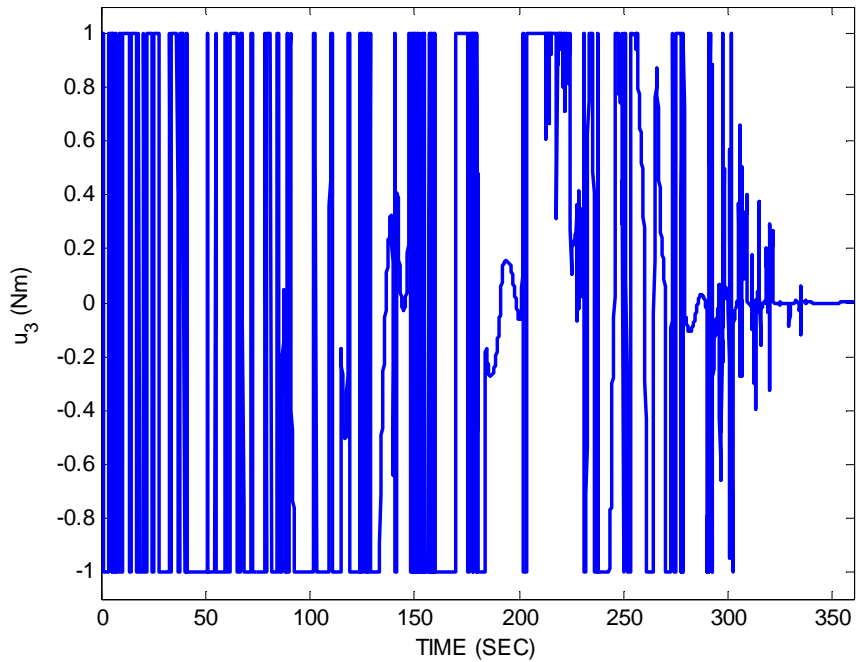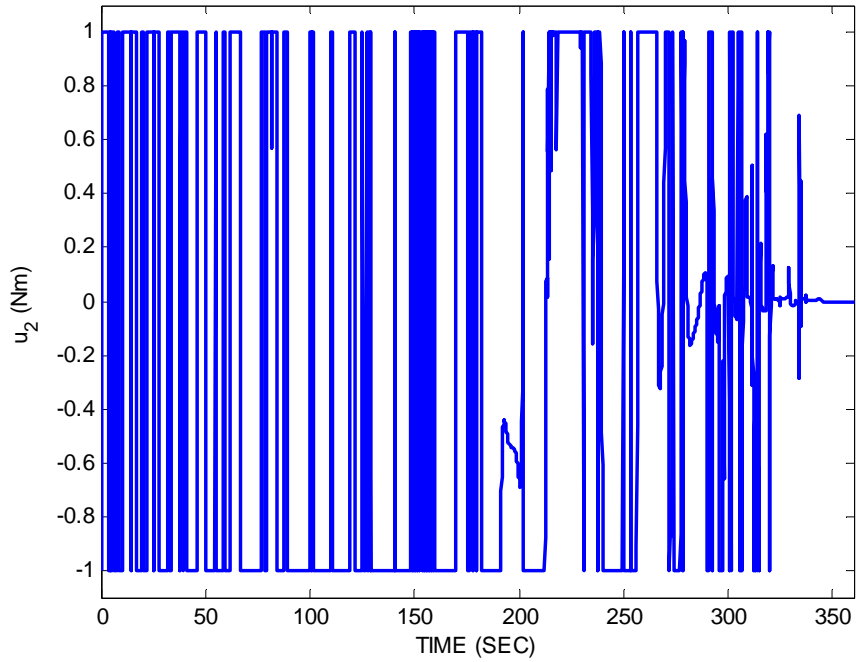
Figure 18.   Time Histories of the Control Torques for a Large Initial Angular Rate to Rest Reorientation Manuever Using the Lyapunov-Function Based Control Law and Nominal Available Control Torque

A three-axis detumbling and reorientation maneuver is considered again with increased torque capabilities as is typically studied in most literature involving underactuated spacecraft control. The quaternions describing the initial and final orientation of $\mathcal{B}_d$ with respect to $\mathcal{I}$ are again taken to be $\hat{\mathbf{q}}(t_f) = \hat{\mathbf{q}}(t_0) = [0,0,0,1]^T$ and the initial angular velocity vector is again taken to be $\boldsymbol{\omega}(t_0) = [1,-1,1] \, rad/s^2$. The final angular velocity vector is $\boldsymbol{\omega}(t_f) = [0,0,0]^T$. The maximum torque is taken to equal to the moment of inertia about the second principal axis so that u_2 is limited to 1 rad/s^2. By assuming the same choice of parameters given above, Figure 19 shows the time histories of the Euler angles and angular rates, demonstrating attitude stabilization in less than 90s. Figure 20 shows the time histories of the control torques. The control noise is clearly evident near the inherent singularities in the null-control vector and its chattering effect on the angular rates.
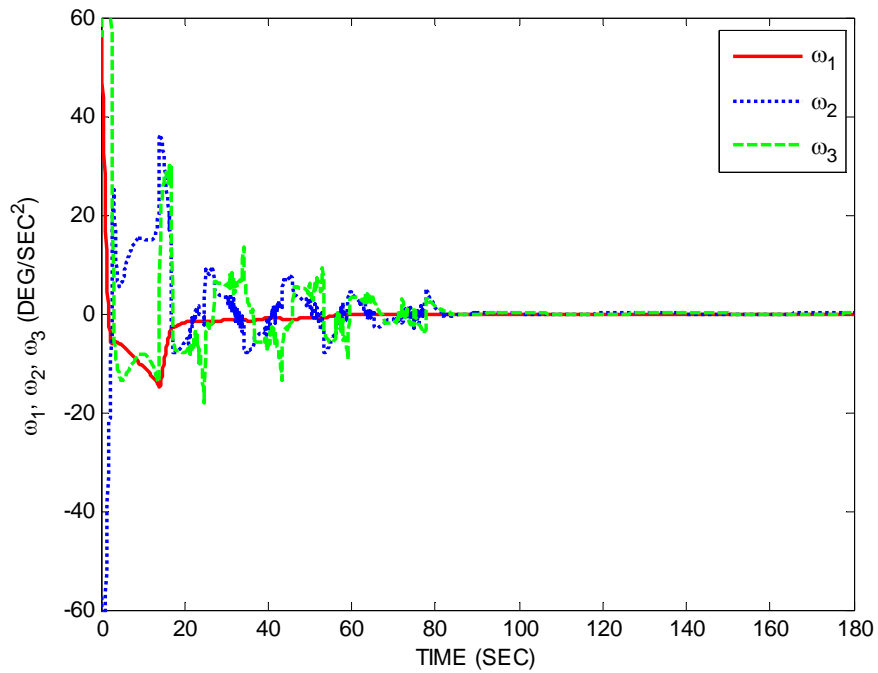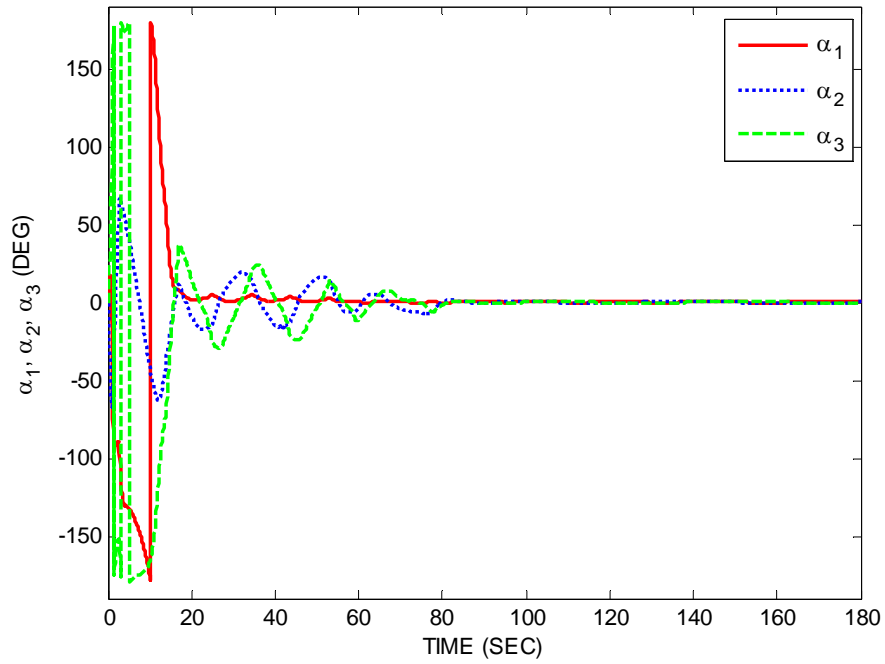
Figure 19.   Time Histories of the Euler Angles and Angular Velocities for a Large Initial Angular Rate to Rest Reorientation Manuever Using the Lyapunov-Function Based Control Law and Large Available Control Torque

Figure 20.   Time Histories of the Control Torques for a Large Initial Angular Rate to Rest Reorientation Manuever Using the Lyapunov-Function Based Control Law and Large Available Control Torque

d. Rest to Rest Reorientation Manuever Given an Initial Angle Offset about Only the Unactuated Axis and Low Available Control Torque

An attitude error stabilization maneuver is considered about the unactuated body-fixed axis with low torque capabilities. The quaternion describing the initial orientation (t_0) of $\mathcal{B}_d$ with respect to $\mathcal{I}$ is taken to be $\hat{\mathbf{q}}(t_0) = [.17, 0, 0, .98]^T$ which, by considering a 3-2-1 sequence of rotations, corresponds to initial Euler angles of $[\alpha_1(t_0), \alpha_2(t_0), \alpha_3(t_0)] = [20, 0, 0]$ deg. The final orientation is taken to be $\hat{\mathbf{q}}(t_f) = [0, 0, 0, 1]^T$. The initial and final angular velocity vector is $\boldsymbol{\omega}(t_0) = \boldsymbol{\omega}(t_f) = [0, 0, 0]^T$. By assuming the same choice of parameters given above, Figure 21 shows the time histories of the Euler angles and angular rates, demonstrating attitude stabilization in less than 70 s. Figure 22 shows the time histories of the control torques and demonstrates significant control noise near the singularities in the control algorithm despite the small initial angular offset.
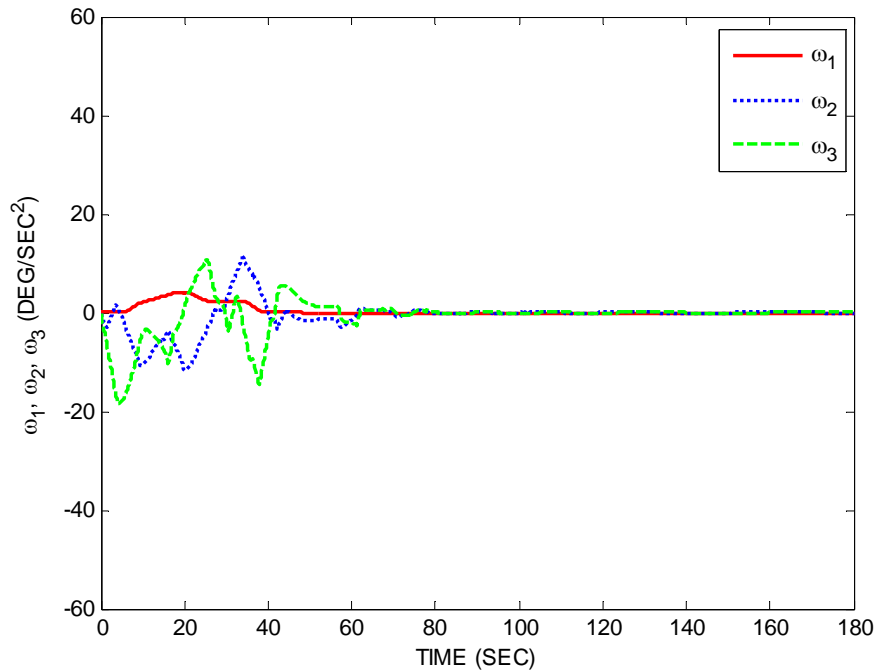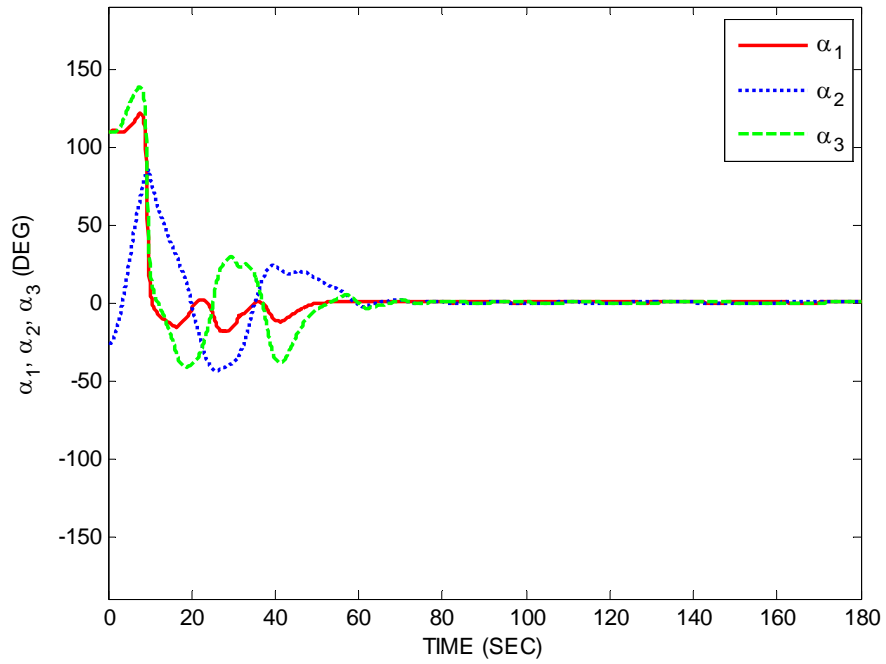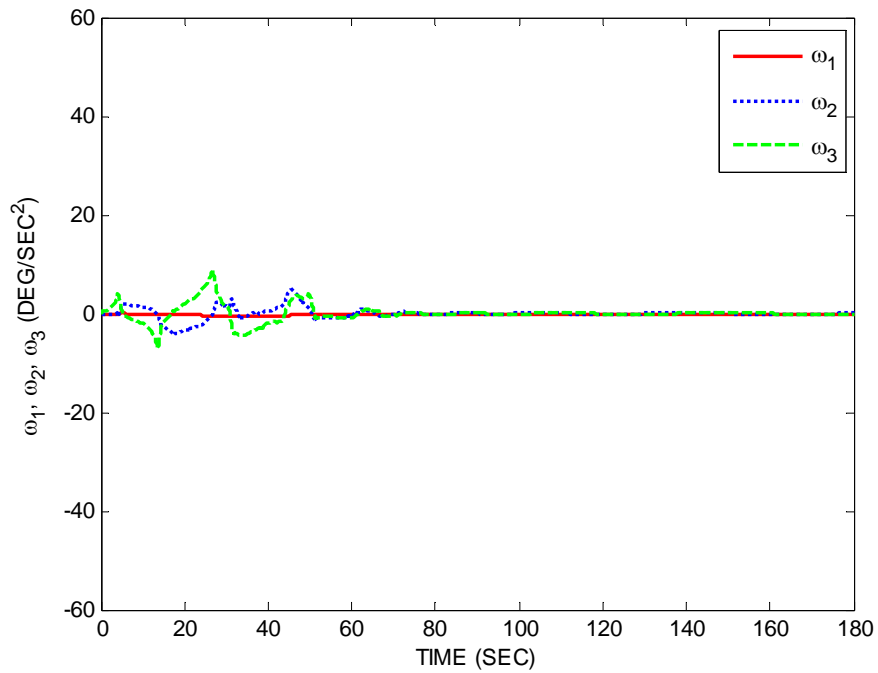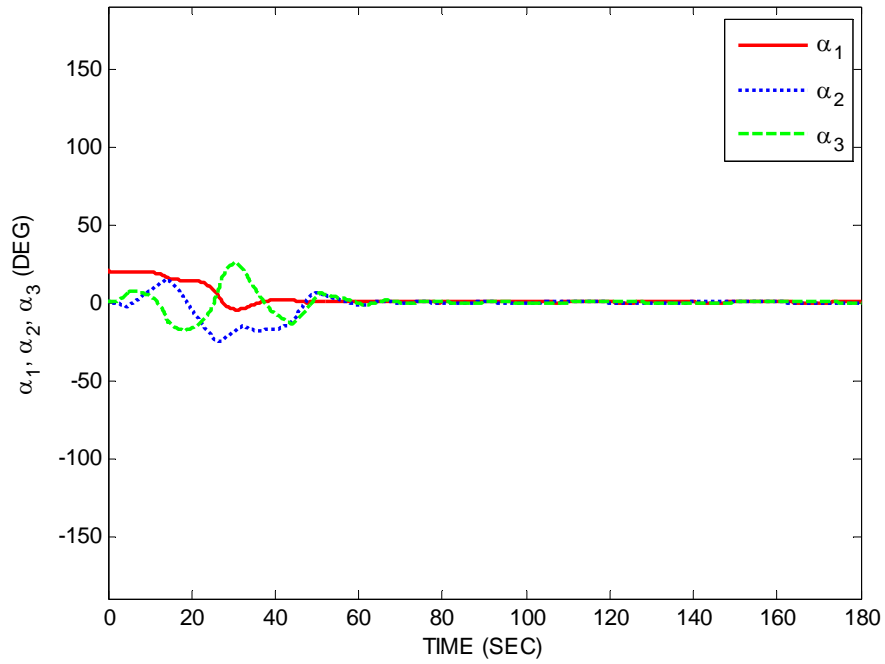
Figure 21.   Time Histories of the Euler Angles and Angular Velocities for a Rest to Rest Reorientation Manuever Given an Initial Angle Offset about Only the Unactuated Axis Using the Lyapunov-Function Based Control Law and Nominal Available Control Torque
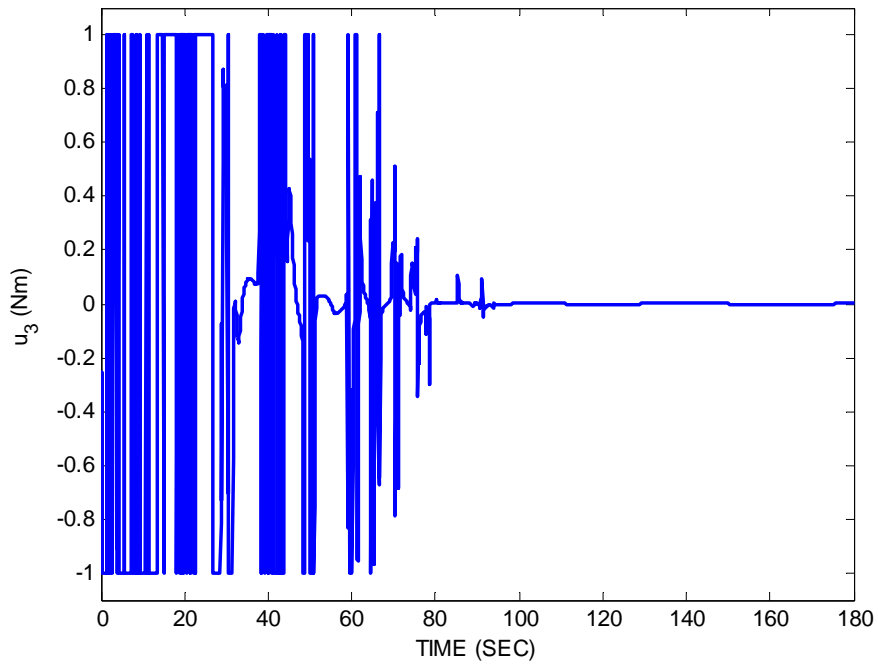
Figure 22. Time Histories of Control Torques for a Rest-To-Rest Reorientation Manuever Given an Initial Angle Offset about Only the Unactuated Axis Using the Lyapunov-Function Based Control Law and Nominal Available Control Torque

112

e.   *Attitude Maintenance in the Presence of Relatively Large Disturbance Torques*

In order to demonstrate a limitation of the presented Lyapunov-function based quaternion feedback regulator with respect to attitude maintenance, an attitude error maintenance scenario is considered with low torque capabilities in the presence of relatively large disturbance torques. The quaternion describing the initial orientation (t_0) of $\mathcal{B}_d$ with respect to $\mathcal{I}$ is taken to be $\hat{\mathbf{q}}(t_0) = [0,0,0,1]^T$ while the final orientation is taken to be $\hat{\mathbf{q}}(t_f) = [0,0,0,1]^T$. The initial and final angular velocity vectors are $\boldsymbol{\omega}(t_0) = \boldsymbol{\omega}(t_f) = [0,0,0]^T$. The same choices of parameters given above are used to include a maximum torque about the two control axes of 1 Nm. Furthermore, a relatively large disturbance torque of .1 Nm is imparted about each body axis. For the presented rigid spacecraft inertia matrix of $J = diag(32.5, 25, 12.5) kgm^2$, this corresponds to angular accelerations of $.003 \, m/s^2$, $.004 \, m/s^2$ and $.008 \, m/s^2$ about the respective body axes. Figure 23 shows the Euler angles and angular rates and demonstrates that although the desired attitude is unable to be maintained, it does remain bounded. Figure 24 reports the control history for the attitude maintenance scenario and again shows the large control effort noise given the near-singularities that exist in the controller.

Figure 23.   Time Histories of Euler Angles and Angular Velocities for an Attitude
Maintenance Scenario in the Presence of Large Disturbance Torques Using the
Lyapunov-Function Based Control Law and Nominal Available Control Torque

Figure 24.   Time Histories of the Control Torques for an Attitude Maintenance
Scenario in the Presence of Large Disturbance Torques Using the Lyapunov-Function
Based Control Law and Nominal Available Control Torque

2. Numerical Simulations using Feedback Linearized Based Quaternion Feedback Regulator

a. *Rest to Rest Reorientation from Large Initial Angle Offset and Low Available Control Torque*

A large-angle rest-to-rest reorientation maneuver is considered. The initial and final conditions of the spacecraft are taken to be equivalent to the considered maneuver above with the Lyapunov-based approach. The chosen gains are

$$\gamma = .70, \alpha = 1.25, d = 7.5, k = 2.25, \beta_1 = 1x10^{-4}$$

Figure 25 shows the time histories of the Euler angles and angular rates, demonstrating attitude stabilization within 100 s. The discontinuity in the Euler angles is due to singularities in the Euler rotation sequence and does not affect the algorithm. Figure 26 shows the time histories of the control torques and demonstrates a significant advantage over the Lyapunov-function based controller with no control noise.
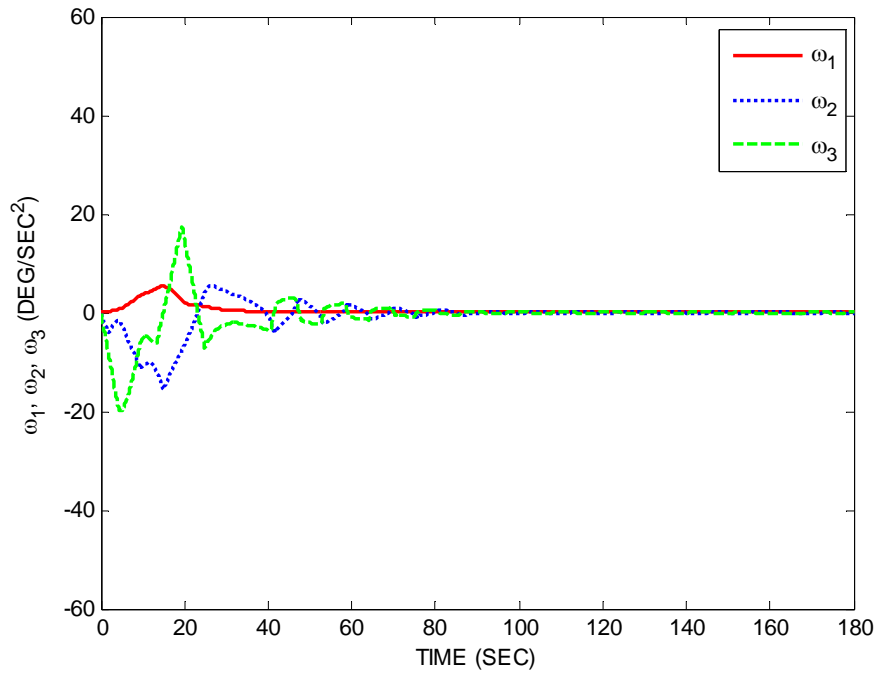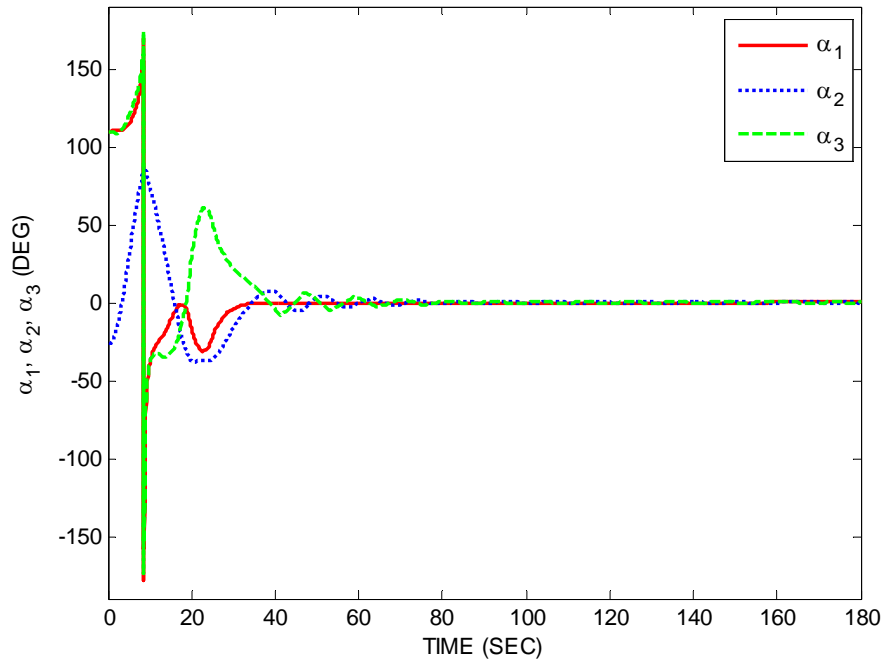
Figure 25. Time Histories of the Euler Angles and Angular Velocities for a Rest to Rest Reorientation Manuever from Large Initial Angle Offset Using the Feedback Linearizing Control Law and Nominal Available Control Torque

117
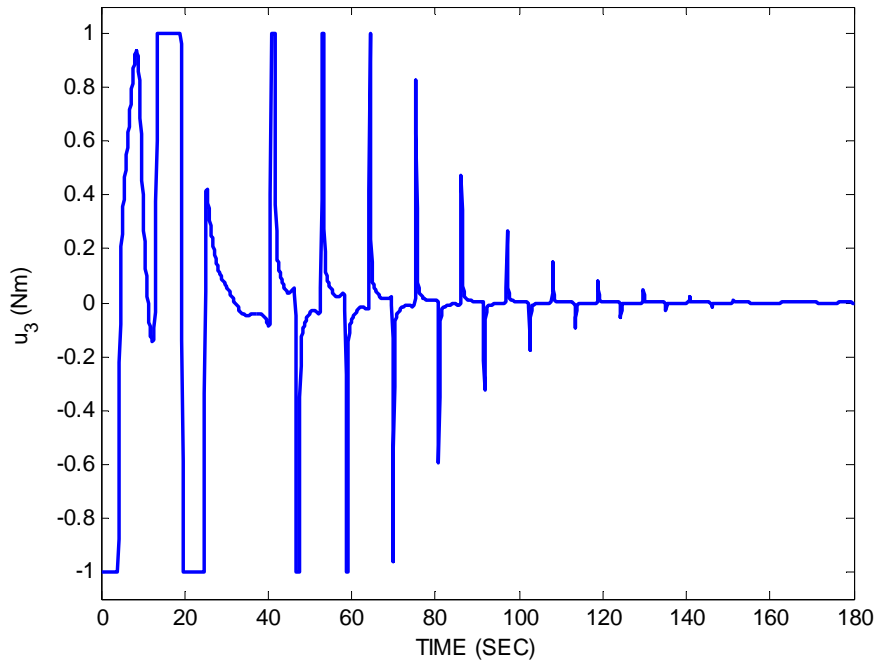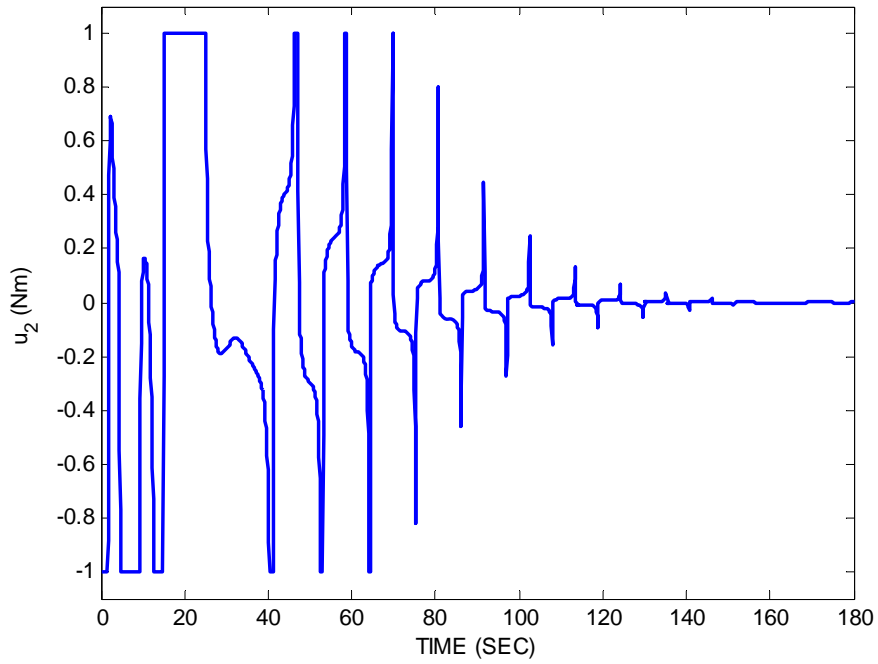
Figure 26.   Time Histories of the Euler Angles and Angular Velocities for a Rest to
Rest Reorientation Manuever from Large Initial Angle Offset Using the Feedback
Linearizing Control Law and Nominal Available Control Torque

118

b.　　　*Rate Stabilization and Reorientation (Low Torque)*

A three-axis detumbling and reorientation maneuver is considered. The initial and final conditions of the spacecraft are taken to be equivalent to the considered maneuver above with the Lyapunov-based approach. By assuming the same choice of parameters, Figure 27 depicts the time histories of the Euler angles and angular rates, demonstrating convergence to the zero state in less than 250 s. Figure 28 shows the time histories of the control torques and again shows significant control effort savings over the Lyapunov-based approach without sacrificing realizability for the system.
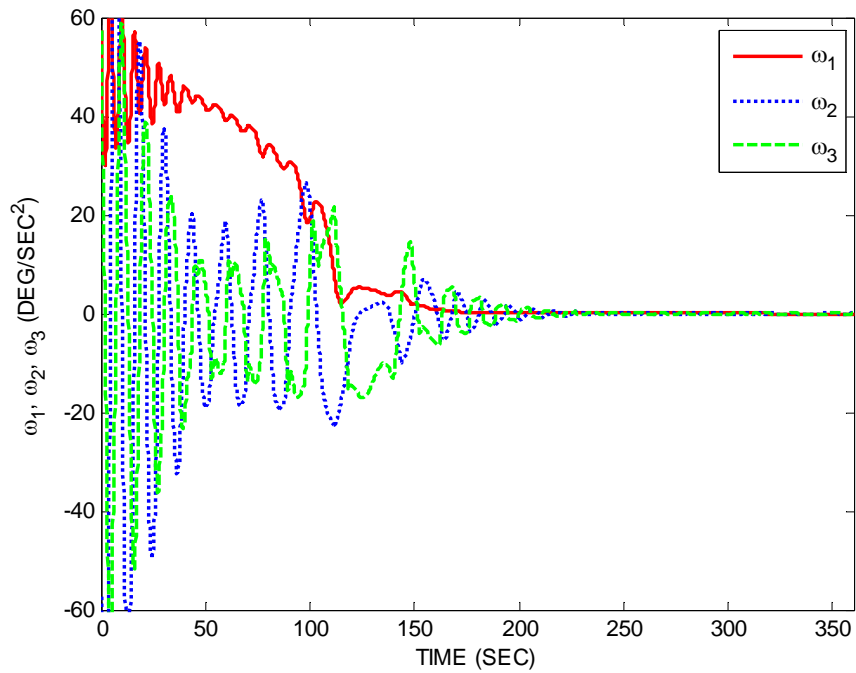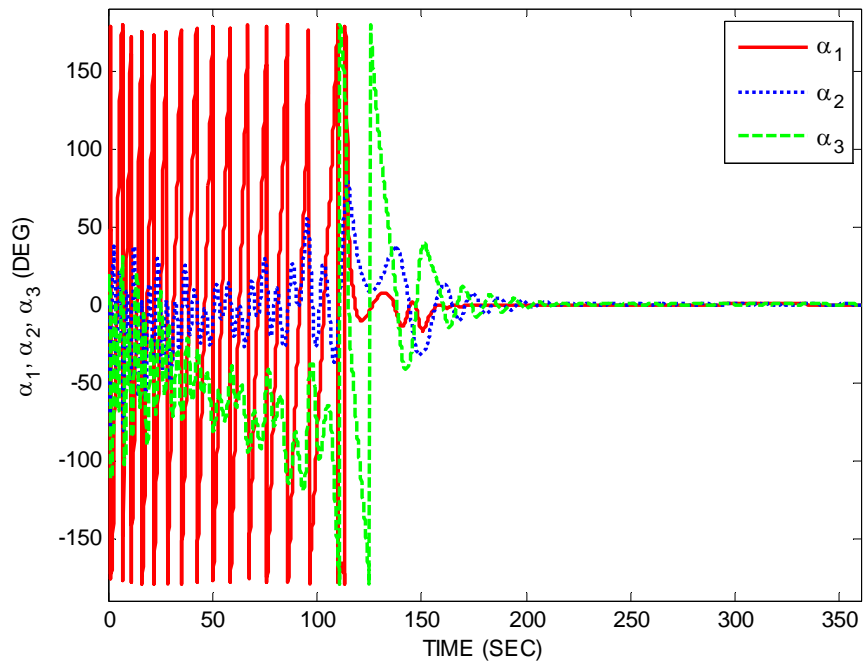
Figure 27.   Time Histories of the Euler Angles and Angular Velocities for a Large
Initial Angular Rate to Rest Reorientation Manuever Using the Feedback Linearing
Control Law and Nominal Available Control Torque
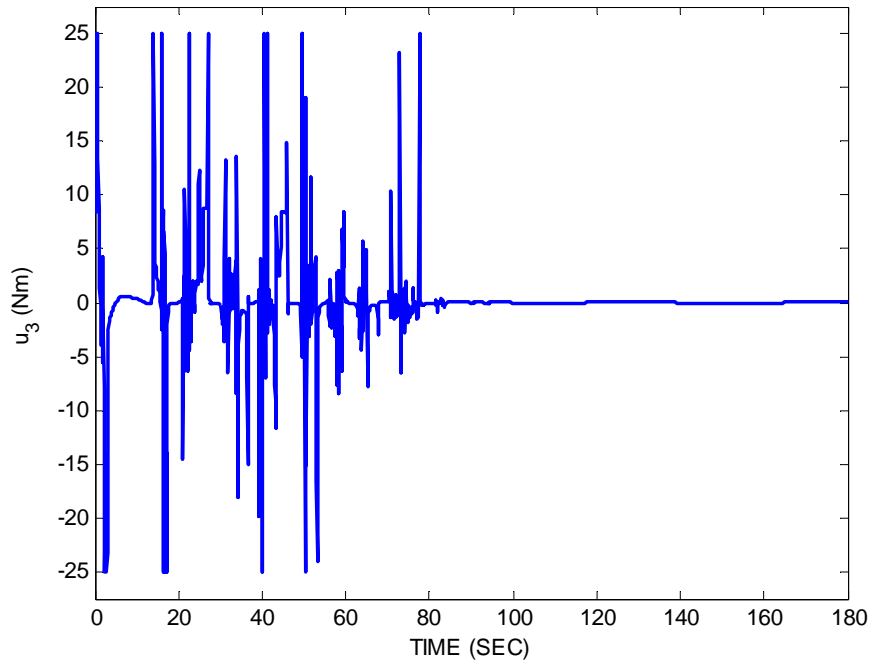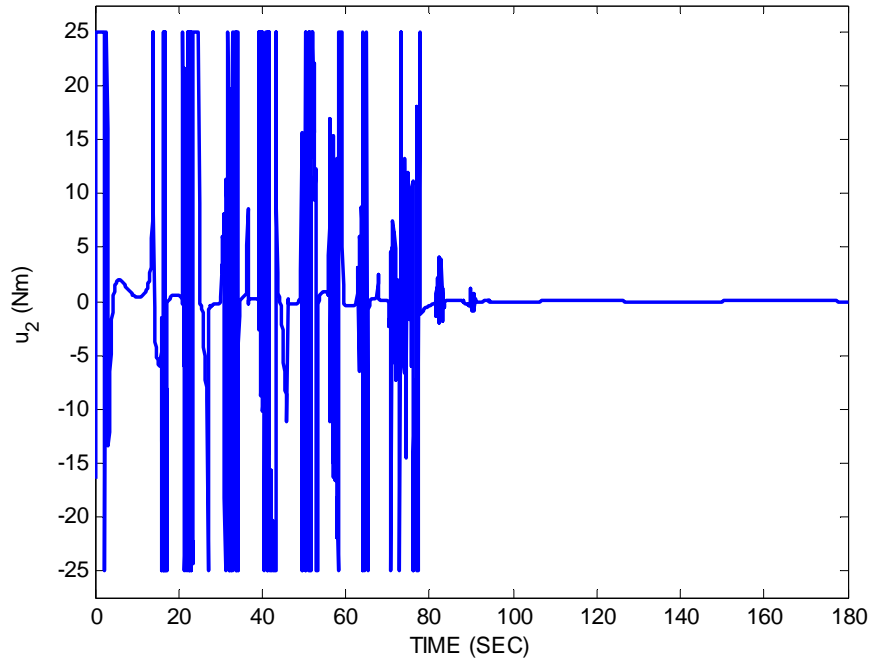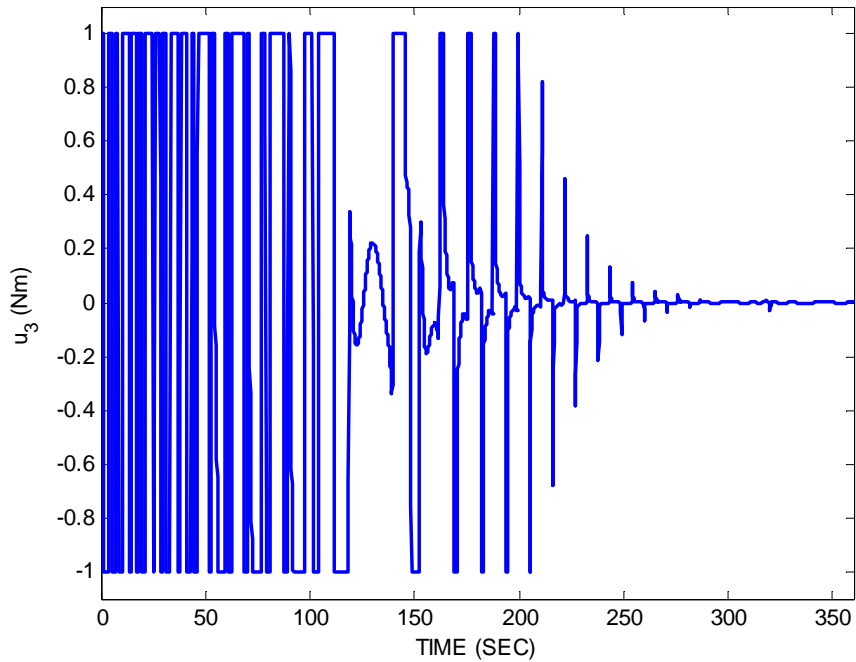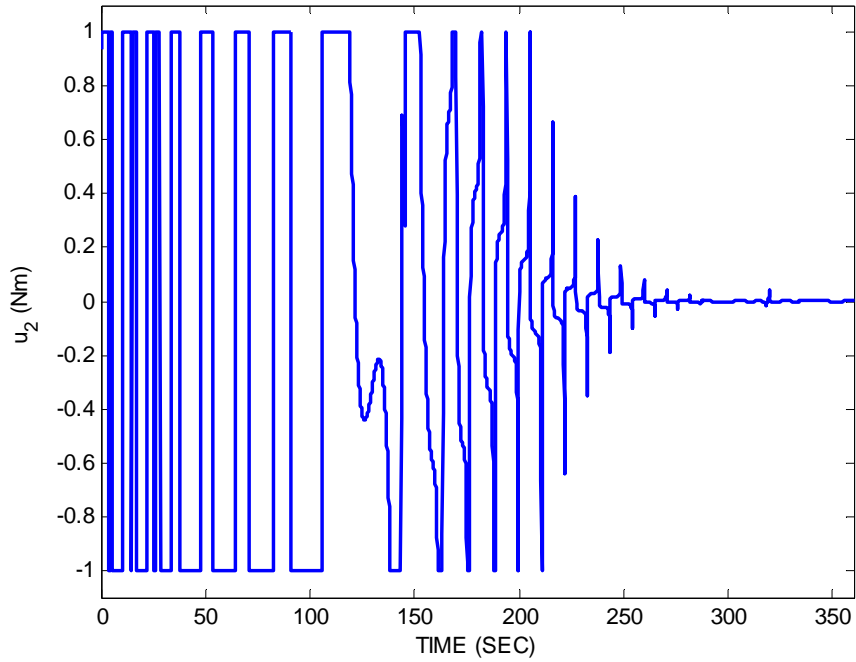
Figure 28.   Time Histories of the Control Torques for a Large Initial Angular Rate to Rest Reorientation Manuever Using the Feedback Linearizing Control Law and Nominal Available Control Torque

121

c. *Rate Stabilization and Reorientation (Large Torque)*

A three-axis detumbling and reorientation maneuver is considered again with increased torque capabilities as is discussed for the Lyapunov-based approach. The initial and final conditions of the spacecraft are taken to be equivalent to the considered maneuver above with the Lyapunov-based approach. By assuming the same choice of parameters given above to include a maximum torque about the second and third body axes so that u_2 is limited to 1 rad/s^2, Figure 29 shows the time histories of the Euler angles and angular rates. Due to the large available torque, the spacecraft is stabilized to the desired attitude in less than 100 s. Figure 30 shows the time histories of the control torques and shows that even with a large available torque, the control does not saturate during the maneuver as is the case with the Lyapunov-based solution.
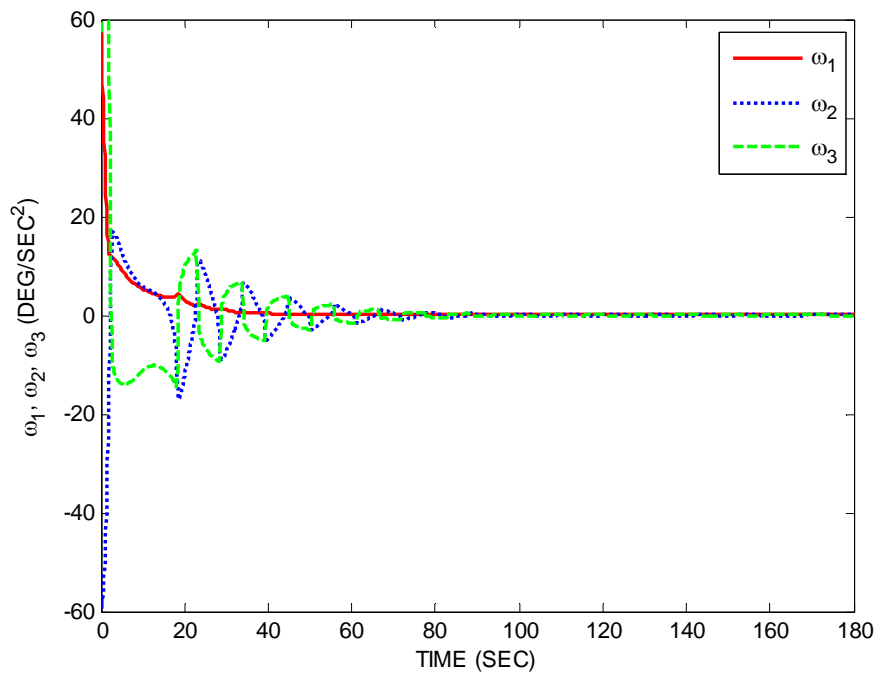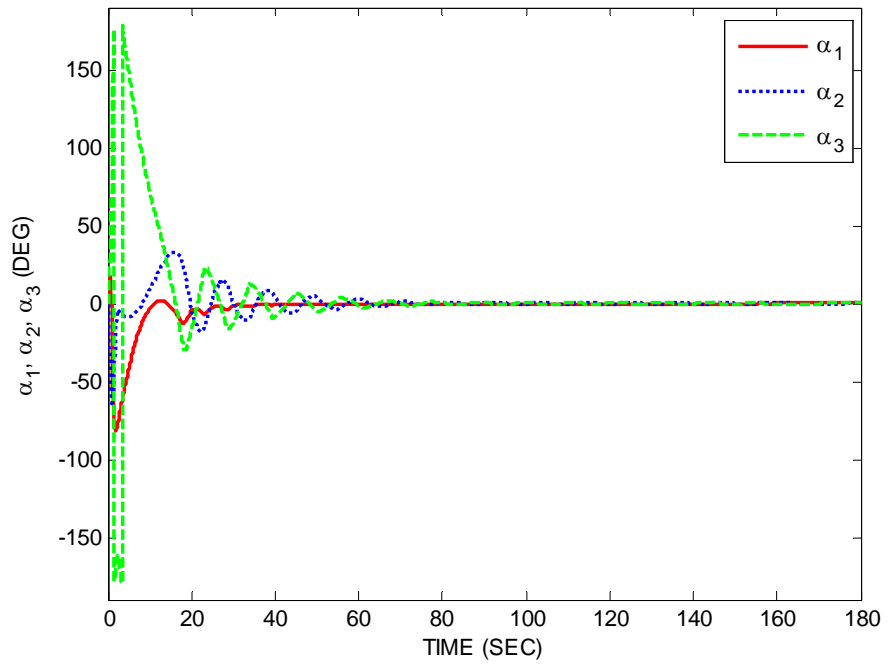
Figure 29.   Time Histories of the Euler Angles and Angular Velocities for a Large
Initial Angular Rate to Rest Reorientation Manuever Using the Feedback Linearizing
Control Law and Large Available Control Torque
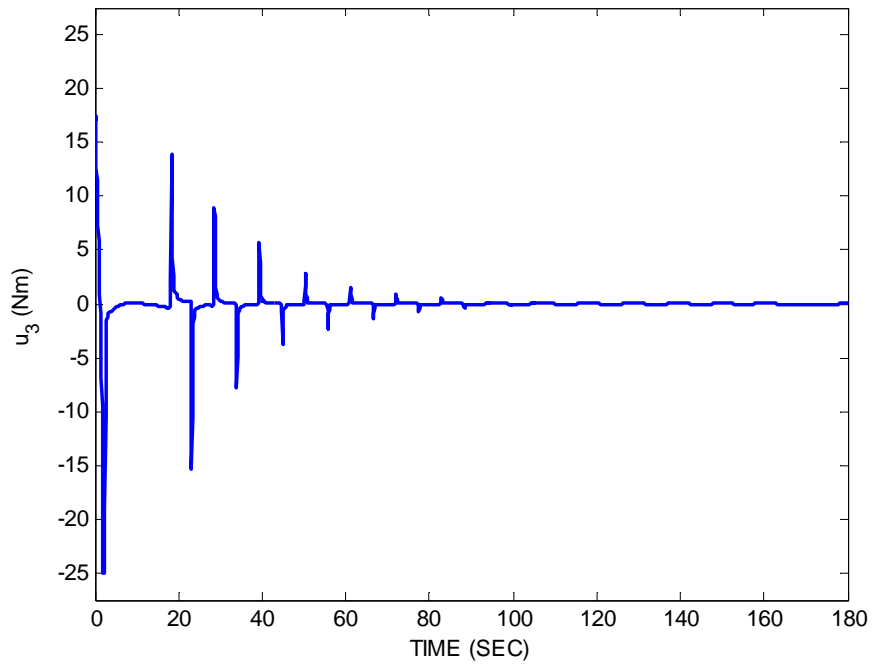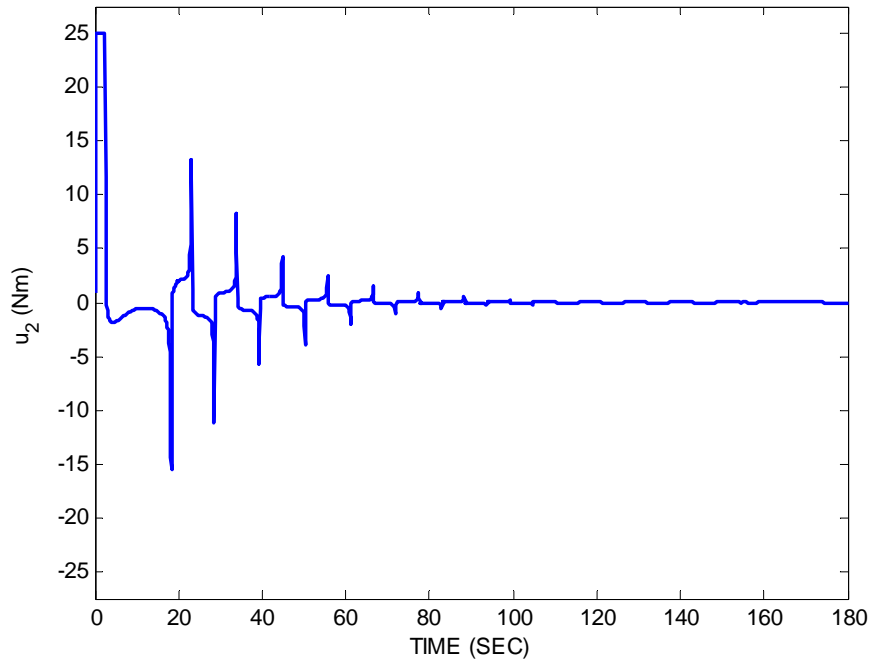
Figure 30.   Time Histories of the Control Torques for a Large Initial Angular Rate to Rest Reorientation Manuever Using the Feedback Linearizing Control Law and Large Available Control Torque

124

d.   *Unactuated Attitude Error Stabilization (Low Torque)*

An attitude error stabilization maneuver is considered about the unactuated body-fixed axis with low torque capabilities. The initial and final conditions of the spacecraft are taken to be equivalent to the considered maneuver above with the Lyapunov-based approach. By assuming the same choice of parameters given above, Figure 31 shows the time histories of the Euler angles and angular rates, demonstrating smooth reorientation to the desired attitude in less than 80 s. Figure 32 shows the time histories of the control torques and shows the advantage in terms of control effort over the Lyapunov-based solution.
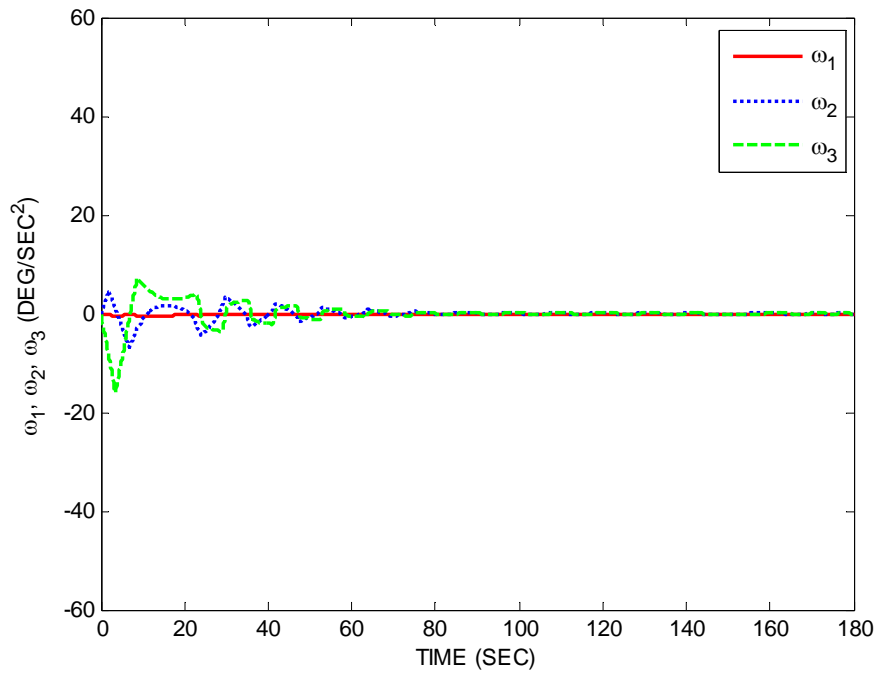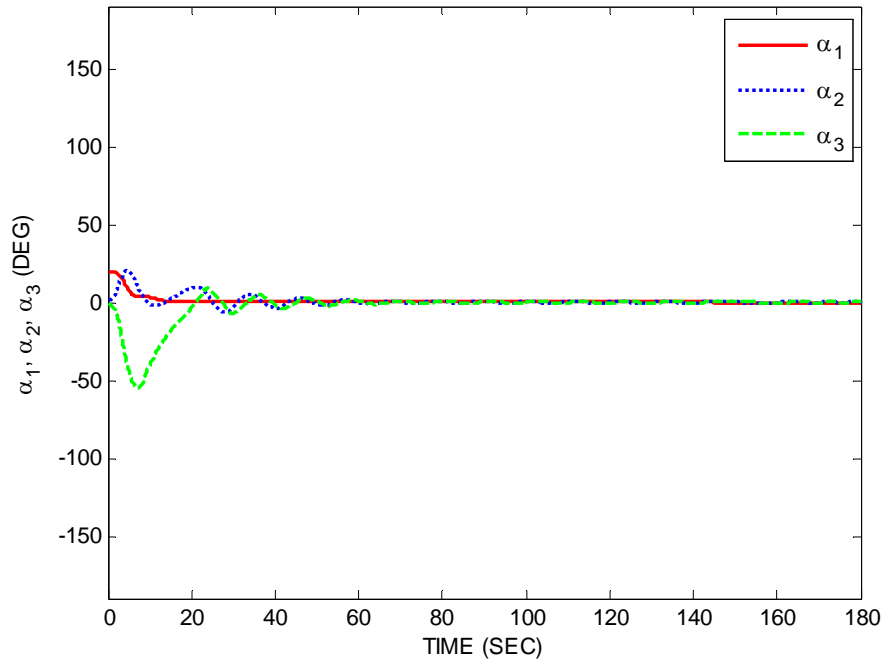
Figure 31.   Time Histories of the Euler Angles and Angular Velocities for a Rest to Rest Reorientation Manuever Given an Initial Angle Offset About Only the Unactuated Axis Using the Feedback Linearizing Control Law and Nominal Available Control Torque
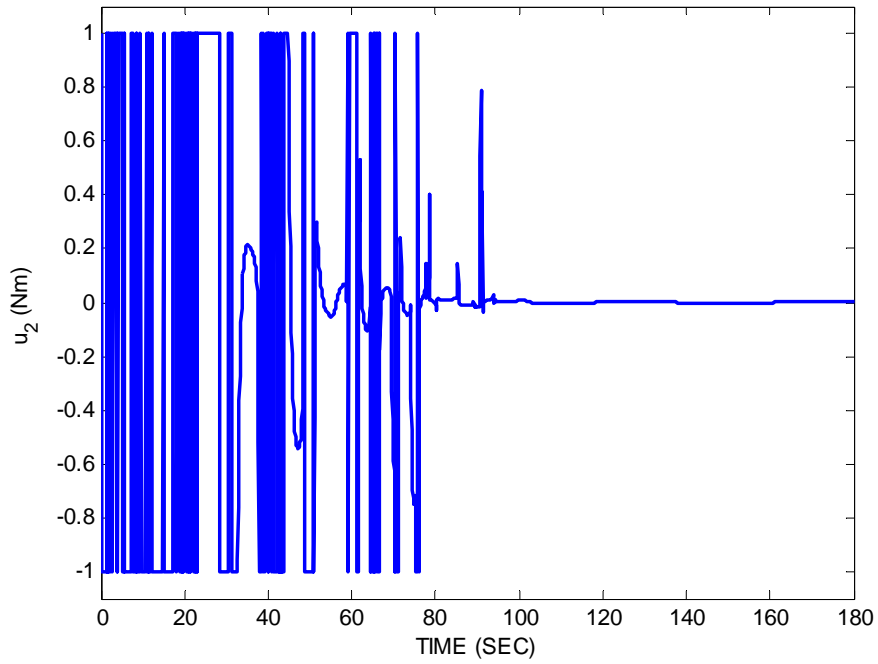
126
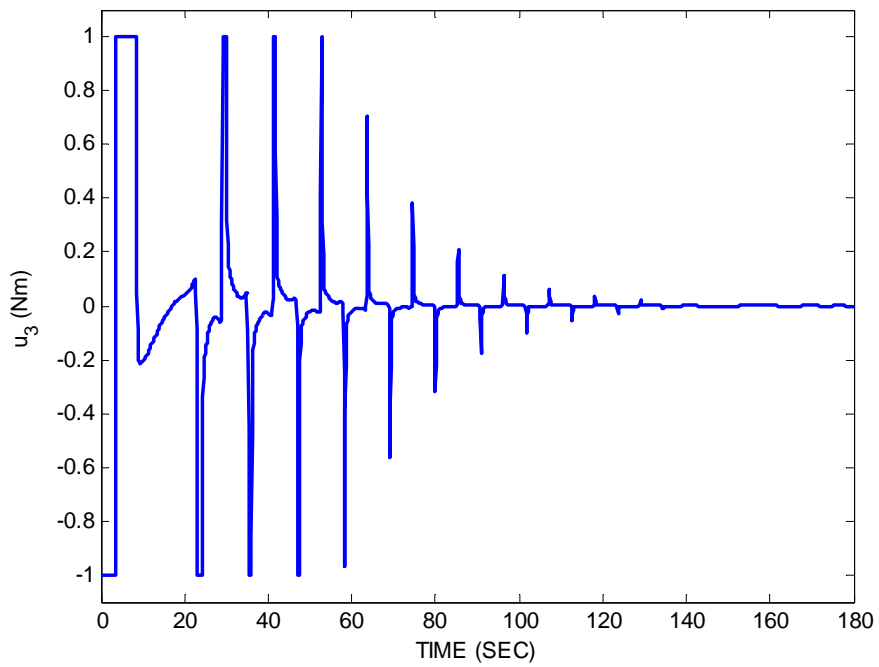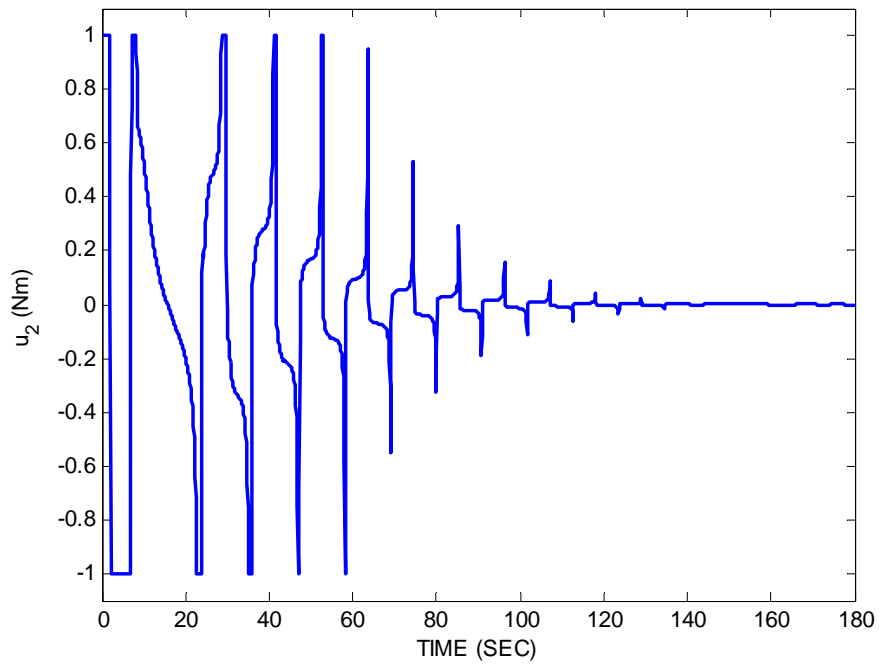
Figure 32.   Time Histories of the Control Torques for a Rest to Rest Reorientation
Manuever Given an Initial Angle Offset About Only the Unactuated Axis Using the
Feedback Linearizing Control Law and Nominal Available Control Torque

e.　　*Attitude Maintenance in the Presence of Relatively Large Disturbance Torques*

An attitude error maintenance scenario is considered with low torque capabilities in the presence of relatively large disturbance torques using the presented feedback linearizing control law. By assuming the same initial and final conditions and parameters used for the Lyapunov-based approach, Figure 33 shows the Euler angles and angular rates and demonstrates that although the desired attitude is unable to be maintained, it remains bounded. By comparison to Figure 23 for the Lyapunov-function based control law, the feedback linearizing control law provides an additional measure of stability by affecting a strictly periodic nature to the spacecraft's attitude and a tighter bounds on the attitude error departures. Figure 34 reports the control history for the attitude maintenance scenario and depicts a relatively smooth control effort throughout the maneuver.
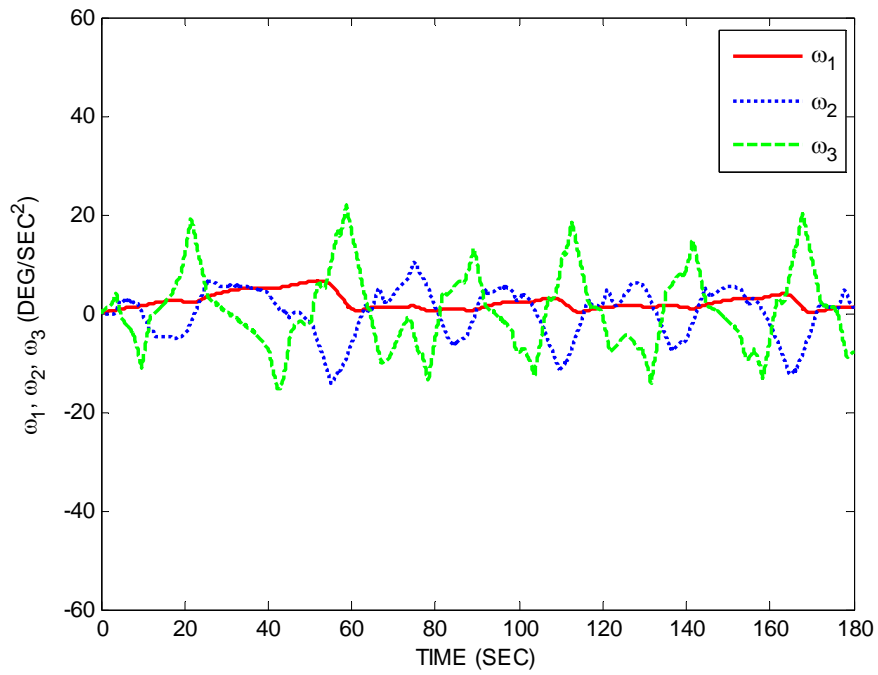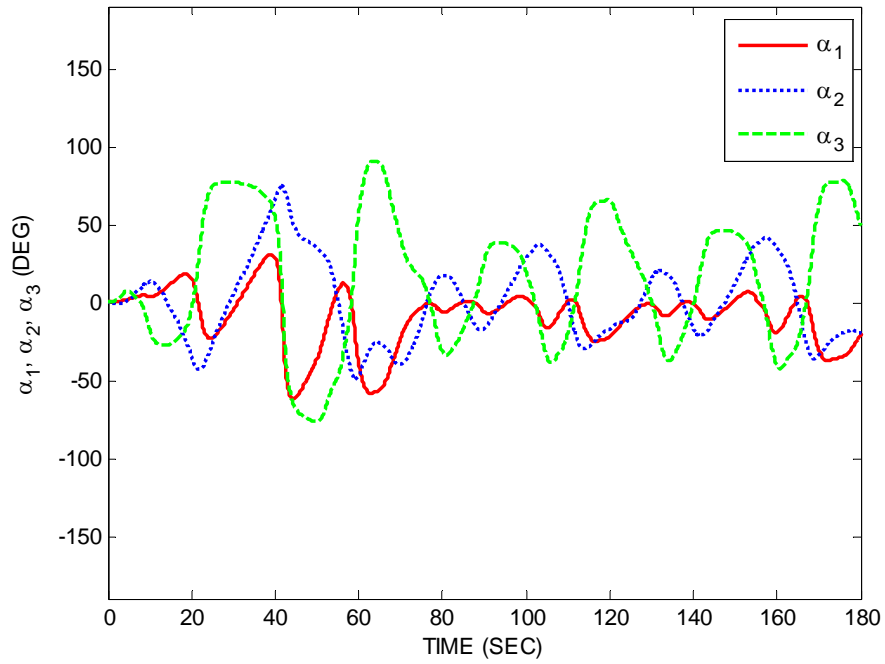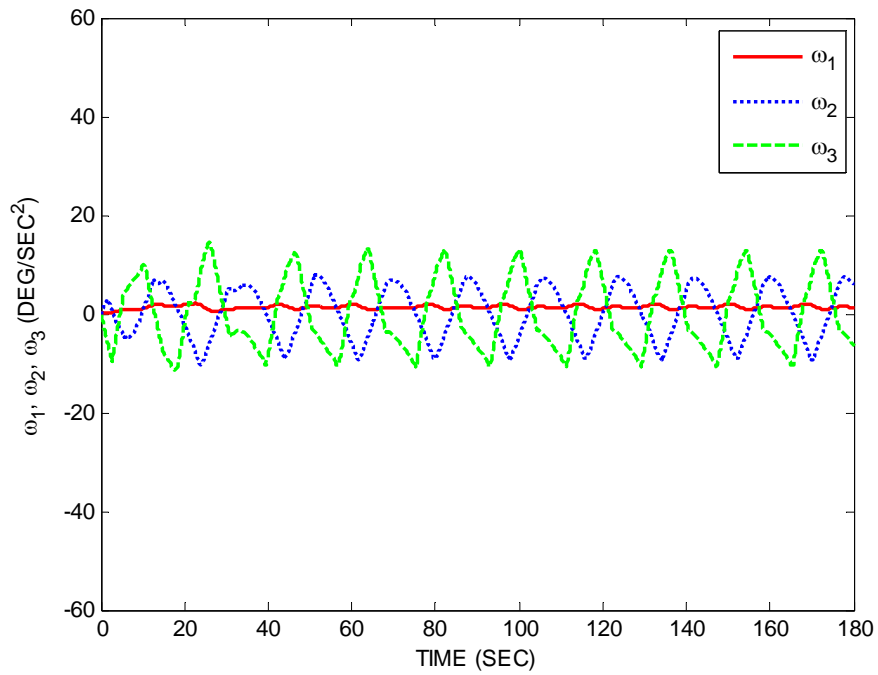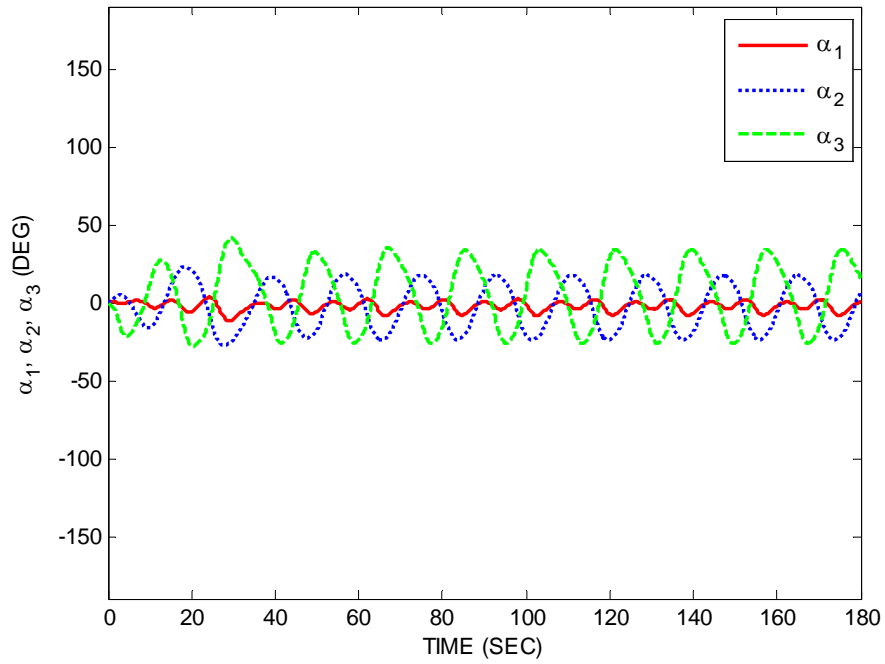
Figure 33.   Time Histories of Euler Angles and Angular Velocities for an Attitude
Maintenance Scenario in the Presence of Large Disturbance Torques Using the Feedback
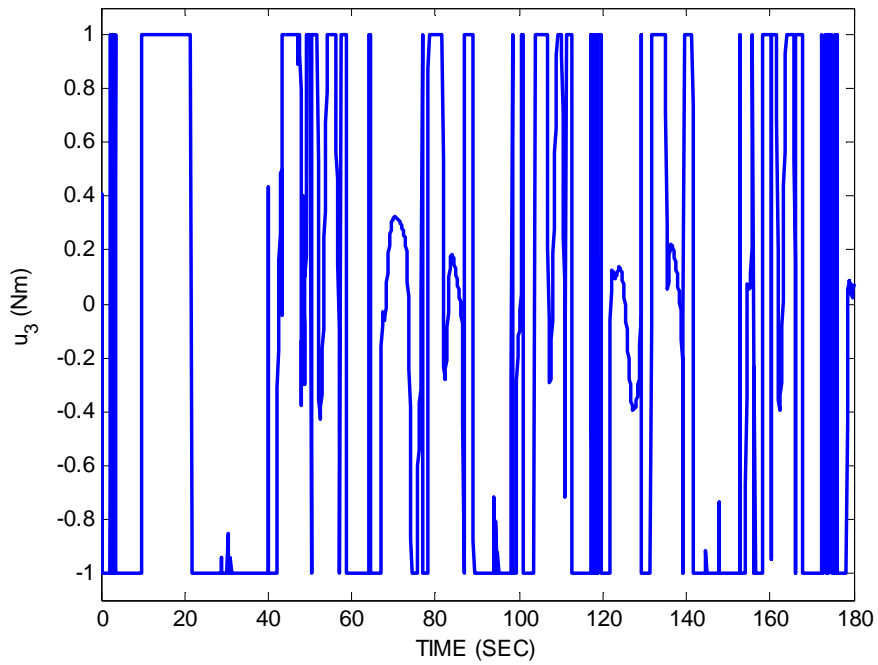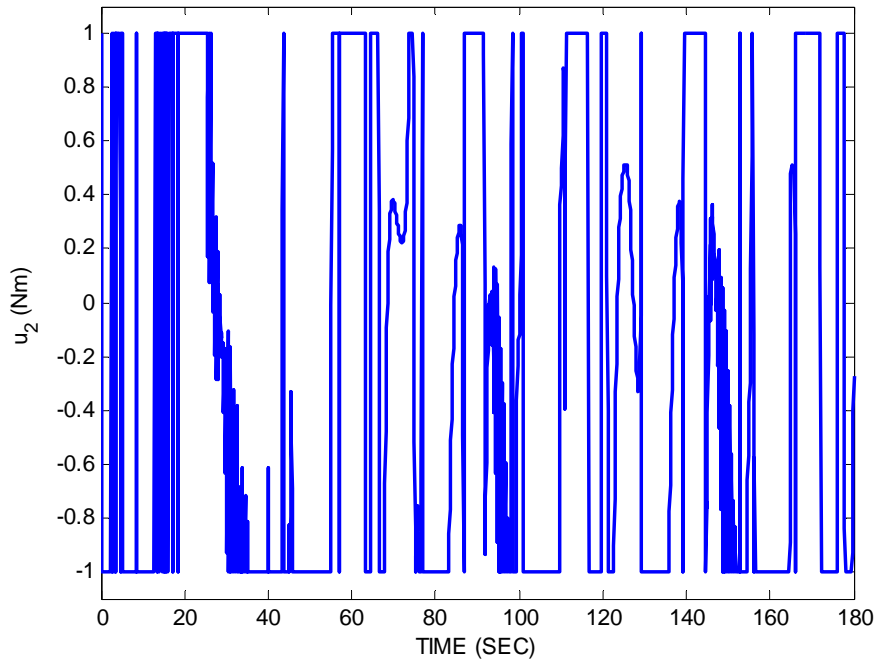Linearizing Control Law and Nominal Available Control Torque
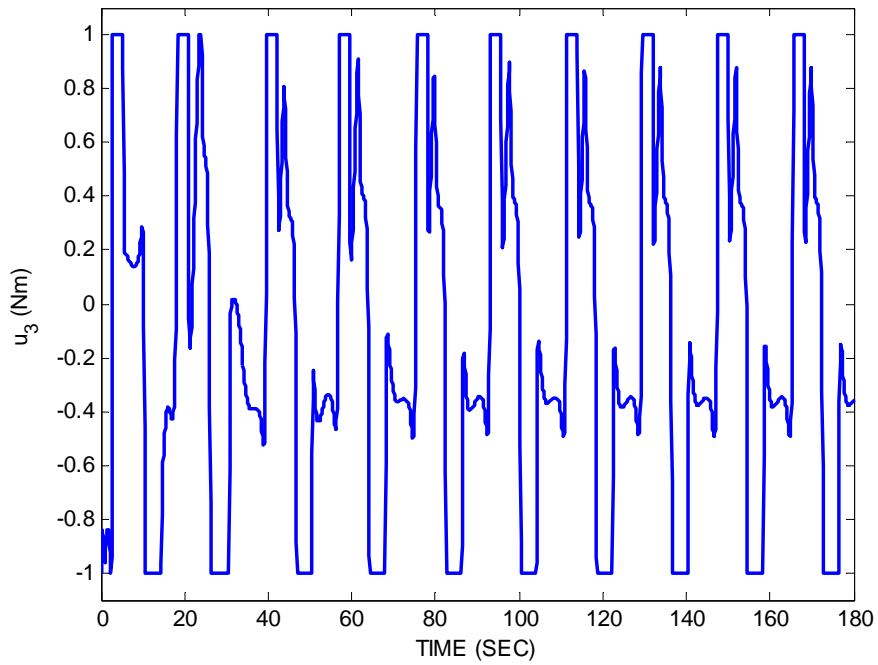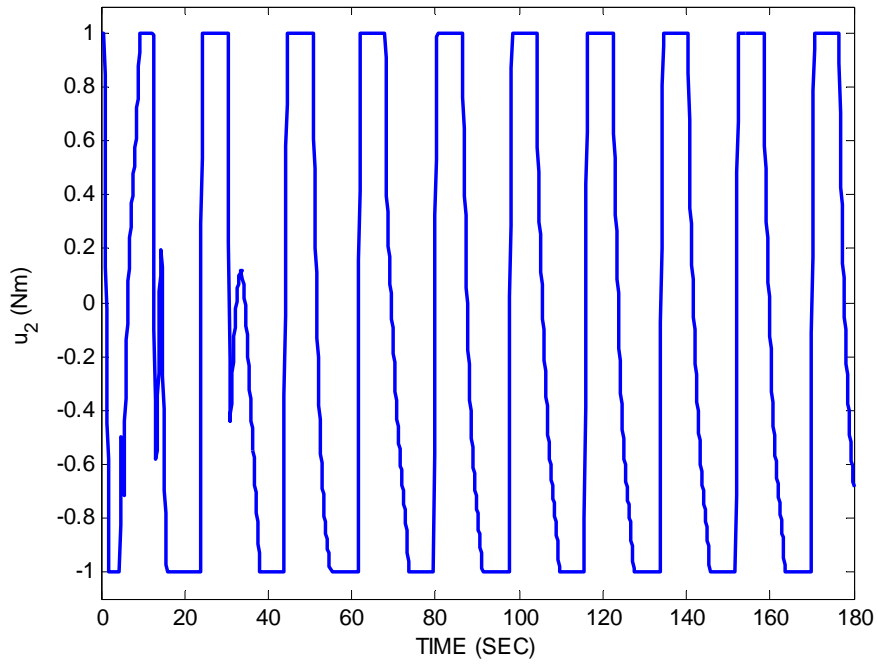
Figure 34.   Time Histories of the Control Torques for an Attitude Maintenance
Scenario in the Presence of Large Disturbance Torques Using the Feedback Linearizing
Control Law and Nominal Available Control Torque

V. CONCLUSION

A. SUMMARY OF CONTRIBUTIONS

A planar laboratory testbed is first introduced for the simulation of autonomous proximity maneuvers of uniquely control actuator configured spacecraft. This testbed consists of a floating robotic simulator via planar air bearings on a flat floor that is equipped with dual vectorable cold-gas thrusters and miniature control moment gyroscope. Inertial position and attitude measurements are obtained and fused with a discrete Kalman filter and linear quadratic estimator for navigation while feedback linearized control coupled with a linear quadratic regulator and Schmitt trigger logic directly command the control moment gyro and command dual in-plane vectorable cold-gas thrusters through a Pulse Width Modulation scheme.

The presented experimental tests of autonomous closed path proximity maneuvers of the spacecraft simulator offer significant sample cases. The experimental results, which show good repeatability and robustness against disturbance and sensor noise, validate the proposed estimation and control approaches and validate, in particular, the analytical small-time local controllability of the uniquely configured system. The achieved accuracy in following the reference trajectory (respectively, ~ 1 cm for translation and ~ .5 deg for rotation given only the vectorable thrusters as control inputs) demonstrates both a feasible and promising actuator configuration for small spacecraft design given size, weight and fuel storage considerations.

Leveraging the research on the 3-DoF robotic testbed, a rigorous small-time local controllability analysis is conducted to determine the minimum number of control actuators for full-order spacecraft in a proximity operations environment. Two potential configurations flow from this analysis. The first involves a traditional approach of fixed thrusters whereby two fixed thrusters are oppositely mounted and used to translate the spacecraft while two sets of paired thrusters provide attitude control. The second configuration involves a novel design consisting of only two hemispherically vectorable thrusters. By combining the vectorable thrusters in an opposing manner, the typical

131

spacecraft system requiring six or more control actuators to achieve 6-DoF control is reduced to only two. Furthermore, by simply adding two additional paired thrusters to provide a torque about the vector that joins the two vectorable thrusters, this system becomes feedback linearizable and similar methods to those presented for the 3-DoF robotic testbed can be employed to control both its attitude and position.

By specifically focusing on the minimal number of control actuators for the 6-DoF system, that is to say where only two vectorable thrusters are required to provide small-time local controllability, a control problem exists where one must achieve three-axis stabilization of the attitude with only two control torques. To solve this problem, a novel quaternion feedback regulator is presented that capitalizes on recent developments in generalized inversion and perturbed feedback linearizing control. A desired second-order linear dynamics in a function of the angular velocity and error quaternion components about the unactuated axis is evaluated along trajectories of the 3-DoF spacecraft angular motion equations that include both Euler's dynamic equations and the error quaternion kinematics. The control variables, which are composed of a particular and auxiliary part, are determined to yield a stable underactuated system. The particular part seeks to realize the desired linear dynamics through generalized inversion of the controls coefficient while the null-control vector in the auxiliary part is selected to yield stability of the full underactuated system. Two control design methodologies are derived that involve separate constructions of the null-control vector. The first is Lyapunov based and yields a stable underactuated spacecraft system while the second involves perturbed feedback linearization and yields stability of the system within a domain of attraction. For both cases, in order to overcome the potential for the control laws to produce numerical instability as the generalized inverse of the controls coefficient becomes singular, the generalized inverse is damped near a bound on the singularity, thus providing smooth control and resulting in stabilization near to the zero error state. As such, neither controller contradicts the conjecture by Byrnes and Isidori (1991) that no smooth, time-invariant state feedback controller can be found to locally asymptotically drive the system to the zero error state. However, given the arbitrary selection of damping coefficients, the region about the zero error state can be reduced to an

insignificant sized ball. Several simulations results are presented for an underactuated asymmetric spacecraft with two, realistically bounded, body-fixed torques to demonstrate the wide-reaching capabilities of both presented null-control vector designs. Included are a large-angle rest-to-rest reorientation maneuver, a large angular velocity detumbling and simultaneous reorientation maneuver and a single-axis reorientation about the unactuated axis. The proposed attitude control method is not intended to provide attitude maintenance or for attitude tracking in the presence of relatively large disturbance torques; however, it may prove widely applicable to detumbling and reorientation maneuvers of spacecraft with only two available control torques.

B.   POSSIBLE FUTURE DEVELOPMENTS

The following iterating research remains open:

1. Validate by numerical and/or experimental methods the feedback linearizing control method proposed in Chapter III for the full 6-DoF relative dynamics problem.

2. Determine a roto-translation control strategy for a spacecraft with two oppositely mounted hemispherical thrusters. A possible solution is to investigate using a Frenet frame waypoint tracking solution where the forward face is first made normal to the path by one of the quaternion feedback regulators presented in Chapter IV and then a separate controller is used to translate the spacecraft.

3. Provide a formal proof of global stability for both the Lyapunov-function based and feedback linearizing underactuated quaternion feedback controllers presented in Chapter IV. Given the presented numerical simulation results that demonstrate a very large domain of attraction, it is possible that global stability for both controllers can be rigorously demonstrated.

4. Compare both underactuated attitude controllers to the optimal solution for each presented case. In this manner, a method of gain tuning may be achieved to ensure a near-optimal solution can be achieved.

THIS PAGE INTENTIONALLY LEFT BLANK

APPENDIX A.   MATLAB CODE TO PERFORM SMALL TIME LOCAL CONTROLLABILITY STUDIES

```matlab
function [L, CO] = nlctrb(fx,Gx,P)

%NLCTRB      Compute the controllability matrix and associated
%            Lie algebra for a nonlinear control-affine system
%            (with or without drift) of the following form:
%
%            xdot = f(x) + G(x)u, f(P) = 0, x->RNx, u->RNu
%
%    The following three cases pertain for the condition of the
%            dimensions of the Lie Algebra Matrix L where Nu is
%            the dimension of the control space and Nx is the
%            dimension of the state space:
%
%    1.  dim(L(Delta)) = Nu      The system is completely integrable
%    2.  Nu < dim(L(Delta)) < Nx The system is nonholonomic, but not
%                                 Small-Time Locally Controllable (STLC)
%    3.  dim(L(Delta)) = Nx      The system is nonholonomic and STLC
%
%    if the system is driftless (i.e. f_0(x) = 0 for all x in X) enter
%        the zero vector for f0(x).
%
%    Evaluate this script to establish symbolic objects for state
%        variables prior to calling function where state = number of
%        state variables
%
%        syms X
%        for a = 1:state
%            x = strcat('x',num2str(a));
%            syms(x);
%            X(a) = x;
%        end
%
%        This algorithm uses the P.Hall Basis algorithm as explained in
%            LaValle, S.M. Planning Algorithms, 2006.
%
%Developed by Jason S. Hall
%Naval Postgraduate School
%Feb 2007
%Modified July 2009 to work with new Symbolic Matlab Toolbox
%%%%%%%%%%%%%%%%%%%%%%%%%%%%%%%%%%%%%%%%%%%%%%%%%%%%%%%%%%%%%%%%%%%%%
%% State Variable Assignment
[Nx,Nu] = size(Gx);
X       = sym(zeros(Nx,1));
for a = 1:Nx
    x   = strcat('x',num2str(a));
    syms(x);
    X(a)= x;
end
%% Vector Variable Assignment
syms h f0
```

```matlab
if isequal(fx,zeros(Nx,1)) == 1
    dimh     = Nu;
    q{1}     = 'h1';
    v        = genvarname('h',who);
    eval([v ' = Gx(:,1)'])
    L{1}     = q{1};
    for a = 2:dimh
        q{a}     = strcat('h',num2str(a));
        v        = genvarname('h',who);
        eval([v ' = Gx(:,a);']);
        L(a)     = q(a);
    end
    st       = 1;
else
    dimh     = Nu + 1;
    q{1}     = 'f0';
    f0       = fx;
    st       = 0;
    for a = 2:dimh
        q{a}     = strcat('h',num2str(a-1));
        v        = genvarname('h',who);
        eval([v ' = Gx(:,a-1);']);
        L(a-1)     = q(a);
    end
end

dim     = ones(1,Nu+1);
Xn      = zeros(Nx,1);
for a = 1:Nx
    if P(a) ~= 0;
        Xn(a) = randn;
    end
end
CO      = Gx;
Ldel_x  = double(subs(Gx,X,Xn));
rhmat   = rank(Ldel_x);
%% Required Index Assignment
[kk,ll] = size(Gx);
k       = 1;
jj      = 1;
%% Algorithm
for a = 2:Nu+5
    [o,p] = size(q);
    if rhmat == Nx
        break
    end
    for b = st:Nu
        if rhmat == Nx
            break
        end
        for c = 1:p
            if rhmat == Nx
                break
            end
            if b == 0
```

```matlab
        r1 = 'f0';
    else
        r1 = strcat('h',num2str(b));
    end
    if iscellstr(q(a-1,c)) && isequal(char(q(a-1,c)),'n') == 0
        r2 = strcat(q(a-1,c));
        r = strcat(r1,',',r2);
        s = sym(char(r));
    else
        r = {'n'};
        s = sym(char(r));
    end
    if strcmp(r1,r2)
        r = {'n'};
        s = sym(char(r));
    elseif (strcmp(r1,'h1') && strcmp(r2,'f0,h1')) ||...
            (strcmp(r1,'h2') && strcmp(r2,'f0,h2'))
        r = {'n'};
        s = sym(char(r));
    else
        if size(r1,2) <= 3
            r3 = char(r2);
            if str2double(r1(2:end)) >= ...
                    str2double(r3(2:end)) && ...
                    isequal(r3(end),'n') == 0
                r = {'n'};
                s = sym(char(r));
            end
        end
        if isequal(r,{'n'})~=1
            q(a,k) = r;
            k = k + 1;
        end
        if length(r1) >= 2 && isequal(char(s),'n') ~= 1
            s2 = s;
        end
        for d = 1:dimh
            if size(r1) == size(char(q(1,d)))
                if r1 == char(q(1,d))
                    for e = 1:Nu+1
                        if length(s) == e+1
                            s1{e}(dim(e),:) = s;
                            kk = dim(e);
                            dim(e) = dim(e) + 1;
                        end
                    end
                end
            end
        end
    end
end
if exist('s2','var')
    fng = eval(s2);
    zz = size(fng,2);
    while zz > 1
        zz = zz -1;
```

137

```matlab
                            fv = fng(:,zz);
                            g = fng(:,zz+1);
                            dfdx = jacobian(fv,X);
                            dgdx = jacobian(g,X);
                            fng(:,zz) = dgdx*fv-dfdx*g;
                        end
                    brack   = fng(:,zz);
                    FNG     = vpa(subs(brack,X,Xn),2);
                    FNG1    = subs(brack,'X','P');
                    hmat    = [Ldel_x,FNG];
                    pp      = size(hmat,2);
                    rhmat   = double(rank(hmat));
                    if rhmat == pp
                        Ldel_x              = hmat;
                        CO                  = [CO,FNG1];
                        qn                  = char(s1{end}(kk,:));
                        L(ll+1)             = cellstr(qn(9:size(qn,2)-2));
                        ll                  = ll + 1;
                    end
                    if rhmat == Nx
                        break
                    end
                    clear s2
                end
            end
        end
        jj = jj+1;
        k = 1;
    end
PHall_Basis = o;

if Nu < Nx && isequal(fx,zeros(Nx,1)) == 1
    if rhmat == Nx
        fprintf('The system is STLC \n \n')
    elseif rhmat == Nu
        fprintf('The system is completely integrable \n \n')
    elseif rhmat < Nx && rhmat > Nu
        fprintf('The system is not STLC \n \n')
    else
        fprintf('The system doesn''t fit \n \n')
    end
elseif Nu < Nx && isequal(fx,zeros(Nx,1)) == 0
    if rhmat == Nx
        fprintf('The system is at least accessible, ')
        fprintf('verify no bad brackets to determine STLC\n \n')
    elseif rhmat == Nu
        fprintf('The system is completely integrable \n \n')
    elseif rhmat < Nx && rhmat > Nu
        fprintf('The system is not accessible \n \n')
    else
        fprintf('The system doesn''t fit \n \n')
    end
end
fprintf('L(Delta) = span {%s',char(L(1)))
for a = 2:length(L)
```

138

```matlab
        fprintf(',%s',char(L(a)))
end
fprintf('} \n')
fprintf('\nThe LRAC is %i \n', rhmat);
fprintf('P.Hall Basis to Depth %i \n',PHall_Basis);
```

THIS PAGE INTENTIONALLY LEFT BLANK

APPENDIX B.   PROOFS OF EMPLOYED LEMMAS

Lemma 1. $\|\boldsymbol{\omega}_a(t)\|$ is uniformly bounded, i.e. $\|\boldsymbol{\omega}_a(t)\| \le c \ \forall t$

Proof.   By rearranging $V = \frac{1}{2}k\|\boldsymbol{\omega}_a\|^2 + 2(1-q_4)$ to yield

$$k\|\boldsymbol{\omega}_a\|^2 = 2V - 4(1-q_4) \tag{255}$$

and then substituting this into $\dot{V} = q_{1e}\phi(\mathbf{x}_u) - \alpha q_u^2 - kd\|\boldsymbol{\omega}_a\|^2$ produces

$$\dot{V} = -2dV + 4d(1-q_4) + q_u\phi(\mathbf{x}_u) - \alpha q_u^2 \tag{256}$$

The desired stable linear dynamics $\ddot{\phi}(\mathbf{x}_u) + 2\gamma\dot{\phi}(\mathbf{x}_u) + \gamma^2\phi(\mathbf{x}_u) = 0$ and the condition $\det[\mathcal{J}_0(\mathbf{x})] \ne 0$ for the infinite set of control laws $\mathbf{u}_d = \bar{\mathbf{u}}_d + P_d(\mathbf{x})\mathbf{y}$ with $\bar{\mathbf{u}}_d = \mathbf{a}_d^+(\mathbf{x})b(\mathbf{x})$ ensure that

$$\lim_{t\to\infty}\phi(\mathbf{x}_u) = 0 \tag{257}$$

for an arbitrarily small selection of that damping coefficient β_1 on the controls coefficient generalized inverse $\mathbf{a}_d^+(\mathbf{x})$. Therefore, given $|q_4| \le 1 \ \forall t$ from the definition of the error quaternion (Cristi and Burl 1993), $V(t)$ is bounded and $\|\boldsymbol{\omega}_a(t)\|$ is bounded.

Lemma 2. *If* $\phi(\mathbf{x}_u)(t) \to 0$ *exponentially, i.e.* $|\phi(\mathbf{x}_u)(t)| \le Ae^{-\gamma t}, t \ge 0$ *for some* $A, \gamma > 0$, *then*

$$\lim_{t\to+\infty}f(t) = f(\infty) < +\infty \tag{258}$$

where $f(t)$ *is defined as*

$$f(t) = \int_0^t \|\boldsymbol{\omega}_a(\tau)\|^2 \, d\tau \tag{259}$$

Proof. For all $t \in \mathbb{R}$ (Cristi and Burl 1993)

$$V(t) = V(0) + \int_0^t \dot{V}(\tau) \, d\tau \tag{260}$$

Substitution of the Lyapunov function V given by $V = \dfrac{1}{2} k \|\boldsymbol{\omega}_a\|^2 + 2(1 - q_4)$ and its

derivative $\dot{V} = q_u \phi(\mathbf{x}_u) - \alpha q_u^2 - kd \|\boldsymbol{\omega}_a\|^2$ yields

$$V(t) = V(0) - kd \int_0^t \|\boldsymbol{\omega}_a(\tau)\|^2 \, d\tau + \int_0^t q_{1e}(\tau)\phi(\mathbf{x}_u)(\tau)\, d\tau - \alpha \int_0^t q_u^2(\tau)\, d\tau \tag{261}$$

Since $V(t) \geq 0 \ \forall t$

$$kd \int_0^t \|\boldsymbol{\omega}_a(\tau)\|^2 \, d\tau \leq V(0) + \int_0^t |\phi(\mathbf{x}_u)(\tau)|\, d\tau \tag{262}$$

Letting $\lambda = 1/kd$ yields

$$\int_0^t \|\boldsymbol{\omega}_a(\tau)\|^2 \, d\tau \leq \lambda V(0) + \lambda \int_0^t |\phi(\mathbf{x}_u)(\tau)|\, d\tau \tag{263}$$

and since $\phi(\mathbf{x}_u)$ exponentially decays through the selection of γ in

$\ddot{\phi}(\mathbf{x}_u) + 2\gamma\dot{\phi}(\mathbf{x}_u) + \gamma^2\phi(\mathbf{x}_u) = 0$ to satisfy the characteristic equation given

by $s^2 + 2\gamma s + \gamma^2 = 0$, the integral is finite. Then for some constant c

$$f(t) = \int_0^t \|\boldsymbol{\omega}_a(\tau)\|^2 \, d\tau \leq c \ \forall t \tag{264}$$

Given (264) is monotonically non-decreasing and upper bounded, it has a finite

limit as $t \to +\infty$ and thus for some constant c

$$f(\infty) = \int_0^{+\infty} \left\| \boldsymbol{\omega}_a(\tau) \right\|^2 d\tau \leq c \tag{265}$$

Lemma 3. *Given* (257),

$$\lim_{t \to \infty} \left\| \phi(\mathbf{x}_u) \right\| = \omega_u + \alpha q_u = 0 \tag{266}$$

which implies that

$$\lim_{t \to \infty} \left| \omega_u(t) \right| = -\alpha q_u(t) \tag{267}$$

Furthermore, with the $\lim_{t \to \infty} \left\| \boldsymbol{\omega}_a(t) \right\| = 0$ *from* (250) *and the kinematic equation for*

the scalar component of the error quaternion given by $\dot{q}_4 = \begin{bmatrix} 0 & -\frac{1}{2} q_u \end{bmatrix} \mathbf{x}_u + \mathbf{q}_p^T \boldsymbol{\omega}_a$

$$\lim_{t \to \infty} \left| \dot{q}_4 \right| = -\frac{1}{2} q_u \omega_u \tag{268}$$

is implied. Therefore, substitution of (267) *into* (268) *yields*

$$\lim_{t \to \infty} \left| \dot{q}_4 \right| = -\frac{1}{2} q_u^2 \tag{269}$$

so that

$$\lim_{t \to \infty} \left| q_4(t) \right| = 0 \tag{270}$$

Additionally, given the kinematic equation for the unactuated component of the

error quaternion expressed by $\dot{q}_u = \frac{1}{2} \left(q_4 \omega_u - \mathbf{q}_p^T \boldsymbol{\omega}_a \right)$ *,the* $\lim_{t \to \infty} \left\| \boldsymbol{\omega}_a(t) \right\| = 0$ *from* (250) *and*

the result from (270) *yields*

$$\lim_{t \to \infty} \left| q_u(t) \right| = 0 \tag{271}$$

And, therefore, from (267),

143

$$\lim_{t \to \infty} \left| \omega_u(t) \right| = 0 \tag{272}$$

and furthermore

$$\lim_{t \to \infty} \left\| \mathbf{x}_u(t) \right\| = 0 \tag{273}$$

Lemma 4. *Given* $\lim_{t \to \infty} \left\| \boldsymbol{\omega}_a(t) \right\| = 0$ *from (250) and* $\lim_{t \to \infty} \left\| \mathbf{x}_u(t) \right\| = 0$ *from (273), and given*

the kinematic equations for the error quaternion as expressed by

$$\dot{\mathbf{q}}_p = \begin{bmatrix} \mathbf{0}_{2x1} & F_{21}(\hat{\mathbf{q}}_{B_dB}) \end{bmatrix} \mathbf{x}_u + F_{22}(\hat{\mathbf{q}}_{B_dB}) \boldsymbol{\omega}_a$$

$$\lim_{t \to \infty} \left\| \mathbf{q}_p(t) \right\| = 0 \tag{274}$$

Proof. From $\dot{\mathbf{q}}_p = \begin{bmatrix} \mathbf{0}_{2x1} & F_{21}(\hat{\mathbf{q}}_{B_dB}) \end{bmatrix} \mathbf{x}_u + F_{22}(\hat{\mathbf{q}}_{B_dB}) \boldsymbol{\omega}_a$, given $\lim_{t \to \infty} \left\| \boldsymbol{\omega}_a(t) \right\| = 0$

from (250) and $\lim_{t \to \infty} \left\| \mathbf{x}_u(t) \right\| = 0$ from (273)

$$\lim_{t \to \infty} \left\| \dot{\mathbf{q}}_p(t) \right\| = 0 \tag{275}$$

$\dot{\boldsymbol{\omega}}_a = -d\boldsymbol{\omega}_a - k\mathbf{q}_p$ can be rewritten as

$$\left(\dot{\boldsymbol{\omega}}_a + \sigma \dot{\mathbf{q}}_p \right) + \kappa \left(\boldsymbol{\omega}_a + \sigma \mathbf{q}_p \right) = \sigma \dot{\mathbf{q}}_p \tag{276}$$

where $\kappa = d > 0, \sigma = kd^{-1} > 0$. By defining

$$\mathbf{e}(t) = \boldsymbol{\omega}_a(t) + \sigma \mathbf{q}_p(t) \tag{277}$$

and substituting this into (276) yields

$$\dot{\mathbf{e}}(t) = -\kappa \mathbf{e}(t) + \sigma \dot{\mathbf{q}}_p(t) \tag{278}$$

From (275) and given $\kappa > 0$

$$\lim_{t \to \infty} \left\| \mathbf{e}(t) \right\| = 0 \tag{279}$$

144

and, therefore, substitution of (279) into (277) yields

$$\lim_{t \to \infty} \left\| \mathbf{q}_p(t) \right\| = 0 \qquad (280)$$

THIS PAGE INTENTIONALLY LEFT BLANK

APPENDIX C.   MATLAB CODE FOR UNDERACTUATED QUATERNION FEEDBACK CONTROLLER

```matlab
function [T]  = RateStable(w, q, qd, wd, J, d, k, gamma,...
                                      Beta1, Beta2, al, select)
% Quaternion Feedback Attitude Regulator for Underactuated Spacecraft

for i = 2:4
    if q(i) == 0
        q(i) = Beta1;
    end
end
for i = 1:3
    if w(i) == 0;
        w(i) = Beta1;
    end
end
q0       = q(1);
q1       = q(2);
q2       = q(3);
q3       = q(4);
qd0      = qd(1);
qd1      = qd(2);
qd2      = qd(3);
qd3      = qd(4);
qdv      = [qd1;qd2;qd3];
qv       = [q1;q2;q3];
qx       = [0 -q3 q2;q3 0 -q1;-q2 q1 0];


q0e      = q0*qd0 + qv'*qdv;
qve      = qd0*qv - q0*qdv + qx*qdv;
q1e      = qve(1);
q2e      = qve(2);
q3e      = qve(3);


we       = w - wd;
w1e      = we(1);
w2e      = we(2);
w3e      = we(3);
wx       = [0 -w3e w2e;w3e 0 -w1e;-w2e w1e 0];


J11      = J(1,1);J12 = J(1,2);J13 = J(1,3);
J21      = J(2,1);J22 = J(2,2);J23 = J(2,3);
J31      = J(3,1);J32 = J(3,2);J33 = J(3,3);

a        = [1/2*(-2*w1e*J11*J13*J22+2*w1e*J11*J12*J23-...
            2*w1e*J31*J22*J33-2*J12*w3e*J13*J32-2*J22*w3e*J23*J32-...
            2*J22*w1e*J12*J23-2*J32*w1e*J12*J33+2*w3e*J13*J12*J23+...
            2*w3e*J33*J23*J32+2*w3e*J12^2*J33+2*w3e*J22^2*J33+...
            2*w1e*J13*J22^2+2*w1e*J13*J32^2-2*w3e*J13^2*J22-...
            2*w3e*J22*J33^2+4*w2e*J12^2*J23+4*w2e*J23*J32^2-...
            4*w2e*J12*J13*J22-4*w2e*J32*J22*J33+...
```
147

```
                  2*w1e*J31*J23*J32-al*q3e*J11*J22*J33+al*q3e*J11*J23*J32+...
                  al*q3e*J21*J12*J33-al*q3e*J21*J13*J32-al*q3e*J31*J12*J23+...
                  al*q3e*J31*J13*J22)/(J11*J22*J33-J11*J23*J32-J21*J12*J33+...
                  J21*J13*J32+J31*J12*J23-J31*J13*J22);
                  1/2*(2*w1e*J11*J12*J33-2*w1e*J11*J13*J32+...
                  2*w1e*J21*J22*J33-2*w1e*J21*J23*J32+2*w2e*J12^2*J33+...
                  2*w2e*J22^2*J33-2*w2e*J13^2*J22-2*w1e*J12*J23^2-...
                  2*w2e*J22*J33^2-4*w3e*J13^2*J32-4*w3e*J23^2*J32-...
                  2*w2e*J12*J13*J32-2*w2e*J22*J23*J32+2*J13*w2e*J12*J23+...
                  2*J23*w1e*J13*J22+2*J33*w2e*J23*J32-2*w1e*J12*J33^2+...
                  2*J33*w1e*J13*J32+4*w3e*J13*J12*J33+4*w3e*J23*J22*J33+...
                  al*q2e*J11*J22*J33-al*q2e*J11*J23*J32-al*q2e*J21*J12*J33+...
                  al*q2e*J21*J13*J32+al*q2e*J31*J12*J23-...
                  al*q2e*J31*J13*J22)/(J11*J22*J33-J11*J23*J32-...
                  J21*J12*J33+J21*J13*J32+J31*J12*J23-J31*J13*J22)];
   Lf2phi  = 1/2*al*w1e*(-1/2*q1e*w1e-1/2*q2e*w2e-1/2*q3e*w3e)+...
                  1/2*al*w3e*(1/2*q3e*w1e+1/2*q0e*w2e-1/2*q1e*w3e)-...
                  1/2*al*w2e*(-1/2*q2e*w1e+1/2*q1e*w2e+1/2*q0e*w3e)+...
                  (1/2*al*q0e+(-(J12*J23-J13*J22)/(J11*J22*J33-...
                  J11*J23*J32-J21*J12*J33+J21*J13*J32+J31*J12*J23-...
                  J31*J13*J22)*J21-(J12*J33-J13*J32)/(J11*J22*J33-...
                  J11*J23*J32-J21*J12*J33+J21*J13*J32+J31*J12*J23-...
                  J31*J13*J22)*J31)*w1e+((J12*J33-J13*J32)/(J11*J22*J33-...
                  J11*J23*J32-J21*J12*J33+J21*J13*J32+J31*J12*J23-...
                  J31*J13*J22)*w3e+(J12*J23-J13*J22)/(J11*J22*J33-...
                  J11*J23*J32-J21*J12*J33+J21*J13*J32+J31*J12*J23-...
                  J31*J13*J22)*w2e)*J11+((J22*J33-J23*J32)/(J11*J22*J33-...
                  J11*J23*J32-J21*J12*J33+J21*J13*J32+J31*J12*J23-...
                  J31*J13*J22)*w3e-(J12*J23-J13*J22)/(J11*J22*J33-...
                  J11*J23*J32-J21*J12*J33+J21*J13*J32+J31*J12*J23-...
                  J31*J13*J22)*w1e)*J21+(-(J22*J33-J23*J32)/(J11*J22*J33-...
                  J11*J23*J32-J21*J12*J33+J21*J13*J32+J31*J12*J23-...
                  J31*J13*J22)*w2e-(J12*J33-J13*J32)/(J11*J22*J33-...
                  J11*J23*J32-J21*J12*J33+J21*J13*J32+J31*J12*J23-...
                  J31*J13*J22)*w1e)*J31+(-(J12*J23-J13*J22)/(J11*J22*J33-...
                  J11*J23*J32-J21*J12*J33+J21*J13*J32+J31*J12*J23-...
                  J31*J13*J22)*J22-(J12*J33-J13*J32)/(J11*J22*J33-...
                  J11*J23*J32-J21*J12*J33+J21*J13*J32+J31*J12*J23-...
                  J31*J13*J22)*J32)*w2e+(-(J12*J23-J13*J22)/(J11*J22*J33-...
                  J11*J23*J32-J21*J12*J33+J21*J13*J32+...
                  J31*J12*J23-J31*J13*J22)*J23-(J12*J33-J13*J32)/...
                  (J11*J22*J33-J11*J23*J32-J21*J12*J33+J21*J13*J32+...
                  J31*J12*J23-J31*J13*J22)*J33)*w3e)*(((( J12*J33-J13*J32)/...
                  (J11*J22*J33-J11*J23*J32-J21*J12*J33+J21*J13*J32+...
                  J31*J12*J23-J31*J13*J22)*w3e+(J12*J23-J13*J22)/...
                  (J11*J22*J33-J11*J23*J32-J21*J12*J33+J21*J13*J32+...
                  J31*J12*J23-J31*J13*J22)*w2e)*J11+((J22*J33-J23*J32)/...
                  (J11*J22*J33-J11*J23*J32-J21*J12*J33+J21*J13*J32+...
                  J31*J12*J23-J31*J13*J22)*w3e-(J12*J23-J13*J22)/...
                  (J11*J22*J33-J11*J23*J32-J21*J12*J33+J21*J13*J32+...
                  J31*J12*J23-J31*J13*J22)*w1e)*J21+(-(J22*J33-J23*J32)/...
                  (J11*J22*J33-J11*J23*J32-J21*J12*J33+J21*J13*J32+...
                  J31*J12*J23-J31*J13*J22)*w2e-(J12*J33-J13*J32)/...
                  (J11*J22*J33-J11*J23*J32-J21*J12*J33+J21*J13*J32+...
                  J31*J12*J23-J31*J13*J22)*w1e)*J31)*w1e+...
```

```
(((J12*J33-J13*J32)/(J11*J22*J33-J11*J23*J32-...
J21*J12*J33+J21*J13*J32+J31*J12*J23-J31*J13*J22)*w3e+...
(J12*J23-J13*J22)/(J11*J22*J33-J11*J23*J32-J21*J12*J33+...
J21*J13*J32+J31*J12*J23-J31*J13*J22)*w2e)*J12+...
((J22*J33-J23*J32)/(J11*J22*J33-J11*J23*J32-J21*J12*J33+...
J21*J13*J32+J31*J12*J23-J31*J13*J22)*w3e-...
(J12*J23-J13*J22)/(J11*J22*J33-J11*J23*J32-J21*J12*J33+...
J21*J13*J32+J31*J12*J23-J31*J13*J22)*w1e)*J22+...
(-(J22*J33-J23*J32)/(J11*J22*J33-J11*J23*J32-...
J21*J12*J33+J21*J13*J32+J31*J12*J23-J31*J13*J22)*w2e-...
(J12*J33-J13*J32)/(J11*J22*J33-J11*J23*J32-J21*J12*J33+...
J21*J13*J32+J31*J12*J23-J31*J13*J22)*w1e)*J32)*w2e+...
(((J12*J33-J13*J32)/(J11*J22*J33-J11*J23*J32-...
J21*J12*J33+J21*J13*J32+J31*J12*J23-J31*J13*J22)*w3e+...
(J12*J23-J13*J22)/(J11*J22*J33-J11*J23*J32-J21*J12*J33+...
J21*J13*J32+J31*J12*J23-J31*J13*J22)*w2e)*J13+...
((J22*J33-J23*J32)/(J11*J22*J33-J11*J23*J32-J21*J12*J33+...
J21*J13*J32+J31*J12*J23-J31*J13*J22)*w3e-...
(J12*J23-J13*J22)/(J11*J22*J33-J11*J23*J32-J21*J12*J33+...
J21*J13*J32+J31*J12*J23-J31*J13*J22)*w1e)*J23+...
(-(J22*J33-J23*J32)/(J11*J22*J33-J11*J23*J32-...
J21*J12*J33+J21*J13*J32+J31*J12*J23-J31*J13*J22)*w2e-...
(J12*J33-J13*J32)/(J11*J22*J33-J11*J23*J32-J21*J12*J33+...
J21*J13*J32+J31*J12*J23-J31*J13*J22)*w1e)*J33)*w3e)+...
(-1/2*al*q3e+((J12*J23-J13*J22)/(J11*J22*J33-...
J11*J23*J32-J21*J12*J33+J21*J13*J32+J31*J12*J23-...
J31*J13*J22)*J11-(J22*J33-J23*J32)/(J11*J22*J33-...
J11*J23*J32-J21*J12*J33+J21*J13*J32+J31*J12*J23-...
J31*J13*J22)*J31)*w1e+J23-J13*J22)/(J11*J22*J33-...
J11*J23*J32-J21*J12*J33+J21*J13*J32+J31*J12*J23-...
J31*J13*J22)*J12-(J22*J33-J23*J32)/  ...
(J11*J22*J33-J11*J23*J32-J21*J12*J33+J21*J13*J32+...
J31*J12*J23-J31*J13*J22)*J32)*w2e+((J12*J33-J13*J32)/...
(J11*J22*J33-J11*J23*J32-J21*J12*J33+J21*J13*J32+...
J31*J12*J23-J31*J13*J22)*w3e+(J12*J23-J13*J22)/...
(J11*J22*J33-J11*J23*J32-J21*J12*J33+J21*J13*J32+...
J31*J12*J23-J31*J13*J22)*w2e)*J12+((J22*J33-J23*J32)/...
(J11*J22*J33-J11*J23*J32-J21*J12*J33+J21*J13*J32+...
J31*J12*J23-J31*J13*J22)*w3e-(J12*J23-J13*J22)/...
(J11*J22*J33-J11*J23*J32-J21*J12*J33+J21*J13*J32+...
J31*J12*J23-J31*J13*J22)*w1e)*J22+(-(J22*J33-J23*J32)/...
(J11*J22*J33-J11*J23*J32-J21*J12*J33+J21*J13*J32+...
J31*J12*J23-J31*J13*J22)*w2e-(J12*J33-J13*J32)/...
(J11*J22*J33-J11*J23*J32-J21*J12*J33+J21*J13*J32+...
J31*J12*J23-J31*J13*J22)*w1e)*J32+((J12*J23-J13*J22)/...
(J11*J22*J33-J11*J23*J32-J21*J12*J33+J21*J13*J32+...
J31*J12*J23-J31*J13*J22)*J13-(J22*J33-J23*J32)/...
(J11*J22*J33-J11*J23*J32-J21*J12*J33+J21*J13*J32+...
J31*J12*J23-J31*J13*J22)*J33)*w3e)*(((-(J11*J33-...
J13*J31)/(J11*J22*J33-J11*J23*J32-J21*J12*J33+...
J21*J13*J32+J31*J12*J23-J31*J13*J22)*w3e-(J11*J23-...
J13*J21)/(J11*J22*J33-J11*J23*J32-J21*J12*J33+...
J21*J13*J32+J31*J12*J23-J31*J13*J22)*w2e)*J11+...
(-(J21*J33-J23*J31)/(J11*J22*J33-J11*J23*J32-...
```

```
J21*J12*J33+J21*J13*J32+J31*J12*J23-J31*J13*J22)*w3e+...
(J11*J23-J13*J21)/(J11*J22*J33-J11*J23*J32-J21*J12*J33+...
J21*J13*J32+J31*J12*J23-J31*J13*J22)*w1e)*J21+...
((J21*J33-J23*J31)/(J11*J22*J33-J11*J23*J32-J21*J12*J33+...
J21*J13*J32+J31*J12*J23-J31*J13*J22)*w2e+(J11*J33-...
J13*J31)/(J11*J22*J33-J11*J23*J32-J21*J12*J33+...
J21*J13*J32+J31*J12*J23-J31*J13*J22)*w1e)*J31)*w1e+...
((-(J11*J33-J13*J31)/(J11*J22*J33-J11*J23*J32-...
J21*J12*J33+J21*J13*J32+J31*J12*J23-J31*J13*J22)*w3e-...
(J11*J23-J13*J21)/(J11*J22*J33-J11*J23*J32-J21*J12*J33+...
J21*J13*J32+J31*J12*J23-J31*J13*J22)*w2e)*J12+...
(-(J21*J33-J23*J31)/(J11*J22*J33-J11*J23*J32-...
J21*J12*J33+J21*J13*J32+J31*J12*J23-J31*J13*J22)*w3e+...
(J11*J23-J13*J21)/(J11*J22*J33-J11*J23*J32-J21*J12*J33+...
J21*J13*J32+J31*J12*J23-J31*J13*J22)*w1e)*J22+...
((J21*J33-J23*J31)/(J11*J22*J33-J11*J23*J32-...
J21*J12*J33+J21*J13*J32+J31*J12*J23-J31*J13*J22)*w2e+...
(J11*J33-J13*J31)/(J11*J22*J33-J11*J23*J32-J21*J12*J33+...
J21*J13*J32+J31*J12*J23-J31*J13*J22)*w1e)*J32)*w2e+...
((-(J11*J33-J13*J31)/(J11*J22*J33-J11*J23*J32-...
J21*J12*J33+J21*J13*J32+J31*J12*J23-J31*J13*J22)*w3e-...
(J11*J23-J13*J21)/(J11*J22*J33-J11*J23*J32-J21*J12*J33+...
J21*J13*J32+J31*J12*J23-J31*J13*J22)*w2e)*J13+...
(-(J21*J33-J23*J31)/(J11*J22*J33-J11*J23*J32-...
J21*J12*J33+J21*J13*J32+J31*J12*J23-J31*J13*J22)*w3e+...
(J11*J23-J13*J21)/(J11*J22*J33-J11*J23*J32-J21*J12*J33+...
J21*J13*J32+J31*J12*J23-J31*J13*J22)*w1e)*J23+...
((J21*J33-J23*J31)/(J11*J22*J33-J11*J23*J32-J21*J12*J33+...
J21*J13*J32+J31*J12*J23-J31*J13*J22)*w2e+...
(J11*J33-J13*J31)/(J11*J22*J33-J11*J23*J32-J21*J12*J33+...
J21*J13*J32+J31*J12*J23-J31*J13*J22)*w1e)*J33)*w3e)+...
(1/2*al*q2e+((J12*J33-J13*J32)/(J11*J22*J33-J11*J23*J32-...
J21*J12*J33+J21*J13*J32+J31*J12*J23-J31*J13*J22)*J11+...
(J22*J33-J23*J32)/(J11*J22*J33-J11*J23*J32-J21*J12*J33+...
J21*J13*J32+J31*J12*J23-J31*J13*J22)*J21)*w1e+...
((J12*J33-J13*J32)/(J11*J22*J33-J11*J23*J32-J21*J12*J33+...
J21*J13*J32+J31*J12*J23-J31*J13*J22)*J12+...
(J22*J33-J23*J32)/(J11*J22*J33-J11*J23*J32-J21*J12*J33+...
J21*J13*J32+J31*J12*J23-J31*J13*J22)*J22)*w2e+...
((J12*J33-J13*J32)/(J11*J22*J33-J11*J23*J32-J21*J12*J33+...
J21*J13*J32+J31*J12*J23-J31*J13*J22)*J13+...
(J22*J33-J23*J32)/(J11*J22*J33-J11*J23*J32-J21*J12*J33+...
J21*J13*J32+J31*J12*J23-J31*J13*J22)*J23)*w3e+...
((J12*J33-J13*J32)/(J11*J22*J33-J11*J23*J32-J21*J12*J33+...
J21*J13*J32+J31*J12*J23-J31*J13*J22)*w3e+...
(J12*J23-J13*J22)/(J11*J22*J33-J11*J23*J32-J21*J12*J33+...
J21*J13*J32+J31*J12*J23-J31*J13*J22)*w2e)*J13+...
((J22*J33-J23*J32)/(J11*J22*J33-J11*J23*J32-J21*J12*J33+...
J21*J13*J32+J31*J12*J23-J31*J13*J22)*w3e-...
(J12*J23-J13*J22)/(J11*J22*J33-J11*J23*J32-J21*J12*J33+...
J21*J13*J32+J31*J12*J23-J31*J13*J22)*w1e)*J23+...
(-(J22*J33-J23*J32)/(J11*J22*J33-J11*J23*J32-...
J21*J12*J33+J21*J13*J32+J31*J12*J23-J31*J13*J22)*w2e-...
(J12*J33-J13*J32)/(J11*J22*J33-J11*J23*J32-J21*J12*J33+...
J21*J13*J32+J31*J12*J23-J31*J13*J22)*w1e)*J33)*...
```

```
             ((((J11*J32-J12*J31)/(J11*J22*J33-J11*J23*J32-...
             J21*J12*J33+J21*J13*J32+J31*J12*J23-J31*J13*J22)*w3e+...
             (J11*J22-J12*J21)/(J11*J22*J33-J11*J23*J32-J21*J12*J33+...
             J21*J13*J32+J31*J12*J23-J31*J13*J22)*w2e)*J11+((J21*J32-...
             J22*J31)/(J11*J22*J33-J11*J23*J32-J21*J12*J33+...
             J21*J13*J32+J31*J12*J23-J31*J13*J22)*w3e-(J11*J22-...
             J12*J21)/(J11*J22*J33-J11*J23*J32-J21*J12*J33+...
             J21*J13*J32+J31*J12*J23-J31*J13*J22)*w1e)*J21+...
             (-(J21*J32-J22*J31)/(J11*J22*J33-J11*J23*J32-...
             J21*J12*J33+J21*J13*J32+J31*J12*J23-J31*J13*J22)*w2e-...
             (J11*J32-J12*J31)/(J11*J22*J33-J11*J23*J32-J21*J12*J33+...
             J21*J13*J32+J31*J12*J23-...
             J31*J13*J22)*w1e)*J31)*w1e+(((J11*J32-J12*J31)/...
             (J11*J22*J33-J11*J23*J32-J21*J12*J33+J21*J13*J32+...
             J31*J12*J23-J31*J13*J22)*w3e+(J11*J22-J12*J21)/...
             (J11*J22*J33-J11*J23*J32-J21*J12*J33+J21*J13*J32+...
             J31*J12*J23-J31*J13*J22)*w2e)*J12+((J21*J32-J22*J31)/...
             (J11*J22*J33-J11*J23*J32-J21*J12*J33+J21*J13*J32+...
             J31*J12*J23-J31*J13*J22)*w3e-(J11*J22-J12*J21)/...
             (J11*J22*J33-J11*J23*J32-J21*J12*J33+J21*J13*J32+...
             J31*J12*J23-J31*J13*J22)*w1e)*J22+(-(J21*J32-J22*J31)/...
             (J11*J22*J33-J11*J23*J32-J21*J12*J33+J21*J13*J32+...
             J31*J12*J23-J31*J13*J22)*w2e-(J11*J32-J12*J31)/...
             (J11*J22*J33-J11*J23*J32-J21*J12*J33+J21*J13*J32+...
             J31*J12*J23-J31*J13*J22)*w1e)*J32)*w2e+(((J11*J32-...
             J12*J31)/(J11*J22*J33-J11*J23*J32-J21*J12*J33+...
             J21*J13*J32+J31*J12*J23-J31*J13*J22)*w3e+(J11*J22-...
             J12*J21)/(J11*J22*J33-J11*J23*J32-J21*J12*J33+...
             J21*J13*J32+J31*J12*J23-J31*J13*J22)*w2e)*J13+...
             ((J21*J32-J22*J31)/(J11*J22*J33-J11*J23*J32-J21*J12*J33+...
             J21*J13*J32+J31*J12*J23-J31*J13*J22)*w3e-(J11*J22-...
             J12*J21)/(J11*J22*J33-J11*J23*J32-J21*J12*J33+...
             J21*J13*J32+J31*J12*J23-J31*J13*J22)*w1e)*J23+...
             (-(J21*J32-J22*J31)/(J11*J22*J33-J11*J23*J32-...
             J21*J12*J33+J21*J13*J32+J31*J12*J23-J31*J13*J22)*w2e-...
             (J11*J32-J12*J31)/(J11*J22*J33-J11*J23*J32-J21*J12*J33+...
             J21*J13*J32+J31*J12*J23-J31*J13*J22)*w1e)*J33)*w3e);
Lfphi    = al*(1/2*q0e*w1e-1/2*q3e*w2e+1/2*q2e*w3e)+(((J12*J33-...
             J13*J32)/(J11*J22*J33-J11*J23*J32-J21*J12*J33+...
             J21*J13*J32+J31*J12*J23-J31*J13*J22)*w3e+...
             (J12*J23-J13*J22)/(J11*J22*J33-J11*J23*J32-...
             J21*J12*J33+J21*J13*J32+J31*J12*J23-...
             J31*J13*J22)*w2e)*J11+((J22*J33-J23*J32)/...
             (J11*J22*J33-J11*J23*J32-J21*J12*J33+J21*J13*J32+...
             J31*J12*J23-J31*J13*J22)*w3e-(J12*J23-J13*J22)/...
             (J11*J22*J33-J11*J23*J32-J21*J12*J33+J21*J13*J32+...
             J31*J12*J23-J31*J13*J22)*w1e)*J21+(-(J22*J33-J23*J32)/...
             (J11*J22*J33-J11*J23*J32-J21*J12*J33+J21*J13*J32+...
             J31*J12*J23-J31*J13*J22)*w2e-(J12*J33-J13*J32)/...
             (J11*J22*J33-J11*J23*J32-J21*J12*J33+J21*J13*J32+...
             J31*J12*J23-J31*J13*J22)*w1e)*J31)*w1e+(((J12*J33-...
             J13*J32)/(J11*J22*J33-J11*J23*J32-J21*J12*J33+...
             J21*J13*J32+J31*J12*J23-J31*J13*J22)*w3e+...
             (J12*J23-J13*J22)/(J11*J22*J33-J11*J23*J32-J21*J12*J33+...
```

```matlab
                    J21*J13*J32+J31*J12*J23-J31*J13*J22)*w2e)*J12+...
                    ((J22*J33-J23*J32)/(J11*J22*J33-J11*J23*J32-J21*J12*J33+...
                    J21*J13*J32+J31*J12*J23-J31*J13*J22)*w3e-(J12*J23-...
                    J13*J22)/(J11*J22*J33-J11*J23*J32-J21*J12*J33+...
                    J21*J13*J32+J31*J12*J23-J31*J13*J22)*w1e)*J22+...
                    (-(J22*J33-J23*J32)/(J11*J22*J33-J11*J23*J32-...
                    J21*J12*J33+J21*J13*J32+J31*J12*J23-J31*J13*J22)*w2e-...
                    (J12*J33-J13*J32)/(J11*J22*J33-J11*J23*J32-...
                    J21*J12*J33+J21*J13*J32+J31*J12*J23-...
                    J31*J13*J22)*w1e)*J32)*w2e+(((J12*J33-J13*J32)/...
                    (J11*J22*J33-J11*J23*J32-J21*J12*J33+J21*J13*J32+...
                    J31*J12*J23-J31*J13*J22)*w3e+(J12*J23-J13*J22)/...
                    (J11*J22*J33-J11*J23*J32-J21*J12*J33+J21*J13*J32+...
                    J31*J12*J23-J31*J13*J22)*w2e)*J13+((J22*J33-...
                    J23*J32)/(J11*J22*J33-J11*J23*J32-J21*J12*J33+...
                    J21*J13*J32+J31*J12*J23-J31*J13*J22)*w3e-(J12*J23-...
                    J13*J22)/(J11*J22*J33-J11*J23*J32-J21*J12*J33+...
                    J21*J13*J32+J31*J12*J23-J31*J13*J22)*w1e)*J23+...
                    (-(J22*J33-J23*J32)/(J11*J22*J33-J11*J23*J32-...
                    J21*J12*J33+J21*J13*J32+J31*J12*J23-...
                    J31*J13*J22)*w2e-(J12*J33-J13*J32)/(J11*J22*J33-...
                    J11*J23*J32-J21*J12*J33+J21*J13*J32+...
                    J31*J12*J23-J31*J13*J22)*w1e)*J33)*w3e;
phi       = w1e + al*q1e;


phidot    = Lfphi;
b         = -Lf2phi - 2*gamma*Lfphi - gamma^2*phi;


wu        = w1e;
wa        = [w2e;w3e];
qa        = qve(2:3);
%qu        = qve(1);


Fw        = -inv(J)*wx*J;
S21       = Fw(2:3,1);
S22       = Fw(2:3,2:3);


if sqrt(a'*a) >= Beta1
   adinv    = a/(a'*a);
else adinv = a/Beta1^2;
end
Pd        = eye(2) - adinv*a';
udbar     = adinv*b;
if select == 1
    %% Lyapunov Function-Based Control Law
    c = wa'*Pd*wa;
    if sqrt(c) >= Beta2
        etad    = wa/(wa'*Pd*wa);
    else etad    = wa/Beta2;
    end
    y = etad*(-wa'*S21*wu - wa'*S22*wa - wa'*udbar - k*qve'*we) - d*wa;
else
    %% Feedback Linearizing Control Law
    y        = (-S21*wu - S22*wa - k*qa - d*wa);
end
```

```
tau_a    = udbar + Pd*y;
tau      = [0;tau_a];
T        = J*tau;
```

THIS PAGE INTENTIONALLY LEFT BLANK

LIST OF REFERENCES

Bajodah, A.H. (2009a), "Generalised Dynamic Inversion Spacecraft Control Design Methodologies," *Control Theory and Applications*, 3 (2), 239–251.

Bajodah, A.H. (2009b), "Asymptotic Perturbed Feedback Linearisation of Underactuated Euler's Dynamics," *International Journal of Control*, 82 (10), 1856-1869.

Battin, R.H. (1987), *An Introduction to the Mathematics and Methods of Astrodynamics*, New York, NY: American Institute of Aeronautics and Astronautics, Inc.

Behal, A., Dawson, D., Zergeroglu, E., and Fang, Y. (2002), "Nonlinear Tracking Control of an Underactuated Spacecraft," *Journal of Guidance, Control and Dynamics,* 25 (5), 979–985.

Bevilacqua, R., Izzo, D., and Valente, C. (2003), "Nonlinear Attitude Control of Satellite Platform Equipped with Variable Speed Control Moment Gyroscopes," in *Proceedings of the XVII AIDAA Congress,* pp. 501–508.

Bevilacqua, R., Hall, J.S., Horning, J., and Romano, M. (2009), "Ad Hoc Wireless Networking and Shared Computation for Autonomous Multirobot Systems," *Journal of Aerospace Computing, Information, and Communication,* 6, 328–352.

Brockett, R.W. (1983), "Asymptotic Stability and Feedback Stabilization," in *Differential Geometric Control Theory,* eds. R.W. Brockett, R.S. Millman, and H.J. Sussman, Boston, MA: Birkhauser, pp. 181–208.

Bryson, A.E. (1994), *Control of Spacecraft and Aircraft*, Princeton, NJ: Princeton University Press.

Bullo, F. and Lewis, A.D. (2005), *Geometric Control of Mechanical Systems*, New York, NY: Springer Science+Business Media, Inc.

Byrnes, C.I. and Isidori, A. (1991), "On the Attitude Stabilization of a Rigid Spacecraft," *Automatica*, 27 (1), 87–95.

Canfield, S.L. and Reinholtz, C.F. (1998), "Development of the Carpal Robotic Wrist," *Lecture Notes in Control and Information Sciences*, 232, 423–434.

Casagrande, D., Astolfi, A., and Parisini, T. (2008), "Global Asymptotic Stabilization of the Attitude and the Angular Rates of an Underactuated Non-symmetric Rigid Body," *Automatica*, 44 (7), 1781–1789.

Cavrois, B., Reynaud, S., Personne, G., Chavy, S., and Strandmoe, S. (2008), "ATV GNC and Safety Functions Synthesis: Overall Design, Main Performance and Operations," in *Proceedings of the AIAA Guidance, Navigation and Control Conference*, pp. 1–22.

Corrazzini, T. and How, J.P. (1998), "Onboard GPS Signal Augmentation for Spacecraft Formation Flying," in *Proceedings of the 11th International Technical Meeting of the Satellite Division of the Institute of Navigation (ION GPS '98)*, pp. 1937–1946.

Coverstone-Carroll, V. (1996), "Detumbling and Reorienting Underactuated Rigid Spacecraft," *Journal of Guidance, Control, and Dynamics*, 19 (3), 708–710.

Crassidis, J.L. and Junkins, J.L. (2004), *Optimal Estimation of Dynamic Systems*, Boca Raton, FL: CRC Press, LLC.

Creamer, G. (2007), "The SUMO/FREND Project: Technology Development for Autonomous Grapple of Geosynchronous Satellites," *Advances in the Astronautical Sciences*, 128, 895–910.

Cristi, R. and Burl, J. (1993), "Adaptive Eigenaxis Rotations," in *Proceedings of the 1993 European Control Conference (ECC '93),* Vol. 2, pp. 770–775.

Crouch, P.E. (1984), "Spacecraft Attitude Control and Stabilization: Applications of Geometric Control Theory to Rigid Body Models," *IEEE Transactions on Automatic Control*, 29 (4), 321–331.

Eikenberry, B.D. (2006), "Guidance and Navigation Software Architecture Design for the Autonomous Multi-Agent Physically Interacting Spacecraft (AMPHIS) Testbed," unpublished M.S. Thesis, Naval Postgraduate School, Dept. of Mechanical and Astronautical Engineering.

Gelb, A. (1974), *Applied Optimal Estimation*, Cambridge, MA: The MIT Press.

Hall, J.S. (2006), "Design and Interaction of a Three Degrees-of-Freedom Robotic Vehicle with Control Moment Gyro for the Autonomous Multi-Agent Physically Interacting Spacecraft (AMPHIS) Testbed," unpublished M.S. Thesis, Naval Postgraduate School, Dept. of Mechanical and Astronautical Engineering.

Hall, J.S. and Romano, M. (2007a), "Autonomous Proximity Operations of Small Satellites with Minimum Numbers of Actuators," in *Proceedings of the 21st AIAA/USU Small Satellite Conference,* pp. 1–14.

Hall, J.S. and Romano, M. (2007b), "Novel Robotic Spacecraft Simulator with Mini-Control Moment Gyroscopes and Rotating Thrusters," in *Proceedings of the 2007 IEEE/ASME International Conference on Advanced Intelligent Mechatronics*, pp. 1–6.

Isidori, A. (1989), *Nonlinear Control Systems: An Introduction*, New York, NY: Springer-Verlag New York, Inc.

Jackson, M. and Gonzalez, R. (2007), "Orion Orbit Reaction Control Assessment," in *Proceedings of the AIAA Guidance, Navigation and Control Conference and Exhibit*, pp. 1–16.

Kennedy, F. (2008), "Orbital Express: Accomplishments and Lessons Learned," *Advances in the Astronautical Sciences*, 131, 575-586.

Kerai, E.Y. (1995), "Analysis of Small-time Local Controllability of the Rigid Body Model," in *Proceedings of the IFAC Symposium on System Structure and Control*, pp. 645–650.

Krishnan, H., McClamroch, H. and Reyhanoglu, M. (1995), "Attitude Stabilization of a Rigid Spacecraft Using Two Momentum Wheel Actuators ," *Journal of Guidance, Control, and Dynamics*, 18 (2), 256–263.

Kurokawa, H. (1998), "A Geometric Study of Single Gimbal Control Moment Gyros – Singularity Problems and Steering Law," Technical Report 175, Mechanical Engineering Laboratory, Tsukuba, Ibaraki, Japan.

Lappas, V.J.; Steyn, W.H. and Underwood, C.I. (2002), "Practical Results on the Development of a Control Moment Gyro Based Attitude Control System for Agile Small Satellites," in *Proceedings of the 16th Annual AIAA/USU Small Satellite Conference*, pp. 1-9.

LaValle, S.M. (2006), *Planning Algorithms*, New York, NY: Cambridge University Press.

Ledebuhr, A.G., Ng, L.C., Jones, M.S., Wilson, B.A., Gaughan, R.J., Breitfeller, E.F., Taylor, W.G., Robinson, J.A., Antelman, D.R., and Nielsen, D.P. (2001), "Micro-Satellite Ground Test Vehicle for Proximity and Docking Operations Development," in *Proceedings of the 2001 Aerospace Conference* (Vol. 5), pp. 2493–2504.

LeMaster, E.A., Schaechter, D.B, and Carrington, C.K. (2006), "Experimental Demonstration of Technologies for Autonomous On-Orbit Robotic Assembly," *Space 2006,* pp. 1–13.

Lewis, A.D. and Murray, R.M. (1997), "Configuration Controllability of Simple Mechanical Control Systems," *Journal on Control and Optimization,* 35 (3), 766–790.

Lugini, C. and Romano, M. (2009), "A ballistic-pendulum Test Stand to Characterize Small Cold-gas Thruster Nozzles," *Acta Astronautica*, 64 (5-6), 615–625.

Machida, K., Toda, Y., and Iwata, T. (1992), "Maneuvering and Manipulation of Flying Space Telerobotics System," in *Proceedings of the 1992 IEEE/RSJ International Conference on Intelligent Robots and Systems* (Vol. 1), pp. 3–10.

Marchesi, M., Angrilli, F., and Venezia, R. (2000), "Coordinated Control for Free-flyer Space Robots," in *Proceedings of the 2000 IEEE International Conference on Systems, Man, and Cybernetics* (Vol. 5), pp. 3550–3555.

Mathieu, C. and Weigel, A. L. (2005), "Assessing the Flexibility Provided by Fractionated Spacecraft," in *Proceedings of the AIAA Space 2005 Conference and Exhibit,* pp. 1–12.

Nolet, S., Kong, E., and Miller, D.W. (2005), "Design of an Algorithm for Autonomous Docking with a Freely Tumbling Target," in *Proceedings of Modeling, Simulation and Verification of Space-based Systems II* (Vol. 5799, No. 123), pp. 123–134.

Price, W. (2006), "Control System of a Three DOF Spacecraft Simulator by Vectorable Thrusters and Control Moment Gyros," unpublished M.S. Thesis, Naval Postgraduate School, Dept. of Mechanical and Astronautical Engineering.

Romano, M., Friedman, A., and Shay, T.J. (2007), "Laboratory Experimentation of Autonomous Spacecraft Approach and Docking to a Collaborative Target," *Journal of Spacecraft and Rockets*, 44 (1), 164–173.

Romano, M. and Hall, J.S (2006), "A Testbed for Proximity Navigation and Control of Spacecraft for On-orbit Assembly and Reconfiguration," in *Proceedings of the AIAA Space 2006 Conference and Exhibit,* pp. 1–11.

Roser, X. and Sghedoni, M. (1997), "Control Moment Gyroscopes (CMG's) and their Applications in Future Scientific Missions," in *Proceedings of the 3rd ESA International Conference on Spacecraft Guidance, Navigation and Control Systems*, pp. 523–528.

Sussman, H.J. (1987), "A General Theorem on Local Controllability," *Journal on Control and Optimization*, 25 (1), 158–194.

Sussman, H.J. (1990), *Nonlinear Controllability and Optimal Control*, New York, NY: Marcel Dekker, Inc.

Slotine, J.E. and Li, W. (1991), *Applied Nonlinear Control*, Upple Saddle River, NJ: Prentice–Hall, Inc.

Tsiotras, P., Corless, M., and Longuski, J.M. (1995), "A Novel Approach to the Attitude Control of Axisymmetric Spacecraft," *Automatica,* 31 (8), 1099–1112.

Tsiotras, P. and Luo, J. (2000), "Control of Underactuated Spacecraft with Bounded Inputs," *Automatica*, 36 (8), 1153–1169.

Tsiotras, P. and Schleicher, A. (2000), "Detumbling and Partial Attitude Stabilization of a Rigid Spacecraft under Actuator Failure," in *Proceedings of the AIAA Guidance, Navigation, and Control Conference and Exhibit*, pp. 1–8.

Tsiotras, P. and Doumtchenko, V. (2000), "Control of Spacecraft Subject to Actuator Failures: State-of-the-Art and Open Problems," in *Proceedings of the R.H. Battin Astrodynamics Symposium*, pp. 1–36.

Ullman, M.A. (1993), "Experimentation in Autonomous Navigation and Control of Multi-Manipulator Free-Flying Space Robots," unpublished Ph.D. Dissertation, Stanford University, Dept. of Aeronautics and Astronautics.

Udwadia, F.E. and Kalaba, R.E. (1996), *Analytical Dynamics, A New Approach*, New York, NY: Cambridge University Press.

Vadali, S.R. (1989), "Variable-structure Control of Spacecraft Large-angle Maneuvers," *Journal of Guidance, Control, and Dynamics*, 9 (2), 235–239.

Vallado, D.A. (2001), *Fundamentals of Astrodynamics and Applications*, El Segundo, CA: Microcosm, Inc.

Wie, B. and Barba, P.M. (1985), "Quaternion Feedback for Spacecraft Large Angle Maneuvers," *Journal of Guidance, Control, and Dynamics,* 8 (3), 360–365.

Wie, B., Weiss, H. and Arapostathis, A. (1989), "Quaternion Feedback Regulator for Spacecraft Eigenaxis Rotation," *Journal of Guidance, Control and Dynamics,* 12 (3), 375–380.

Wie, B. (1998), *Space Vehicle Dynamics and Control*, Reston, VA: American Institute of Aeronautics and Astronautics, Inc.

Zhou, K., Doyle, J.C., and Glover, K. (1996), *Robust and Optimal Control,* Upper Saddle River, NJ: Prentice Hall

THIS PAGE INTENTIONALLY LEFT BLANK

INITIAL DISTRIBUTION LIST

1.   Defense Technical Information Center
        Ft. Belvoir, Virginia

2.   Dudley Knox Library
        Naval Postgraduate School
        Monterey, California